Detector-Based Traceability Chain for Spectral Irradiance using Tunable Laser-Based Facility at PTB

Von der Fakultät für Elektrotechnik, Informationstechnik, Physik
der Technischen Universität Carolo-Wilhelmina
zu Braunschweig

zur Erlangung des Grades eines
Doktors der Naturwissenschaften
(Dr.rer.nat.)
genehmigte
D i s s e r t a t i o n

von Alaa-Eldin Ahmed Abd-Elmageed Ahmed
aus Kairo, Ägypten

1. Referent: Priv. Doz. Dr. Stefan Kück
2. Referent: Prof. Dr. Andreas Hangleiter

eingereicht am: 18. Januar 2011
mündliche Prüfung (Disputation) am: 24. März 2011
Druckjahr: 2011

Dedication

to my

Parents,

Wife and Kids,

Brothers and Sisters

Acknowledgments

First of all, whole praise is to **ALLAH**, the lord of the world, the source of all knowledge, the knower of everything, and who pleased me to finish this work during the period from 2007 to 2011 at the Physikalisch-Technische Bundesanstalt (PTB), Germany.

I am heartily thankful to my supervisor **Prof. Dr. Stefan Kück**, head of the Optical Technologies Department at PTB, whose encouragement, supervision and support from the preliminary to the concluding level enabled me to develop an understanding of the subject.

I would like to express my deepest thanks to **Prof. Dr. Andreas Hangleiter**, head of the Institute of Applied Physics of the Technical University of Braunschweig, for his continuous supervision and assistance's during my thesis.

From the depth of my heart, I am greatly indebted to **Dr. Stefan Winter**, the head of Solar Cells Group at PTB, for his innovative and constructive ideas that led to this research topic. He follows my work almost day by day with his valuable comments, ideas, and guidance as well as for his encouragement, patience, and interest throughout the course of the study.

I would like also to express my deepest thanks to **Dr. Saulius Nevas**, head of the Source-Based Spectroradiometry Group at PTB, for his assistance whenever necessary and for sharing his scientific and experimental knowledge.

Sincerely thanks to **Dr. Armin Sperling**, head of the Photometry Group at PTB, for using Tunable Laser In Photometry (TULIP) setup in my facility, and **Dr. Peter Sperfeld**, Source-Based Spectroradiometry Group at PTB, for using the Blackbody system for intercomparison with my facility.

Special thanks to **Mr. Mario Taddeo** and **Mr. Dietrich Schlüssel**, Photometry Group at PTB, for their help in setting up the experiments.

I wish also to convey my gratitude to my colleagues at Photometry and Applied Radiometry Division for providing a good working atmosphere, and for sharing their scientific knowledge.

Great thanks to the Egyptian Culture Affair and Mission Sector under the Egyptian Government for supporting me financially during the study period, also great thanks for my institute in Egypt, the National Institute of Standards (NIS), for selecting me to take this scholarship.

Great thanks also to the International Graduate School of Metrology (IGSM) in Braunschweig for the useful metrological lectures during my thesis and continuous help and support.

Finally, I am deeply thankful and profoundly grateful to my parents, my wife, my daughter (Hoda), my son (Omar), my sisters and my brother for their love, care, pray, support, patience, and encouragement during the study period. Without them, I would have never the chance to achieve lots of things.

Vorveröffentlichungen der Dissertation

Teilergebnisse aus dieser Arbeit wurde mit Genehmigung der Fakultät für Elektrotechnik, Informationstechnik, Physik, vertreten durch den Mentor Priv. Doz. Dr. Stefan Kück, in folgenden Beiträgen vorab veröffentlicht:

1- S. Winter, A. Abd-Elmageed, S. Kück, P. Sperfeld, S. Nevas, A. Sperling, "Detector based traceability chain for spectral irradiance using tunable lasers, independent from blackbody radiators." Accepted paper in 27th International Commission on Illumination (CIE) conference, Sun City, South Africa, 10-15 July (2011).

2- A. Abd-Elmageed, S. Winter, S. Kück, P. Sperfeld, S. Nevas, A. Sperling, "Detector-based irradiance measurement using wavelength-tunable lasers." Accepted paper in 8th National Lighting Congress, Istanbul, Turkey, 14-17 April (2011).

3- A. Abd-Elmageed, S. Winter, S. Nevas, P. Sperfeld, S. Kück, A. Sperling, "Detector based traceability chain for spectral irradiance using tunable lasers, independent from blackbody radiators." Proceeding of BulLight 2010, the XIV National Conference with International Participation, Varna, Bulgaria, ISSN 1314-0787, 10-12 June (2010).

4- T. Keawprasert, K. Anhalt, R.D. Taubert, A. Abd-Elmageed, A. Sperling, J. Hartmann, "Monochromator based absolute calibration of radiation thermometers." Proceeding of TEMPMEKO&ISHM 2010, Portorož - Slovenia, 31 May-04 June (2010).

5- T. Keawprasert, K. Anhalt, R. Taubert, A. Abd-Elmageed, A. Sperling; J. Hartmann, “Absolute calibration of spectral responsivity for a radiation thermometer.” Proceedings of NEWRAD 2008, the 10th International Conference on New Developments and Applications in Optical Radiometry, Daejeon, South Korea, 12-15 October (2008).

6- S. Nevas, A. Sperling, S. Winter, A. Abd-Elmageed, P. Blattner, “Measurements of the spectral responsivity and f_1' values of photometers. ” Proceedings of the CIE Expert Symposium on Advances in Photometry and Colorimetry, (CIE X: 033), Turin, Italian, 07-08 July (2008).

TABLE OF CONTENTS

1 Introduction

The principle functions of the National Metrology Institutes (NMIs) are the maintenance of national primary standards and to transfer technical leadership and advice upon request to industry and other sectors for problems related to measurements and calibration of high precision measuring devices for scientific, medical, legal, industrial and technological laboratories. In Germany, the Physikalisch-Technische Bundesanstalt (PTB) is responsible for operating the national measurement system and for providing the national standards of measurement. Part of its work is concerned with the practical realization of the base units of the International System of Units (SI), and its derived units [1, 2].

Optical radiation measurement is one of the main areas of metrology developed and realized at NMIs and distributed by them to many users in the industrial, retail, engineering and scientific communities. Many applications require better accuracies than are currently available, and therefore there is a continuous need for the improvement of the primary scales realized by NMIs and for the development of methodologies to transfer those scales to customers [3-5].

1.1 The Aims of Optical Radiation Measurements

An enormous amount of electromagnetic energy with a wide spectral range occupies our surrounding environment (see Fig. 1.1). Therefore, for measuring and controlling this energy many requirements have to be taken into account. Optical radiation metrology covers both the measurement of light as a physical quantity (radiometry) and the effect of the light on a human (photometry) [6-8].

Radiometry is of fundamental importance in an extremely wide range of applications [5, 6]. Many of these applications require visible radiant

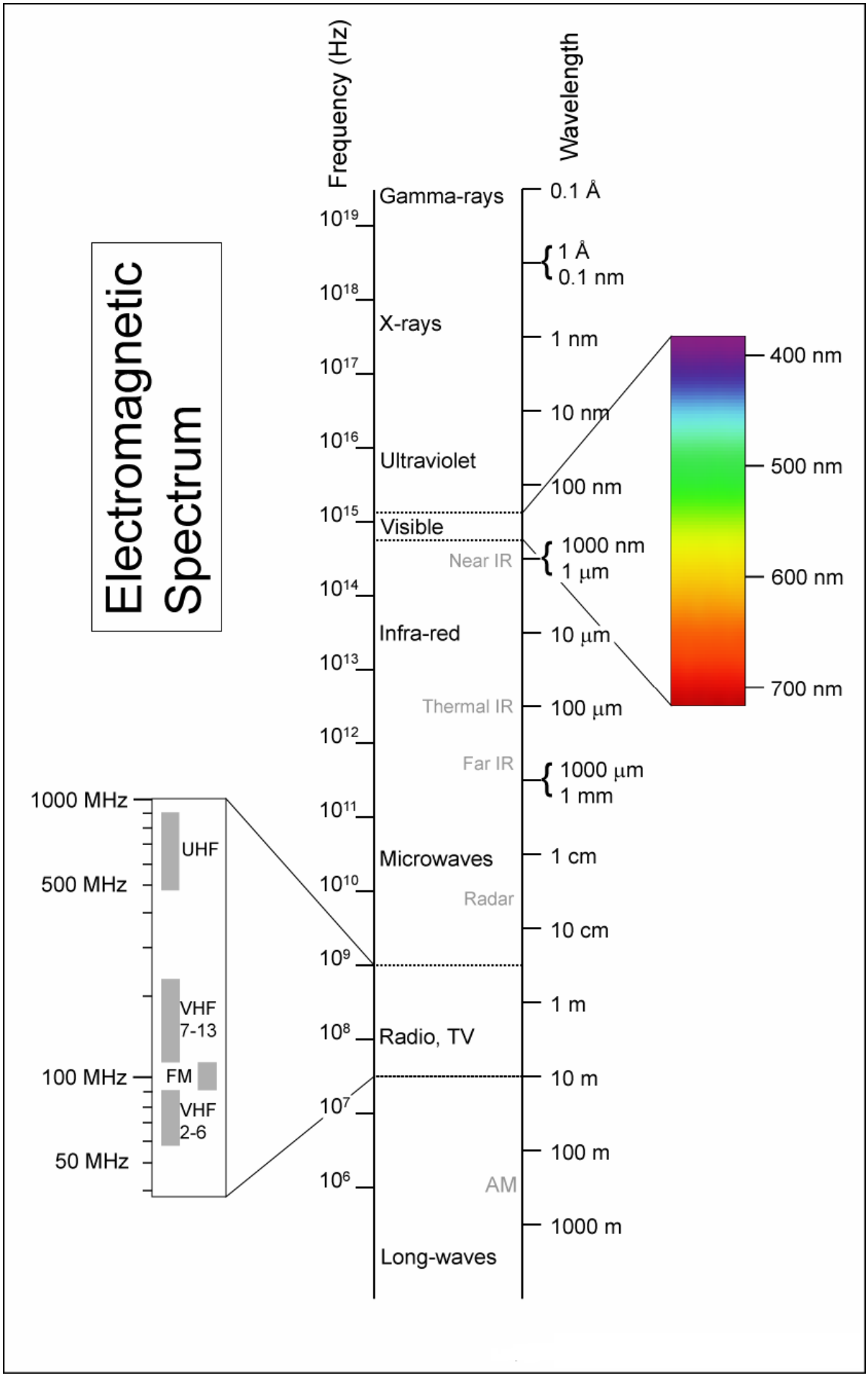

Fig. 1.1 Electromagnetiec spectrum [7].

energy and systems which produce the information that detected and observed by the human vision. Some examples of these applications are photometry, photography, television, visual information displays, applications of color science, and vision research. Moreover, scientific areas also have different applications inside radiometry. Some of these applications are in the areas of planetary astronomy, astrophysics, metrology and atmospheric physics, material science, photobiology, and photochemistry. Application in military defense areas prolongs the range of human vision over longer distances. It includes environmental conditions where unaided human vision is limited at night and weather effects. Night vision instruments use in the infrared region of the spectrum, where the radiant energy from objects at ambient temperatures reaches its maximum [5].

Table 1.1 Some applications of radiometry and the corresponding spectral regions of primary interest [5]**.**

Application	UV	VIS	IR
Astrophysics	*	*	*
Clinical medicine	*	*	*
Colorimetry		*	
Earth resources satellites		*	*
Illumination engineering		*	
Laser measurements	*	*	*
Materials science	*	*	*
Metrology and atmospheric physics		*	*
Military electro-optical sensor		*	*
Photobiology and photochemistry	*	*	*
Photographic systems	*	*	*
Photometry		*	
Radiation heat transfer			*
Solar energy		*	
Television systems		*	
Visual information display		*	
Vision research		*	

At present the invention and development of laser sources in all spectral regions from the ultraviolet (UV) to the visible (VIS) and infrared (IR) has led to a closer examination of the fundamentals of radiometry. Before that, the available sources of radiant energy were incoherent. The using of the laser with its high degree of spatial and temporal coherence has led to the development of new types of radiometric instrumentation as well as the expansion of related theoretical concepts. A brief summary of some of the application areas and spectral regions of primary interest is shown in Table 1.1 [5, 9, 10].

1.2 The Aims of this Research

The aim of this research is to setup and to characterize a completely detector based irradiance measurement ***independent*** from the primary standard sources, e.g. the high temperature blackbody radiator and the synchrotron radiation. Thus a SI traceability of the spectral irradiance is obtained without any use of intermediate calculable radiant sources [11-13] for the wavelength regions used within this thesis.

Unlike the other setups of a detector-based traceability chain as implemented at different NMIs [14, 15], the new setup utilizes tunable lasers (TUnable Laser In Photometry (TULIP) facility at PTB [16-19]). This laser-based facility provides an absolute-calibrated spatially-uniform irradiance field with high spectral resolution and high flux levels [20-23].

In this thesis, results of a spectral irradiance calibration of a broadband source, e.g. FEL lamp, will be described. The absolute irradiance responsivity of a continuously scannable spectroradiometer is derived from the spectral responsivity of a silicon trap detector [24-26], traceable to the primary cryogenic radiometer of PTB [27-35]. This spectroradiometer can subsequently be used to calibrate the spectral irradiance of photometric and radiometric sources.

With this new calibration chain, the two commonly used calibration steps to measure the blackbody temperature using calibrated filter-radiometers are replaced by the single calibration of the responsivity of the spectroradiometer against a trap detector (see Fig. 1.2). Due to fewer steps in the traceability chain, this can lead to a more convenient and accurate way of realizing the irradiance calibration of arbitrary sources with the potential to a significant reduction of the uncertainty compared to the traditional methods.

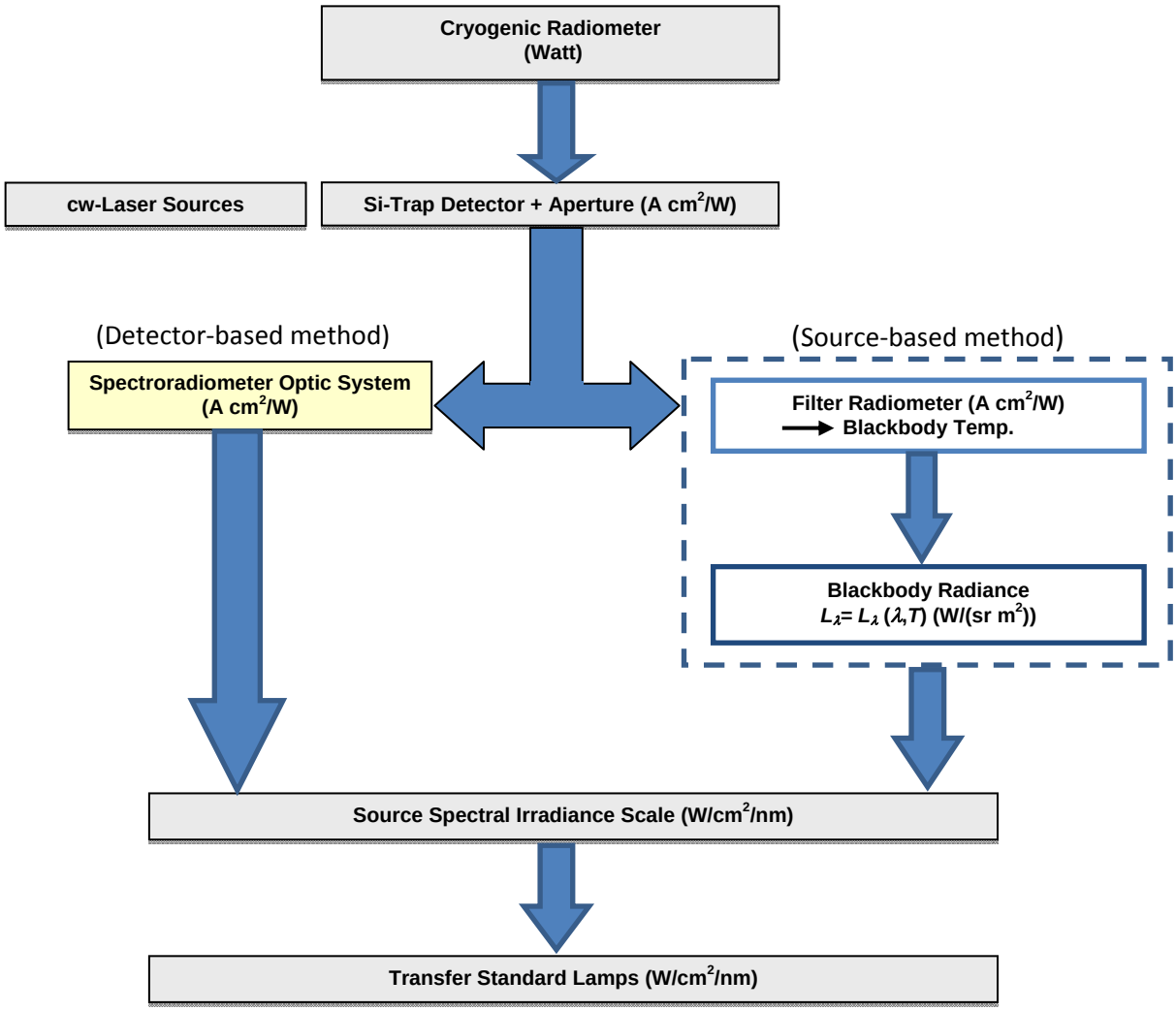

Fig. 1.2 New calibration chain leading to spectral irradiance scale. With the detector-based method the two commonly used calibration steps to measure the blackbody irradiance in source-based method are replaced by the single calibration of the responsivity of the spectroradiometer in detector-based method.

2 Theory and Background

2.1 Radiometric Terms and Concepts

2.1.1 Radiometry and Photometry

The propagation of energy by radiation from a source to a detector through the electromagnetic spectrum is described by radiometry and photometry. Radiometry deals with this problem in a purely physical way, in the form of power or energy and the geometry within which the propagation takes place. In photometry in principal the same problem is described, but the analysis is based on the visual effect on a standard human observer that this power would produce [8-10]. Radiometry and photometry deal necessarily with a source of radiation, a receiver, and the space between them. In photometry the receiver is the human eye or a detector approximating the human eye. The concept of photometry is considered more difficult, because of the "strange" quantities and units in this field of optics. Like the other physical detector of radiation, the human eye reacts to electromagnetic radiation only in a certain part of the spectrum, that is to a limited wavelength range of about 380-830 nm. The goal in photometry is thus to measure light in such a way that the results matched nearly as possible with the visual sensation that would be detected by a standard human observer exposed to the same radiation.

A photometric quantity X_v is related to the corresponding radiometric quantity $X_{e,\lambda}$ as described by Eq. (2.1),

$$X_v = K_m \int_{380}^{830} X_{e,\lambda} V(\lambda) d\lambda. \qquad (2.1)$$

The constant, $K_m = 683$ lm/W, relates the photometric quantities and radiometric quantities, and is called the maximum spectral luminous efficacy of radiation. $V(\lambda)$ is the relative spectral sensitivity of the average human eye [8].

2.1.2 Radiant Flux

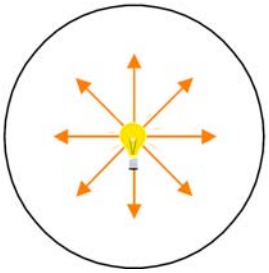

Fig. 2.1 Flux.

The optical flux, Φ, is the energy radiated by a source per unit time. If Q denotes energy, then,

$$\Phi = \frac{dQ}{dt}. \tag{2.2}$$

In radiometry this is the radiant flux and its unit is watt (1 W = 1 J /s). In photometry this is known as luminous flux, Φ_v, and is measured in lumen (lm) [8, 9].

2.1.3 Radiant Intensity

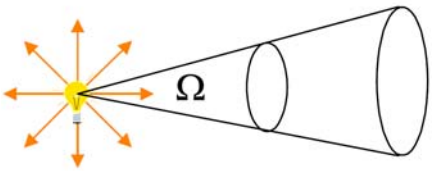

Fig. 2.2 Intensity.

The flux per unit steradian in a specified direction is called the radiant intensity, I, and radiant intensity is measured in W/sr, whereas luminous intensity, I_v, is measured in candela (cd). The intensity of a source is independent of the distance at which it is measured. However, a larger detector is required to measure the same solid angle at a larger distance. Intensity is defined by:

$$I = \frac{d\Phi}{d\Omega}. \tag{2.3}$$

The candela is one of the seven SI base units. The candela is defined as the luminous intensity, in a given direction, of a source that emits monochromatic radiation of frequency 540×10^{12} Hz and that has a radiant intensity in that direction of 1/683 W sr^{-1}. This definition links radiometric and photometric quantities [8, 9].

The frequency chosen is in the visible spectrum near green, corresponding to a wavelength of about 555 nanometers. The human eye is most sensitive to this frequency, when adapted for bright conditions. At other frequencies, more radiant intensity is required to achieve the same luminous intensity, according to the frequency response of the human eye [36, 37]. The luminous intensity is given by:

$$I_v = K_m \int_{380}^{830} I(\lambda)V(\lambda)d\lambda, \tag{2.4}$$

where I_v is the luminous intensity in candelas, $I(\lambda)$ is the radiant intensity in W/sr and $V(\lambda)$ is the relative spectral sensitivity of the average human eye (dimensionless). If more than one wavelength is present (as is usually the case), one must sum or integrate over the spectrum of wavelengths present to get the total luminous intensity as seen in Eq. (2.4).

2.1.4 Irradiance and Exitance

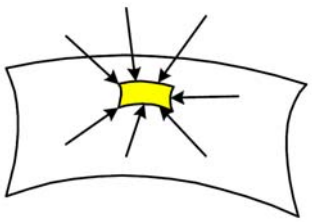

Fig. 2.3 Irradiance of a small area of a surface.

The radiometric concept of irradiance, E, and its photometric equivalent illuminance, E_v, deals with the measurement of the flux incident on a surface. Irradiance is the flux per unit area incident on a surface from the entire hemisphere above.

Irradiance is given as:

$$E = \frac{d\Phi}{dA}. \tag{2.5}$$

Its unit is W m^{-2}. Illuminance has the unit of lumens per square meter, or lux.

Exitance, *M*, is the formal term for flux emitted from an area of source surface into the hemisphere in front of it. Mathematically the relationship for an emitter the same as irradiance to a detector but exitance is a source quantity.

In addition, it is common to describe "the irradiance of a lamp". This means the irradiance at a surface due to the lamp at a defined distance from it, as shown in Fig. 2.4.

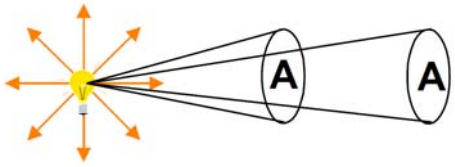

Fig. 2.4 Irradiance of a point source.

According to the inverse square law, the irradiance of a point source is inversely proportional to the square of the distance from that source because the same area receives less flux [8, 9].

2.1.5 Radiance

Radiance, *L*, is the light emitted by part of an extended source into a particular solid angle. It is the amount of flux emitted per unit projected area of surface into a unit solid angle in a given direction. Radiance has the unit of W m^{-2} sr^{-1} and its photometric equivalent, luminance, has units of cd m^{-2}.

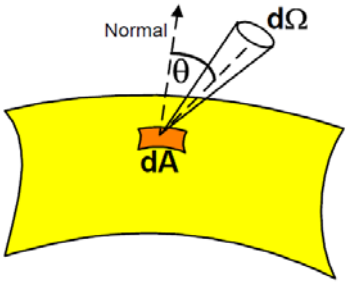

Fig. 2.5 Radiance of an extended source.

Radiance is defined by:

$$L = \frac{d^2\Phi}{d\Omega dA\cos\theta}. \tag{2.6}$$

Table 2.1 gives the basic radiometric and photometric quantities, their usual symbols and their metric definitions [8, 9].

Table 2.1 Basic radiometric and photometric quantities, their symbols and their metric definitions [8].

Radiometric Quantity	Symbol	Units		Units	Symbol	Photometric Quantity
Radiant Energy	Q	J		Lm s	Q_v	Luminous energy
Radiant Flux (power)	P , Φ	W		Lm	Φ_v	Luminous Flux
Irradiance and Exitance	E	W / m^2		lm/m^2	E_v	Illuminance
Radiance	L	W/(m^2 sr)		lm/(m^{2}sr), (cd/m^2)	L_v	Luminance
Radiant Intensity	I	W / sr		lm/sr, (cd)	I_v	Luminous Intensity

J = joule, W = watt, lm = lumen, m = meter, sr = steradian, s = second, cd = candela

2.1.6 Lambertian Source

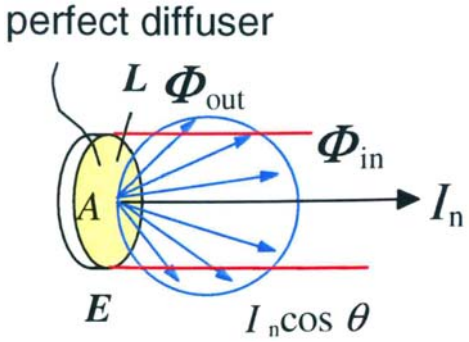

Fig. 2.6 Perfect diffuser as a Lambertian source [38].

The source that has the same radiance over its entire surface area and in all directions is known as a Lambertian source. Practically many diffusely reflecting surfaces act as approximations to a true Lambertian source. Integrating sphere sources and practical blackbody are designed to be near from Lambertian. For a Lambertian source there is a direct relationship between radiance and exitance [8, 9],

$$M = \pi L \tag{2.7}$$

2.2 Absolute Detector Radiometry

In the past two decades, the improvement of detector-based technology opened a new era in the field of optical radiation measurements [3]. From Albert C. Parr, the historical state of the art for developing absolute detector radiometry has been described as follows in [40]: “The 1979 redefinition of the candela was a major driving force in radiometry and photometry that spurred the need for, and subsequent development of, improved optical radiation detectors in the visible wavelength region. While light sensors such as photomultiplier tubes and cadmium sulfide devices were well known, such technologies were not suitable as fundamental standards. Fortunately, at the time the redefinition was formulated, technology had progressed. Newer types of photodetectors allowed photometry and radiometry to become detector-based, rather than based on

traditional thermal source techniques." See also [4, 11-13], "By the 1970s, silicon photodiodes had become available with unprecedented stability. Advances in semiconductor technology provided a wealth of new types of solid-state photodetectors, both from silicon and other materials. Solid-state devices are particularly attractive as sensors since they can directly deliver an electrical signal, usually current, which can be proportional to the input optical signal over many orders of magnitude. Their internal impedance and other electronic characteristics allow for easy mating with modern solid-state electronics and thereby provide a high-quality and inexpensive sensor system for many applications of optical radiation measurement. At about the same time silicon devices were being perfected for use in radiometry, more advanced electrical-substitution radiometers were also developed." See also [39], "These included cryogenic devices operating near liquid-helium temperatures with a relative combined standard uncertainty of 0.01 % or better." See also [28-35], "Electrical Substitution Radiometers (ESRs) are constructed by devising an absorbing receiver that collects optical power and as a result undergoes a temperature rise. The optical power is determined by using electrical power to produce the same temperature rise or, in most practical implementations, to maintain a steady-state temperature as the optical power load varies. The equality of the electrical and optical power is implied because of their equivalent thermal effect on the system. Electrical substitution devices are often referred to as absolute detectors, because they determine the radiant flux incident upon them by direct reference to physical laws and do not depend upon another optical power-measuring device for their calibration. The presumption of the equivalence of electrical power and optical power heating of a system is verified by careful characterization of the radiometer. Similarly, in the case of silicon, the knowledge of the semiconductor physics is thought to be adequate for describing the internal quantum efficiency and hence the response of the device to optical radiation. The measurement of high power and pulsed lasers poses challenging technical

problems that have led to the development of specialized detectors, including electrically calibrated ones. The national laboratories check the veracity of their absolute optical power measuring instruments through a continual series of international intercomparisons and other activities designed to establish equivalence of techniques. While a device such as a silicon photodiode can be considered an absolute detector under specified conditions, the actual accomplishment of the task may require considerable expertise and careful attention to specified procedures. Checking the procedures and practices used in the realizations of absolute optical power measurement with a particular detector system is the main impetus for the intercomparisons carried out by the national laboratories. ” See also [41, 42].

Progress in radiometry is associated with progress in the development of detectors; an ideal detector used in radiometric measurement should have the following properties [9]:

1- Uniform response across its active area.
2- High signal-to-noise ratio.
3- Be linear.
4- Short time constant.
5- Spectral responsivity stable with time.
6- Independently known, and preferably flat, spectral response.

Due to their importance in modern radiometry and photometry, we will briefly review the use of silicon photodetectors and cryogenic radiometers from the ESRs, while leaving discussion of the many other detectors to the literature references cited in this thesis.

2.2.1 Silicon Photodiodes and Trap Detectors

The theory of silicon photodiodes and trap detectors was described in details by Albert C. Parr [40]. Here we adopt again "When photons are absorbed by silicon they create pairs of electrons and holes. When this occurs in the junction region of a silicon diode, an electrical current is generated which is proportional to the number of photons absorbed. The energy of the photon must exceed the band-gap energy of silicon, which is about 1.12 eV and which corresponds to light with wavelengths less than about 1200 nm. Silicon's band-gap allows it to be used as a photodetector from the near infrared into the soft x-ray region.

The responsivity of a silicon photodiode is its output electrical signal per unit of input optical power. The electrical signal is usually the photocurrent measured in amperes and the optical power is measured in watts; hence, responsivity is typically expressed in units of A/W. When this quantity is measured as a function of wavelength, it is referred to as the spectral responsivity of the detector. In most cases the silicon photodiode is coupled to a current-to-voltage amplifier that provides an output voltage that is easily measured with widely available high-quality voltmeters. Top quality silicon photodiodes have proven to be generally stable, uniform, and sensitive. In addition, Geist and Zalewski showed that in the visible and near IR wavelength regions the absolute response of certain silicon detectors could be determined by a procedure that they called "self-calibration". This procedure relies upon the fact that the internal quantum efficiency of silicon is very close to unity over the wavelength region of 500 nm to 950 nm and that the reflectance of the diodes can be accurately measured using ordinary optical techniques. The internal quantum efficiency is the ratio of the number of electron-hole pairs created per absorbed photon. By accounting for the reflected light that is not absorbed, the number of photons incident on the silicon detector can be determined by measuring the electrical current produced. This procedure can, with some care, provide absolute calibrations of silicon

detectors used to measure optical power, with a relative standard uncertainty of less than 0.05 %.

The reflectance of a silicon photodiode can change as its surface changes, because of additional oxidation, contamination, or even humidity changes in ordinary laboratory atmospheres. Nevertheless, Zalewski and Duda showed how these effects can be minimized by using multiple photodiodes in a "trap" configuration. In a trap configuration, a collimated beam of light reflects off from one photodiode onto another, and then another, until a sufficient number of photodiodes absorb substantially almost all of the light. A trap detector is so named, because almost none of the incident light escapes. Most importantly, small changes in the reflectance of an individual surface do not significantly affect the total absorption of the whole device." See also [39, 43], "The light flux not absorbed, Φ_{na}, is related to the reflectance as shown in Eq. (2.8):

$$\Phi_{na} = \Phi_{\circ}\rho^{n}, \tag{2.8}$$

where ρ is the reflectance, n is the number of reflections, and Φ_0 is the incident flux. Since ρ is typically about 0.2, Φ_{na} is a small fraction of the incident flux for $n \geq 3$. Typically, over 99.9 % of the light is absorbed and converted to electrical signal. Since the internal quantum efficiency is near unity for a substantial wavelength region, trap detectors can be used as absolute standards based upon their known physical properties. In many other cases the inherent stability of trap detectors leads to their use as transfer standards. These are first calibrated against another radiometer, typically a cryogenic radiometer (see sec. 2.2.3.1).

In many applications a quantity like irradiance or illuminance needs to be measured and hence a precision aperture is required to define the acceptance area of the detector system. In radiance or luminance measurements it is sometimes necessary to define the configuration factor of a system. This also requires a precision aperture in order to account properly for the flux transferred from one region to another". See also [44, 45].

2.2.2 Reflection and Transmission Trap Detectors

Trap detectors have many different configurations such as: reflection, transmission, wedge and tunnel trap detectors. Three-detector reflection trap and the six-detector transmission trap are the two common configurations (see Fig. 2.7 [9]). In the reflection trap detector, the incident radiation is reflected successively from the three detectors at 45^o, 45^o, 0^o, 45^o, 45^o until the residual radiation emerges from the trap back along the direction of incidence. In the transmission trap detector, the radiation is transmitted through the trap co-axially with the incident beam, after suffering six successive reflections at 45^o. Fig. 2.8 shows a comparison between the total reflectance or transmittance of the two trap detectors shown in comparison with a single detector at normal incidence (S1337 detectors assumed) [9]. The residual reflectance is < 1 %, above 400 nm. One important property of these two designs is that the trap is nearly polarization-independent, i.e. the spectral responsivity is independent of polarization of the incident radiation. This is true in the ideal case of perfectly collimated radiation incident exactly along the optical axis of a perfect trap in which the individual diodes have identical radiometric properties and are perfectly aligned. Polarization independence is an important property for traps as transfer radiometers since laser radiation is usually highly polarized. Practically, such traps have a small residual polarization sensitivity due to a deviation from these ideal conditions [46, 47], therefore the trap must be fabricated very carefully.

To overcome the interference effect, trap detectors are used without windows. Usually, they are calibrated in air, but calibration in vacuum is possible. Proved by measurements and calculations, the effect on responsivity of air versus vacuum operation is a few parts in 10^5 [9, 46, 47].

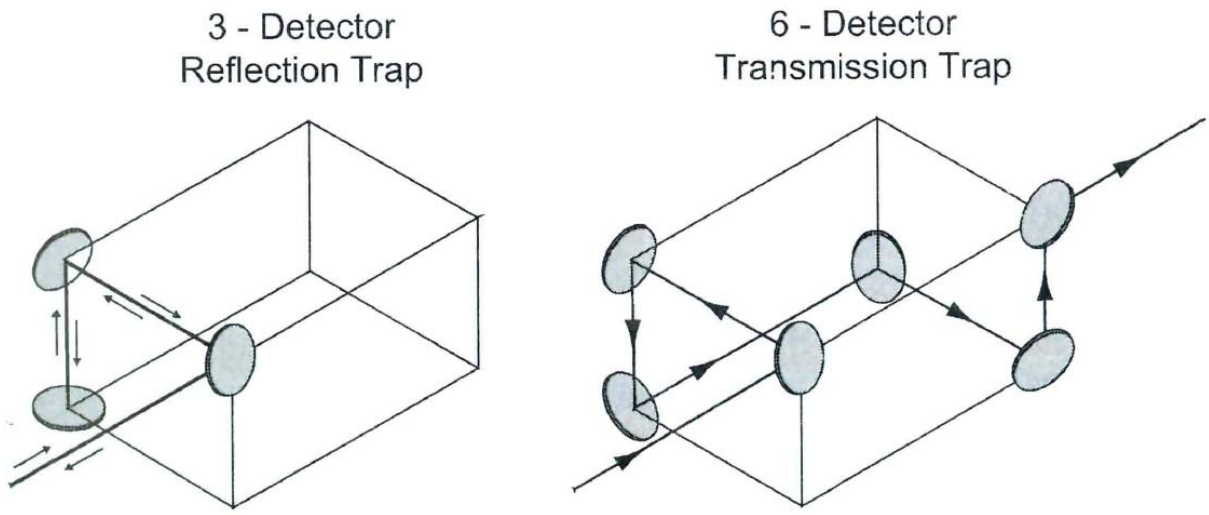

Fig. 2.7 Configuration of a 3-detetcor reflection trap and a 6-detetctor transmission trap [9].

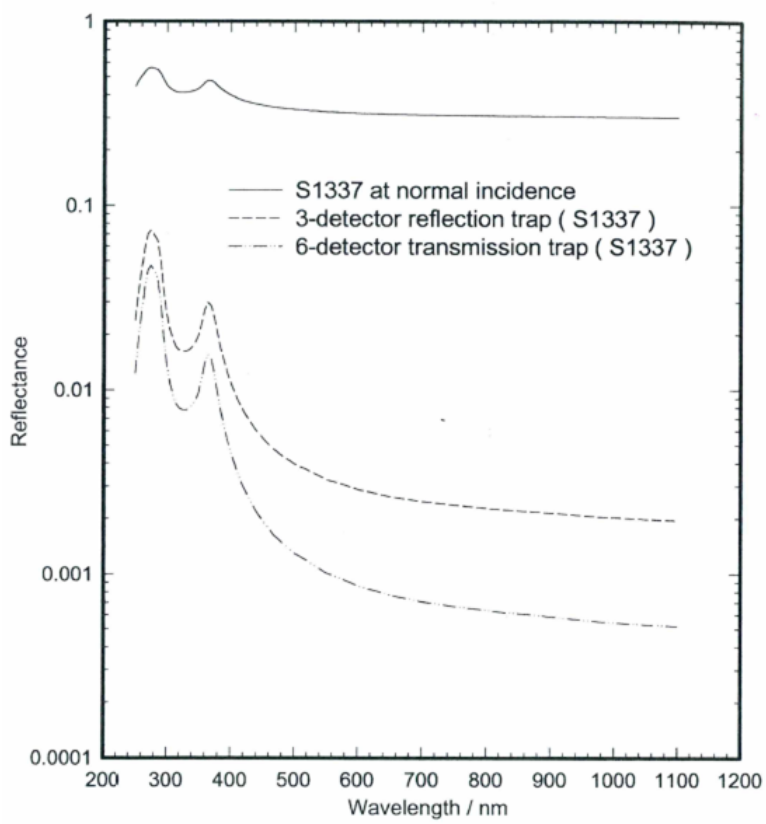

Fig. 2.8 Total reflectance of a 3-detector reflection trap and a 6-detetcor transmission trap [9].

2.2.3 Electrical Substitution Radiometers (ESRs)

Electrical Substitution Radiometers (ESRs) or Electrically Calibrated Radiometers (ECRs) are considered as absolute radiometers. ESRs are devices that measure radiation power equivalent to the same amount of electrical power. From Albert C. Parr in [36, 40], the basic idea of ESRs can be understood by reference to Fig. 2.9.

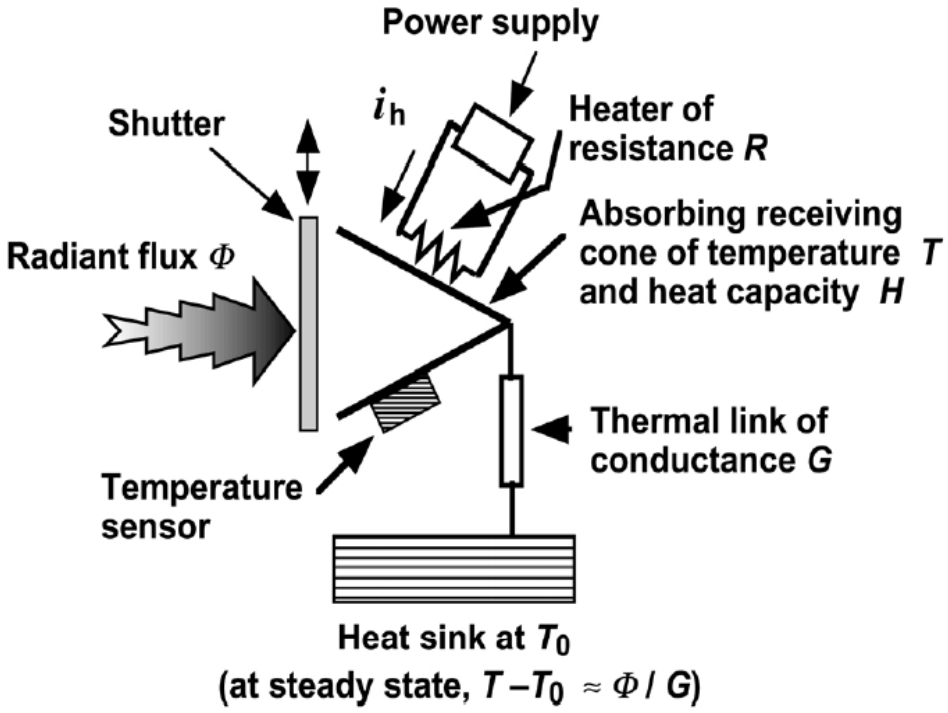

Fig. 2.9 Schematic diagram of the essential components of an electrical substitution radiometer [36].

The radiant power or flux Φ incident onto a cavity that is designed to accumulate radiation in nearly optimal way. The cavity (receiver) will suffer a temperature rise upon absorption of the power. The cavity is joined to a thermal conductor G to a constant temperature heat sink maintained at a reference temperature T_o. By ignoring losses caused by radiation, convection, and stray thermal conductance, the long-time equilibrium temperature rise is given by:

$$T - T_\circ = \Phi / G. \tag{2.9}$$

The equivalent amount of power provided by an electrical heater would have the same effect. Practically, by maintaining the receiving cavity at a constant temperature with the electrical heater, ESR performance could be improved. To create a specific temperature rise, power is supplied to the heater when a shutter is imposed to stop the light beam. A feedback loop decreases the electrical power when the shutter is opened. This feedback is involved to keep the same cavity temperature. By ignoring corrections and losses, the radiant power is given by:

$$\Phi = (i_{closed}^2 - i_{open}^2)R, \tag{2.10}$$

where i_{closed} is the current applied through the heater of resistance R when the shutter is closed and i_{open} is the current when the shutter is opened.

The main idea of ESR is used to calibrate optical detectors like bolometers and pyroelectric instruments. Usually these used for laser power and energy measurements. In order to apply appropriate corrections to the power equivalence relationship, ESRs must be carefully characterizing the various loss mechanisms.

Since 85 years or more ESRs have been in use. By Hengstberger, their history and development have been described in details [48]. By Coblentz at the National Bureau of Standards (NBS) during the early part of this century ESR technology was innovated [49]. Coblentz developed a number of radiometers and used them for several purposes in photometry and radiometry as well as a measurement of the Stefan-Boltzmann constant. During the 1970s and 1980s, the limited wavelength range with solid-state detector promotes the development of much-improved ESRs. A new significant design and construction of an ESR was innovated during this period that operated at cryogenic temperatures. This resulted in an increased responsivity with lower uncertainties due to convective and radiative losses.

2.2.3.1 Cryogenic Radiometer

Cryogenic radiometers provide an absolute basis for optical power (flux) measurements at the lowest possible uncertainties. They are used as primary standards for optical power at many national laboratories [28-34]. The cryogenic radiometer was designed to improve the accuracy and the spectral range of the primary standard for optical power. The cryogenic radiometer is an Electrical Substitution Radiometer (ESR) that operates at cryogenic temperatures by comparing the temperature rise caused by optical power absorbed in a cavity to the electrical power needed to cause the same temperature rise by ohmic resistive heating [50]. This links the measurement of optical power to the watt. Cryogenic radiometers use liquid helium as the cryogenic medium.

Several advantages are gained by operating at cryogenic temperatures (≈ 5 K) instead of room temperature. The heat capacity of copper is decreased by a factor of approximately 1000, thus allowing the use of a relatively large cavity, leading to a higher absorption, with a time constant up to ≈ 4 min. Moreover, the thermal radiation emitted by the cavity or absorbed from the surroundings is reduced by a factor of $\approx 10^7$, which rejects the radiative effects on the equilibrium temperature of the cavity. Finally, the cryogenic temperature allows the use of superconducting leads to the heater which removes the lead "self-heating" and thus improves the equivalence of the optical and the substituted electrical power. The relative combined standard uncertainty of the cryogenic radiometer measurements is 10^{-5} in the visible region of the spectrum [21, 27]. The largest components of the uncertainty are those due to the systematic correction for the Brewster angle window transmittance and the non-equivalence between electrical and optical heating. A schematic diagram of a cryogenic radiometer is shown in Fig. 2.10.

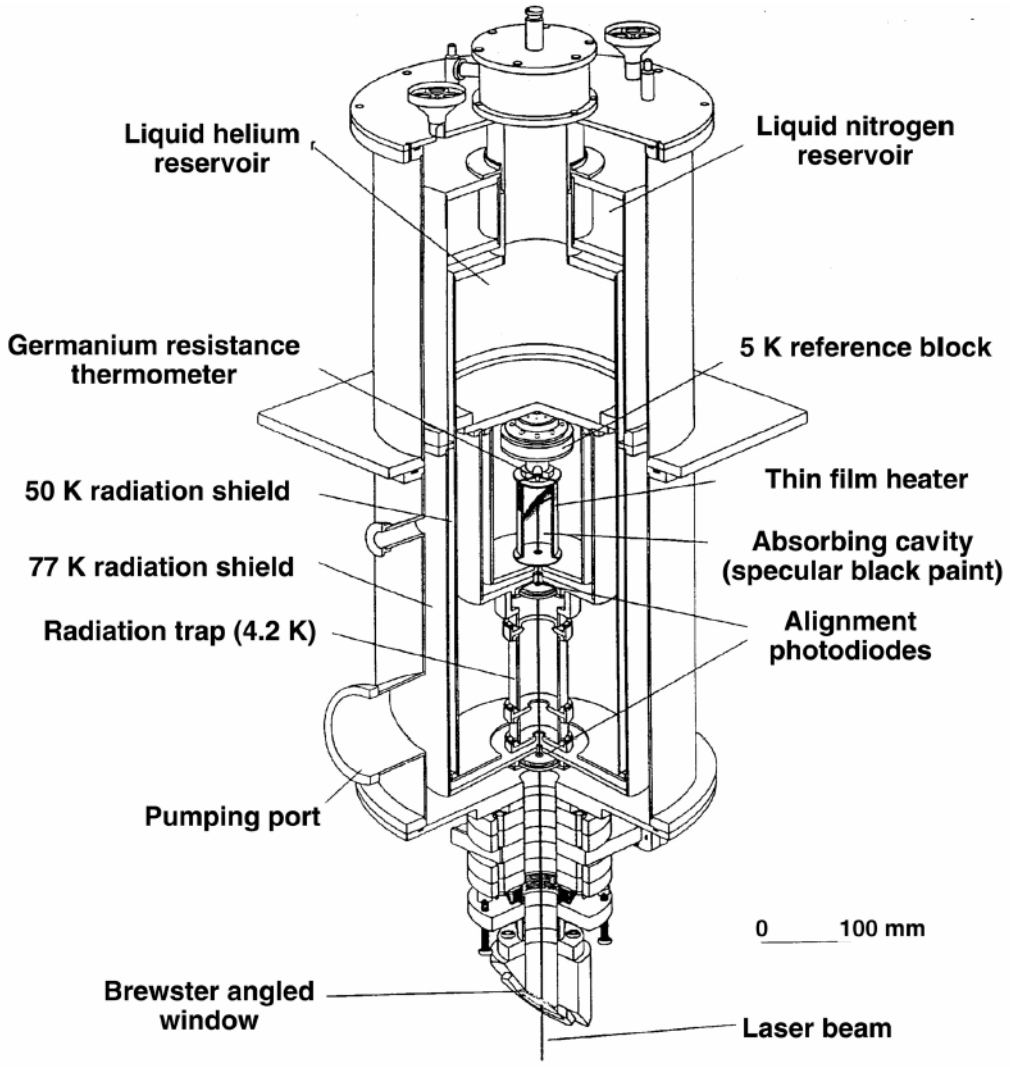

Fig. 2.10 Schematic drawing of a cryogenic radiometer [40]

2.3 Spectral Responsivity

One of the main goals of detector-based radiometry is to determine the absolute spectral responsivity of any photodetector in the form of the spectral responsivity of an absolute national standard. In many different radiometric, photometric and colorimetric applications, knowledge of the spectral responsivity function of photoelectric detectors is a fundamental requirement [21, 22, 26, 28, 51, 52]. Spectral responsivity, $s(\lambda)$, generally refers to the electrical signal generated by a photodetector, $I(\lambda)$, when irradiated with a known radiant flux of a specific wavelength, $\Phi(\lambda)$, and is determined using the relationship:

$$s(\lambda) = I(\lambda) \Big/ \Phi(\lambda). \tag{2.11}$$

The output signal of the detector can be in amperes, volts, counts/s, etc. The spectral responsivity of a photodetector can be either power or irradiance response. A power response generally requires under filling the detector with monochromatic flux, whereas an irradiance response has to uniformly overfilling the detector with monochromatic flux. It is possible to convert from power to irradiance response, if the area of the receiver (sensitive portion of the photodetector) is known and if the receiver is uniform in its responsivity.

Photodetectors are calibrated for spectral power responsivity in the ultraviolet, visible and near-infrared wavelength regions at different NMIs [21, 22, 26, 28, 51, 53]. These photodetectors deliver a photocurrent electric signal related to the radiant power incident on it. This relation defines the spectral responsivity to be determined.

Consider a beam of radiant energy incident on a photon detector. The spectral radiant power in the beam is Φ_λ. Since each photon has the energy $Q = h\nu$, the number of photons per unit time arriving at the detector is $\Phi_\lambda / h\nu$. Each of these photons produces an electron hole pair with quantum efficiency η. Thus the number of signal electron-hole pairs produced per unit time is $n = \eta\Phi_\lambda / h\nu$.
If each signal electron contributes to the output current, then the electronic current is nq, where q is the electronic charge. The current is then,

$$I_\lambda = (\eta q / h\nu)\Phi_\lambda. \tag{2.12}$$

So that, by the definition of the spectral responsivity,

$$s(\lambda) = I_\lambda / \Phi_\lambda = \eta q / h\nu. \tag{2.13}$$

Fig. 2.11.a shows an ideal case of the spectral responsivity curve for a typical photon detector. In the figure the responsivity of a photodiode is limited by the

cutoff wavelength, λ_g, established by the energy gap, E_g, of the semiconductor material, where $\lambda_g = hc / E_g$.

The slope for $\lambda < \lambda_g$ is a consequence of the wavelength dependence in Eq. (2.13), which can be rewritten as:

$$s(\lambda) = \eta q \lambda / hc, \text{where } \nu = c / \lambda. \tag{2.14}$$

The quantum efficiency of the photodiode in the ideal case is $\eta = 1$ (100 %). The resulted responsivity is then,

$$s_{ideal}(\lambda) = \frac{1}{1.24}\lambda \text{ [A/W]}, \tag{2.15}$$

where λ is given in μm.

This ideal case is only possible, if each photon with an energy greater than the semiconductor band gap will generate precisely one hole-electron pair. In the real case quantum efficiency of the photodiode is normally lower than 100 % where $\eta = s(\lambda) / s_{ideal}(\lambda)$ (see Fig. 2.12).

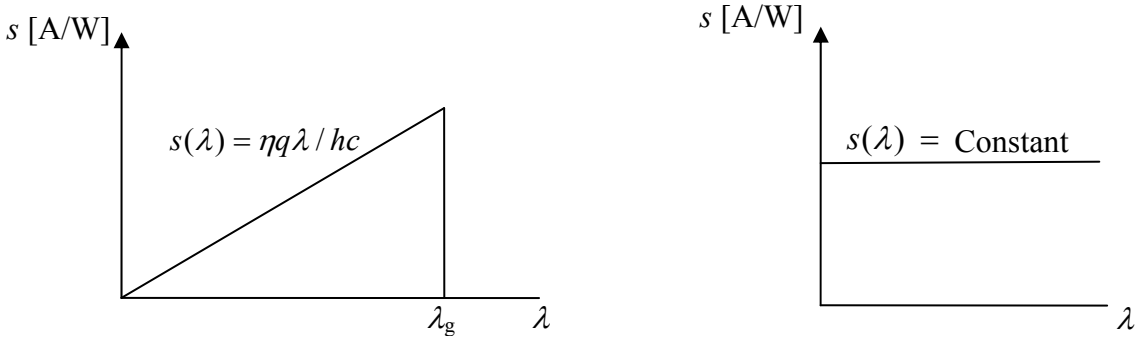

Fig. 2.11 Ideal spectral responsivity, s, versus wavelength, λ, for a photon detector (a) and for a thermal detector (b).

The responsivity of silicon detectors has maximum responsivity between 850 and 950 nm and is about 0.6 A/W at the maximum peak. Above 950 nm the responsivity decreases because the absorption coefficient becomes small. Therefore, the silicon thickness required is about 3.4 cm to absorb 99.9 % of λ = 1100 nm light, which is much longer than the thickness of the silicon substrate

wafers that normally used from 0.031 cm to 0.036 cm. At wavelengths above λ_g=1.1 μm, the rapid fall-off in responsivity wavelength of silicon is caused by increasing transparency of the silicon crystal at those wavelengths. Photons with energy less than energy gap, E_g, are not absorbed, i.e. pass through the crystal without being usefully detected.

The thermal detector responsivity, shown in Fig. 2.11b, is essentially spectrally flat (wavelength independent) since the detection mechanism depends only on total absorbed power or energy.

The responsivities of the working standard detectors below 1100 nm are derived by comparing their responsivities against those of silicon trap detectors calibrated relative to ESRs or cryogenic radiometers.

Fig. 2.12 shows typical responsivity curves of different types of photodiodes.

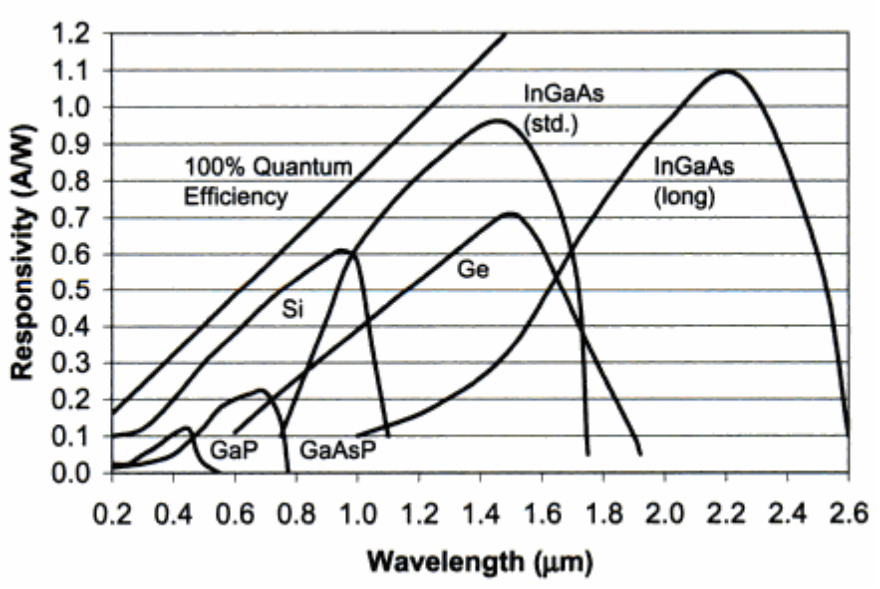

Fig. 2.12 Photodiodes of different semiconductor material show responsivity in different wavelength regions, limited at long wavelength by their energy gap. 100 % quantum efficiency means that one photon produces one hole-electron-pair [54].

2.4 Laser-Based Methods

Laser-based methods are used when the highest level of accuracy in measurement at NMIs are required [18, 20, 41, 42]. The main advantages of laser-based calibrations are [9]:

1- Very accurately known wavelengths.
2- Very small bandwidth, i.e. a high spectral purity.
3- High signal-to-noise level; this is particularly important when using absolute radiometers.
4- The laser radiation can be stabilized to a high degree using electro-optic or acousto-optic modulators.
5- Very low stray light level.
6- Good beam geometry-low beam divergence and easy alignment.

The use of tunable lasers in realizing the source scales leads to take the full advantage of detector-based calibrations at the highest level of accuracy, compared to traditional monochromator-based setups, and to avoid the use of traditional sources like blackbody radiator as transfer standards.

2.5 Blackbody Radiator and its Related Problems

A blackbody is defined as a body that will absorb all incident electromagnetic radiation at all wavelengths and from all directions [4, 11-13]. When a blackbody is in thermal equilibrium, it must also be a perfect emitter, emitting exactly what it absorbs. It is not possible for a source at a given temperature to emit more energy than a blackbody at that temperature. The radiance of a blackbody at a given temperature is given by Planck's equation,

$$L_\lambda = \frac{2hc^2}{\lambda^5 (e^{hc/\lambda kT} - 1)}, \tag{2.16}$$

where λ is the wavelength, h is Planck's constant, c is the speed of light, k is Boltzmann's constant and T is the thermodynamic temperature. Thus, when T is known, the radiance of a blackbody radiator can be calculated.

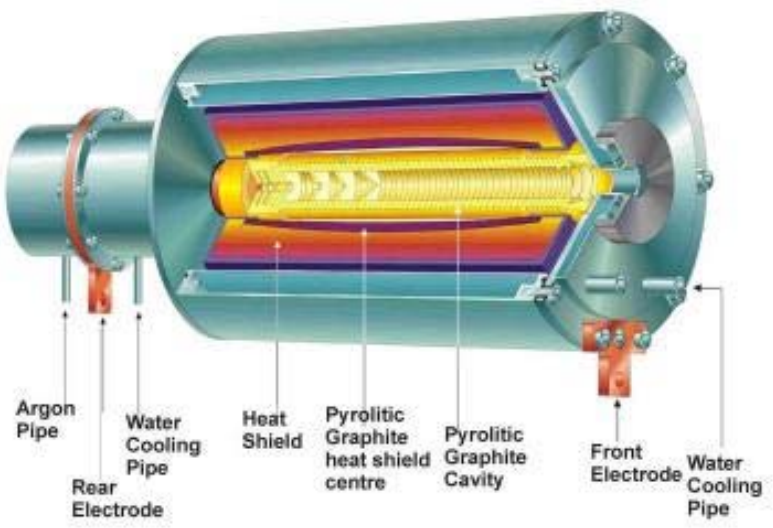

Fig. 2.13 Blackbody radiator [55]

Practically, absorption bands have been observed in e.g. carbon-cavity blackbodies at very high temperatures, which spectrally decrease the emissivity of the blackbody. From P. Sperfeld and others at PTB [12], these absorption bands are mainly caused by C_2, or some other carbon compounds such as CN or C_2N_2. Absorption bands have been observed around 210 nm, 360 nm, 385 nm, 420 nm, 470 nm, 510 nm and 590 nm. The strongest and the broadest absorption band appears around 385 nm. Fig. 2.14 gives an example of a blackbody spectrum with high absorption. Reasons of such absorption effects are very difficult to explain due to poor reproducibility and the unknown effect of a large number of factors such as argon flow, age of the cavity and graphite impurity. However, the use of high-temperature blackbody cavities as primary standard radiators is restricted because of the presence of these absorptions bands in the affected spectral ranges.

Extensive care must be taken into account to determine and to eliminate absorption lines and bands in the emitted spectra, when using high-temperature blackbody cavity as a primary radiometric standard. To identify absorptions, a small array-spectroradiometer can be used as well as several improvements can

be implemented to prevent absorptions. However, at temperatures above 3100 K absorptions cannot be avoided due to an increased sublimation rate of carbon (see Fig. 2.15). In the UV spectral range, the width of the emerging absorption bands may prohibit the use of high-temperature cavity radiators a primary radiometric standard [12].

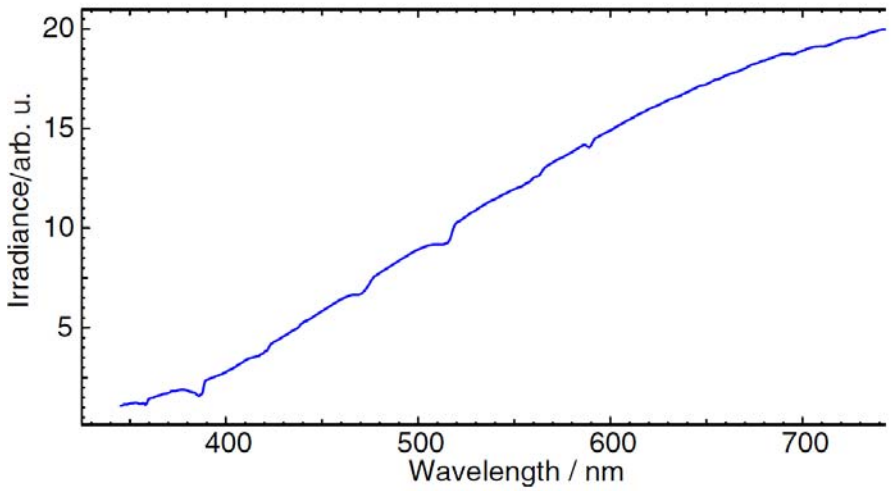

Fig. 2.14 Blackbody spectrum with evident absorptions [12]

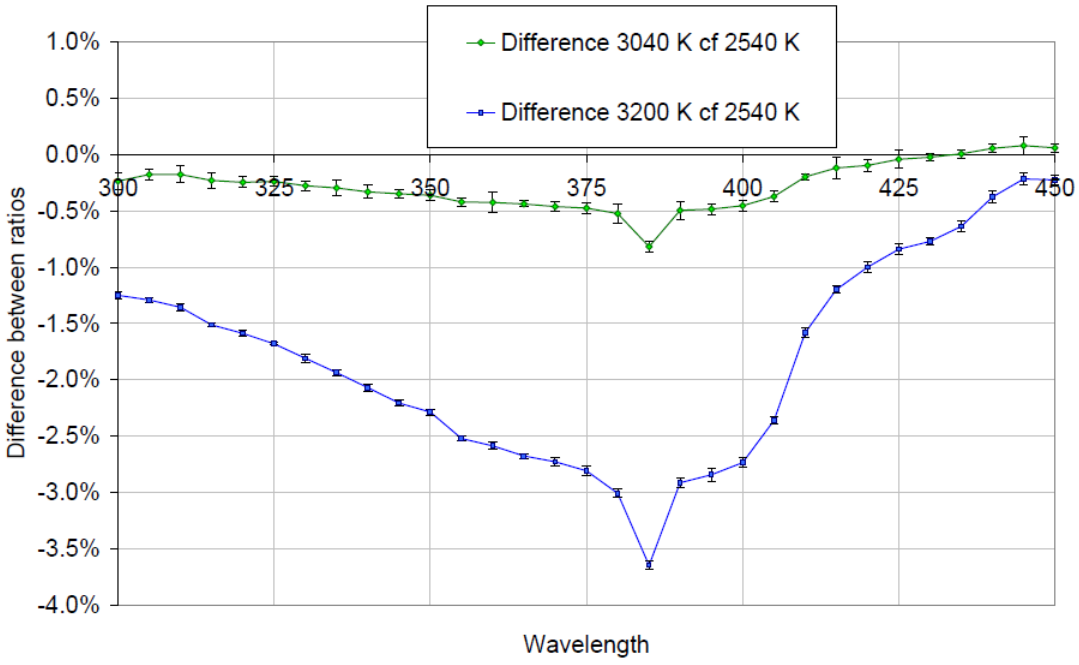

Fig. 2.15 Comparing the measurements of a blackbody operating at 3040 K and 3200 K with the operating at 2540 K [4]

2.6 Spectral Source Scale and Chain

The word “scale” in radiometry and photometry is used to describe a methodology by which a given quantity is measured over a defined spectral range [56]. For example, the current PTB spectral irradiance scale is how PTB measures absolute spectral irradiance from 250 nm to 2500 nm. At present, the realization of the spectral irradiance scale is traceable to the cryogenic radiometer, as shown in Fig. 2.16. The cryogenic radiometer is used to calibrate other detectors. These detectors form the top of the spectral responsivity scales chain. Usually the transfer standard calibrated directly against the cryogenic radiometer is the trap detector. Trap detectors are used to calibrate either filter radiometers or photometers. The photometers are used directly to realize the photometric scales. The filter radiometers are used to measure the temperature of the blackbody and this gives its spectral irradiance. In this way the source scale, based on the blackbody radiator, are connected to the most accurate detector scales. The scale must then be “transferred” to transfer standard lamps.

It is neither practical nor economic for the majority of customers that calibrations are made against the primary standard cryogenic radiometer. The spectral irradiance scale is transferred on a set of transfer standard lamps to the measurement service unit, and so the PTB scale seen by most customers is depend on these transfer standard lamps. However, for routine calibrations, these lamps are not used, as they would age very fast with continuous use. So “working standard” lamps are calibrated, which then calibrate customer lamps. With the same reasons, the customers will not use the lamps that they have measured at PTB for routine measurements. They will calibrate their own working standards against these lamps. This sequence forms part of the traceability chain [18, 58]. If each step in the traceability chain is attested, audited and has a full uncertainty budget, then any measurement in the chain can be considered to be “traceable to primary standards” of a particular NMI, and through the Mutual Recognition Arrangement to SI [4, 57].

Accuracy and uncertainty for the end user can be improved by identifying the part of the calibration chain, which introduces the largest step in uncertainty. In this case, the uncertainty of the FEL-lamp transfer standard is rather large. Thus, part of the calibration chain could be improved.

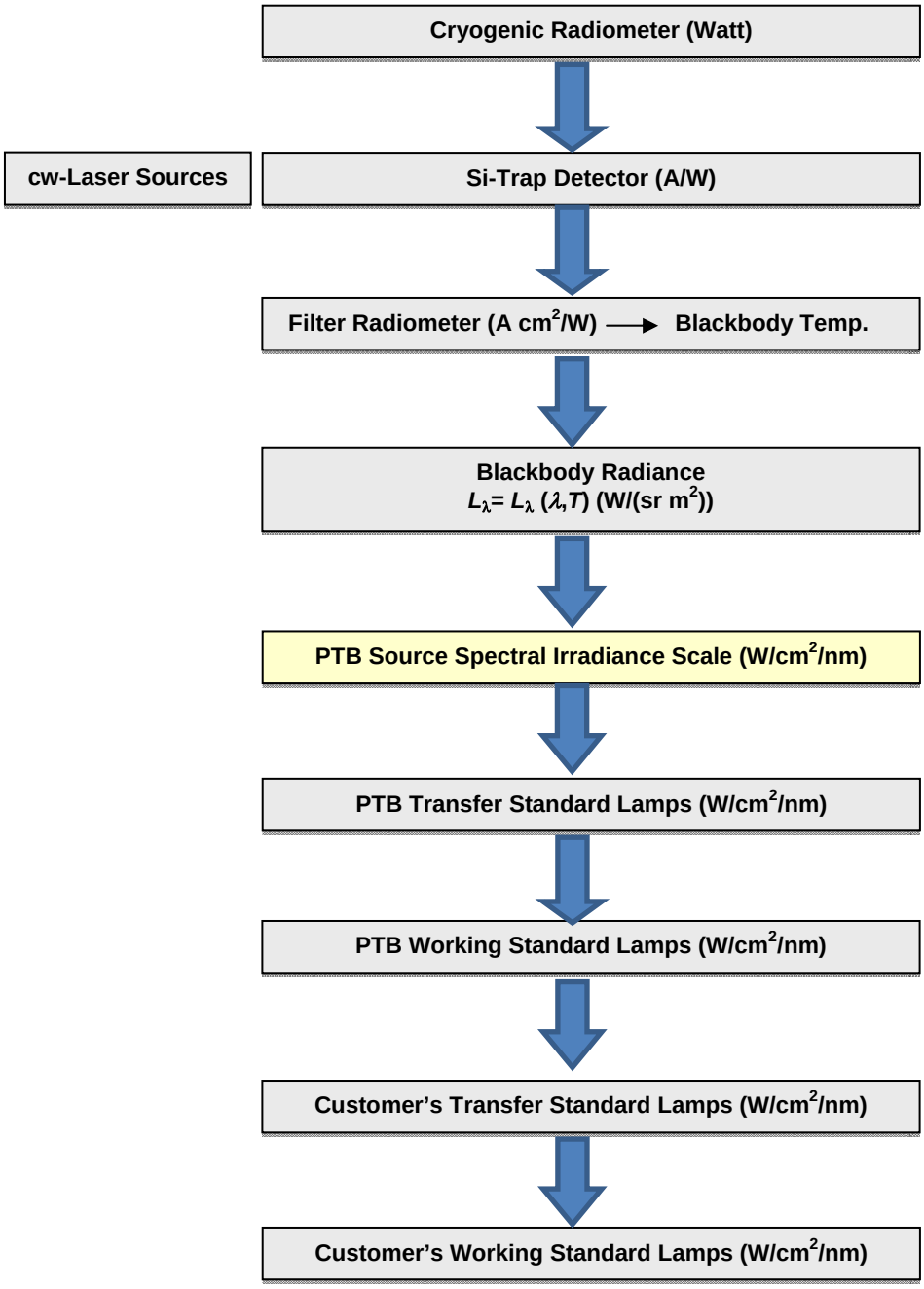

Fig. 2.16 Current calibration chain for spectral irradiance at PTB

3 The Detector-Based Spectral Irradiance Facility

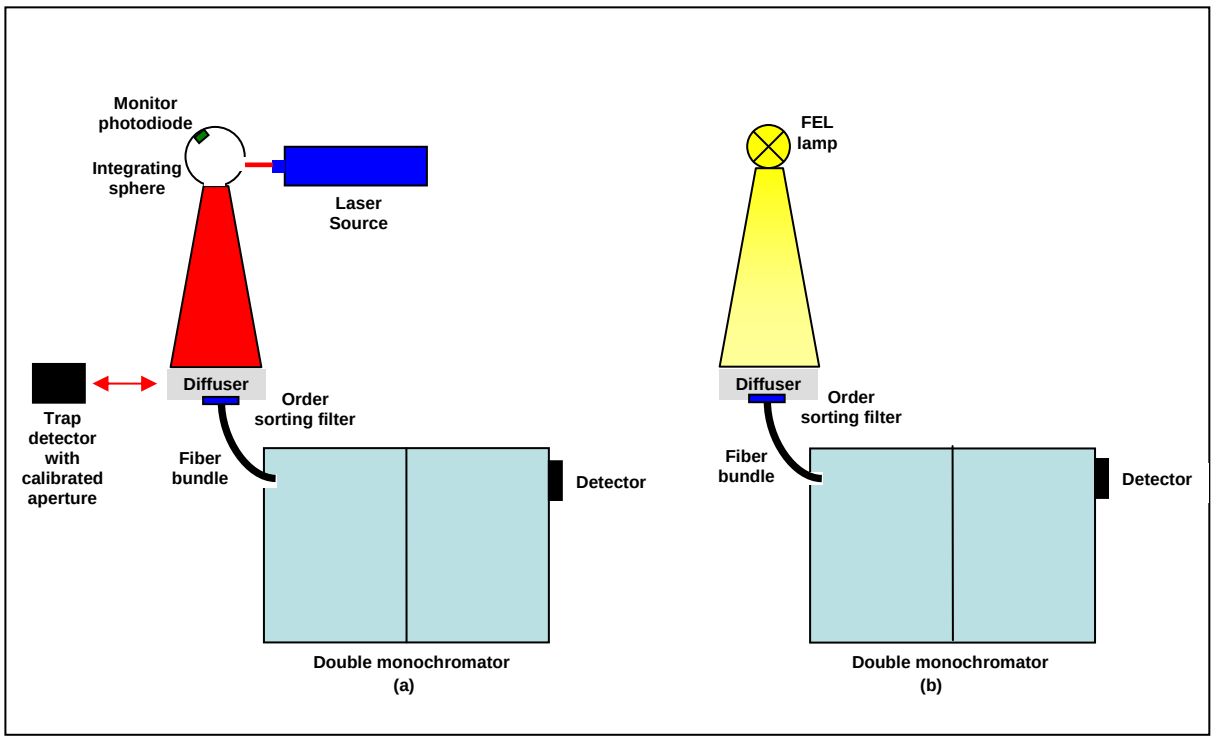

Fig. 3.1 Schematic diagram of the facility

3.1.a Irradiance responsivity of the spectroradiometer

3.1.b Irradiance measurement of FEL lamp with the calibrated spectroradiometer

The completely detector-based spectral irradiance facility is the facility used to disseminate the spectral irradiance of radiometric sources, like e.g. FEL lamps. Within the frame of this work, the spectral range is limited to 565 nm to 970 nm due to the availability of appropriate laser sources.

The facility, shown schematically in Fig. 3.1, is based on a calibrated silicon trap detector, traceable to the primary cryogenic radiometer of PTB, in combination with a well calibrated aperture. Moreover, a spectroradiometer with appropriate input optics (a double monochromator with a silicon detector and fiber bundle-based input optics) is used as a wavelength tunable-filter radiometer. This chapter describes the different parts of this facility.

3.1 Lasers

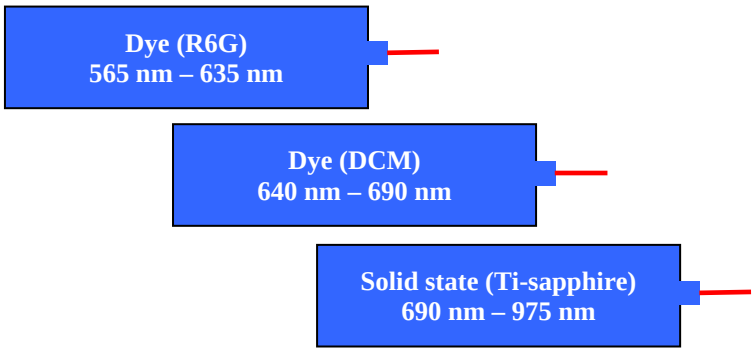

Fig. 3.2 Laser types used in the facility

A number of different continuous wave (cw) lasers are used from the TUnable Laser In Photometry (TULIP) facility at PTB to cover the spectral range from 565 nm to 970 nm [16-19]. The use of tunable lasers gives high-power, tunable and cw light in the visible range. Continuous tunability is provided by a Rhodamine 6G dye laser (565 nm – 635 nm), a DCM dye laser (640 nm – 680 nm) and a Ti:sapphire solid state laser (690 nm – 970 nm) (see Fig. 3.2), which are all pumped by a frequency-doubled Nd:vanadate laser (10 W at 532 nm). The use of tunable lasers leads to a higher signal-to-noise ratio and spectral resolution compared to traditional monochromator-based setups [15, 23, 41, 42]. With the help of the TULIP laser-based setup we can reach very accurately known wavelengths, very small bandwidth, i.e. a high spectral purity, a high signal-to-noise level, as the laser radiation can be stabilized to a high degree, a very low stray light level, good beam geometry and low beam divergence.

3.2 Integrating Spheres

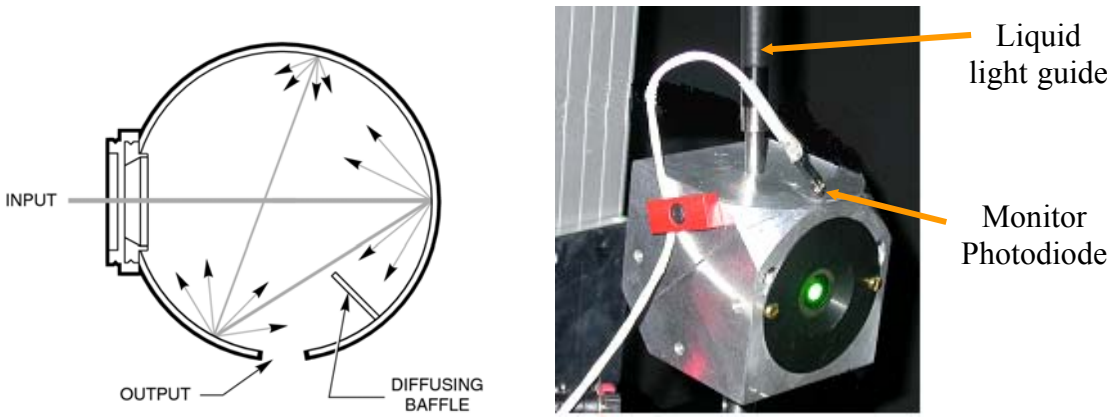

Fig. 3.3 Facility integrating sphere, left figure from [65]

An integrating sphere is a spherical shell that is coated internally with a highly reflecting material, whose reflectance is approximately the same at all positions (spatially uniform) and directions (uniformly diffuse). Depending on the application, it has a specific numbers of ports. Light enters through one port and is diffusely scattered multiple times before leaving through the exit port (see Fig. 3.3). This gives a uniform, nearly Lambertian source, regardless of the spatial properties of the input beam with radiance homogeneity up to 99.8 % [59-64].
Integrating spheres are commonly used in radiometry and photometry [63]. Small integrating spheres of 30-100 mm in diameter are used at the input of monochromators and detectors. Medium sized spheres, around 300 - 500 mm in diameter, serve as large area uniform radiance sources; and large spheres, around 1-5 m in diameter, are used in photometry to measure the total flux of a lamp [4, 62]. A really uniform output requires a sphere where the port sizes are far smaller than the sphere. This requirement must, however, be compromised because with a large input port more light is available and with a small sphere, more light is transmitted.

The transmittance, τ, of a sphere is given by the following equation [62, 65]

$$\tau = \frac{\Phi_e}{\Phi_i} = \frac{\rho A_e / A_s}{(1 - \rho(1 - A_p / A_s))}, \tag{3.1}$$

where:

Φ_e = Total flux exiting port

Φ_i = Total incident flux

A_e = Area of exit port

A_s = Surface area of sphere

A_p = Sum of all port areas

ρ = sphere wall reflectance

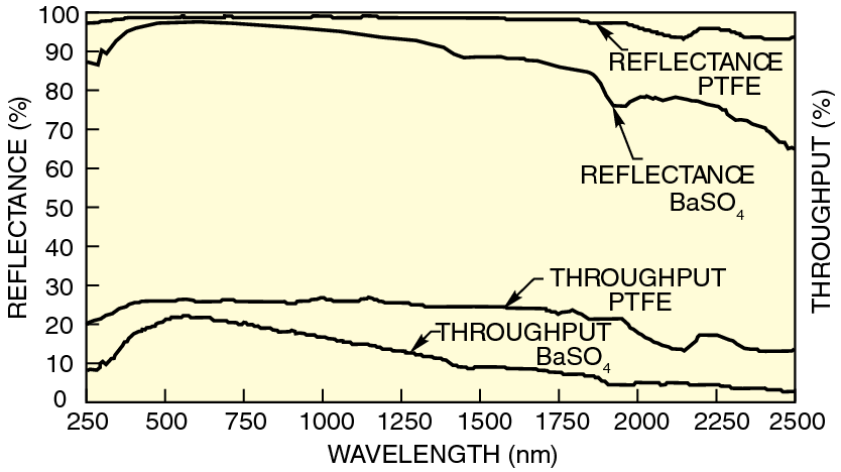

Fig. 3.4 Reflectance and throughput of 4 inch PTFE and $BaSO_4$ Spheres [65].

It is clearly important to get a reflectance as close to 1 as possible. Integrating spheres are coated with a barium sulphate ($BaSO_4$) or a polytrafluorethylene (PTFE). By using PTFE, better reflectance is achieved with comparison to $BaSO_4$, especially in the spectral ranges below 275 nm and above 1100 nm (see Fig. 3.4). However, a weak fluorescence has been observed from PTFE coatings [64]. The fluorescent excitation occurs at wavelengths below 290 nm, and the fluorescent emission is primarily between 310 nm and 350 nm. Therefore when the unknown source and the standard have greatly different irradiances in the

UV, a significant error may result in the 310 nm to 350 nm region. In this case, the use of an integrating sphere that is coated with powdered $BaSO_4$ is preferred rather than with PTFE.

The integrating sphere in our facility is typically 80 mm in inner diameter, coated with barium sulphate, with a 20 mm input port and a 20 mm exit port that matches with a fiber-optic probe. This integrating sphere is self-made inside PTB.

3.3 Monitor Detectors

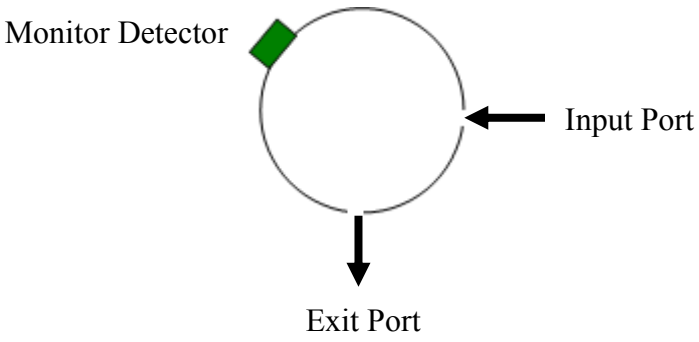

Fig. 3.5 Monitor detector mounted at an exit port of the integrating sphere

To stabilize the radiant power of the source, a third port is added to the integrating sphere, at right angles to the other two ports, onto which is mounted a monitor photodiode (see Fig. 3.5). This monitor correct for any small changes that occur during a calibration caused by fluctuations in the laser power input into the integrating spheres. To avoid interference fringes in the monitor signal the window of the detector is removed [63].

The monitor detector used on the facility is a silicon detector from Hamamatsu [66].

3.4 Transmission Diffusers

Fig. 3.6 Quartz glass diffuser [67]

Transmission diffusers are used as entrance optics for various detectors in order to achieve good cosine response and uniform light distribution in terms of incidence angle [68-72]. A diffuser (see Fig. 3.6) is a device that diffuses, spreads out or scatters light in to give uniform light distribution. When illuminating an ideal diffuser with a homogeneous plane wave, its rear surface radiates the light as the cosine distribution of the incident angle of its front surface. In practical diffuser devices, light is then coupled either into an optical fiber (spectroradiometers) or a filtered radiometer (broadband UV meters and luxmeters). Mostly, diffusers have been designed to be installed onto an optical fiber bundle.

Different methods are used in optical diffusers to diffuse light and can include opal glass, holographic, ground glass, teflon, and grayed glass diffusers. A transmitting diffuser is commonly a thin sheet of polytetraflouroethyline (Teflon) or a quartz or glass plate with its surfaces roughened or a stack of such plates [9].

The diffusers used on the facility are OM-100 diffusers from (Heraeus) with thicknesses of 2 mm used in the 565 nm – 630 nm and 690 nm - 790 nm wavelength range and of 1 mm used in the 640 nm - 680 nm wavelength range, respectively. These diffusers are a transparent quartz glass plates with very good transmission and opaque plates with high reflectivity [73].

3.5 Fiber-optic probes

Fiber-optic probes are optical fibers used to carry light to/or from areas which are difficult to reach, e.g. monochromators or integrating spheres. They are particularly useful, when the positioning or the aligning of the measuring device with respect to the source is difficult. A probe can be used without additional input optics, in combination with entrance optics such as an integrating sphere (for spectral irradiance or spectral radiant intensity measurements), or for the direct coupling of the input optics to the monochromator [74].

3.5.1 Fiber Bundles-Circular to Rectangular

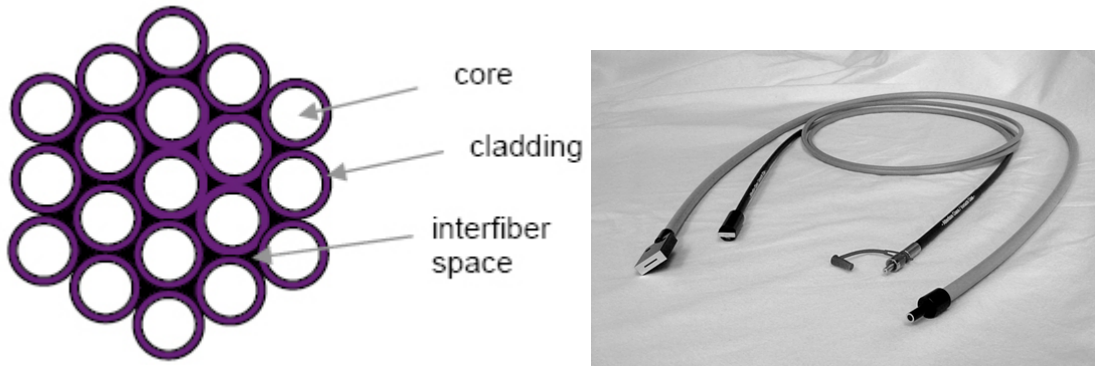

Fig. 3.7 Fiber bundles-circular to rectangular [75]

Light guides or fiber bundles are made from glass or silica fibers within diameters around 50 µm – 100 µm. These thin fibers are very flexible and allow large diameter fiber bundles to be fabricated with much smaller bend radii than possible with single fibers of similar diameter. For simple light transmission and more throughputs in the visible region, lower cost glass or polymer fibers can be used. Protective jackets in plastic or stainless steel can be fitted.

With monochromators and spectrographs, circular to rectangular fiber bundles are mainly used. The rectangular end can replace the input and output slit of a monochromator or spectrograph (see Fig. 3.7) [74, 75].

The fiber used in our facility is a glass fiber bundle, circular to rectangular, from Roper Scientific company. Fiber length is 2 m with a rectangular end of 4 mm height and 3 mm width and its round end is approximately 3.9 mm in diameter. A single fiber is 105 micron in diameter [76].

3.6 Monochromator

Fig. 3.8 Double Monochromator [77]

A monochromator is an instrument that uses a dispersive element to separate white light into a spectrum and transmit only a small band of this spectrum. The dispersing elements with a high dispersion could be gratings or prism-gratings, but require the use of order sorting filters. The following section describes the specific design of the monochromator used on the facility.

3.6.1 Double Monochromators

A double monochromator consists of two single monochromators working in series but using a single drive mechanism and housing (See Fig. 3.9) [75]. Theoretically, double monochromators have four slits - an entrance and exit for each of the single monochromator components. Practically, the exit of one is the entrance of the other and hence only three slits are used, the entrance, middle and exit. The influence, and hence selection, of the middle slit largely depends on whether the double monochromator is additive or subtractive.

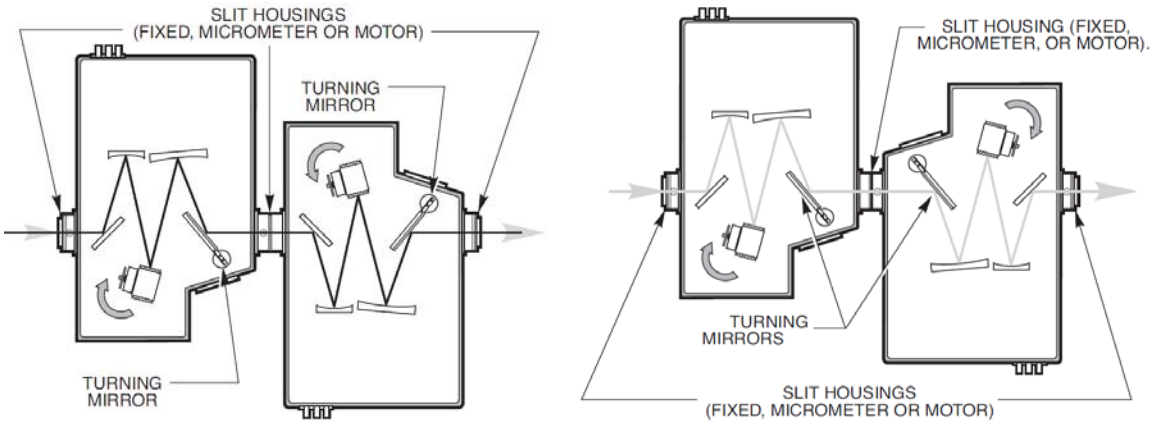

(a) **(b)**

Fig. 3.9 Schematic diagram for double monochromator in (a) subtractive and (b) additive configuration [75].

Additive means that light that is dispersed by the first monochromator is further dispersed by the second [8]. The dispersion is the wavelength range in nm in 1 mm distance in the plane of the slit. Thus, if a single monochromator has a dispersion of 2 nm/mm, then the same type and design of a double additive monochromator would have a dispersion of 1 nm/mm. Subtractive means the second component monochromator combines (the opposite of disperse in this context) any light dispersed by the first component monochromator. Subtractive monochromators have two main applications. The first is to perform extremely fast measurements, of the order of picoseconds. Here, the difference in path lengths through an additive monochromator might spread out a pulse because of the finite speed of light, but the symmetrical arrangement of a subtractive double monochromator provides a constant length for all paths. The second application, for measurements such as detector spectral response, is more common. In additive double monochromators, the small difference in wavelength between the left and right edges of the slit can cause serious errors if the detectors are not uniform. Subtractive double monochromators have no residual dispersion at the exit slit, thus eliminating this source of error.

However, in subtractive mode the coordination of the two monochromators is still important, and since there is no effective movement of the image at the exit slit. By Casimer DeCusatis in his book [8] it is prudent to:

i. have the exit slit slightly narrower than the entrance slit.
ii. have the entrance slit slightly narrower than the middle slit.

These two conditions are to achieve a good stability, which is necessary in spectroradiometry. They made also a compromise to get the narrowest bandpasses and triangular slit function. If a triangular slit function is required, equal entrance and middle slits should be chosen. If the narrowest bandpass is also required, then the entrance and middle slits should be equal to the exit slit, but the inherent instability of this arrangement may be occurred.

3.6.2 Monochromator Bandwidths and Slit Sizes

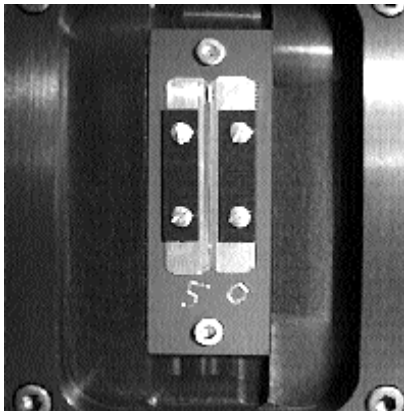

Fig. 3.10 Monochromator slit width [77]

Monochromator slits are rectangular and in general they are much taller than wide (see Fig. 3.10) [77]. Slits are positioned as the long side is perpendicular to the plane of the monochromator that is usually vertical). Selection of appropriate slits is critical in obtaining correct spectroradiometric results.

At the exit slit, the monochromator forms an image of the entrance slit when using a monochromatic source. Therefore the exit slit is considered as a mask, specifying the part of the image that reaches the detector. The slit function and hence the bandpass of the monochromator is determined by measuring the

output signal of the monochromator as a function of scanning wavelength under monochromatic irradiation [78, 79]. The slit function (bandpass) can be calculated simply for a monochromator. There are two different possible shapes present: if the entrance and exit slits are equal and the other if they are different. If the detector responds equally to all light passing through the exit slit then, as shown in Fig. 3.11, the signal is proportional the overlap area between the image of the entrance slit and the mask formed by the exit slit. This gives a triangular slit function for equal slits and a skewed normal distribution with a flattened top function for different slits [8].

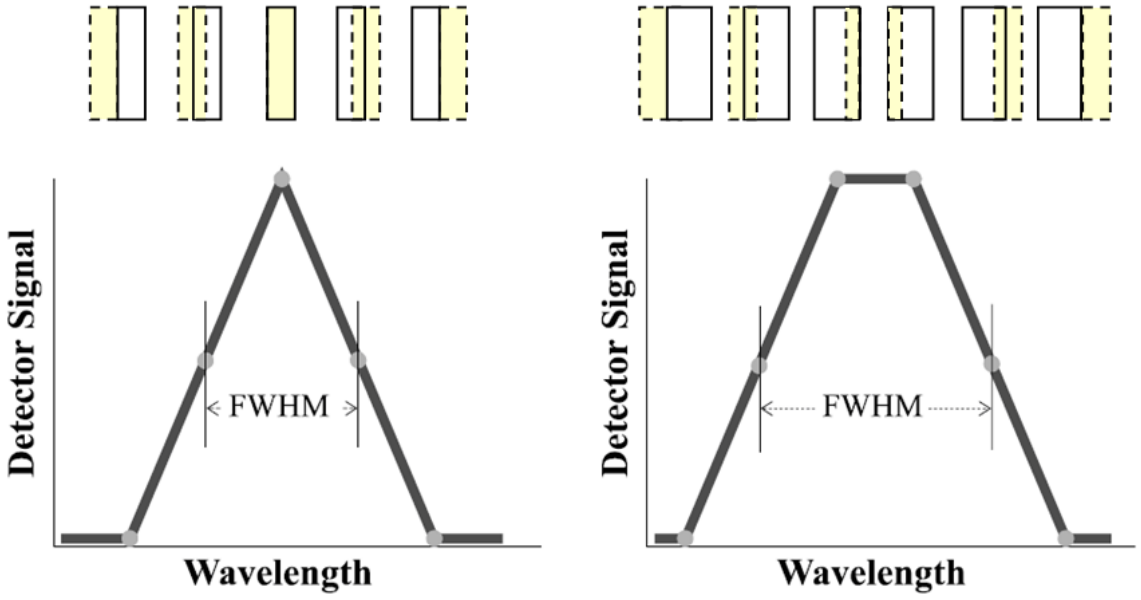

(a) **(b)**

Fig. 3.11 Slit function and bandpass for (a) equal slits and (b) different slits [8].

The maximum signal at any bandpass can be provided in the equal slits case. This gives accurate peak areas with most scan intervals less than the FWHM. Experimentally, the triangular function will have a rounded top and baseline intercept. Moreover, if the slits are very narrow, the function resembles a skew-Gaussian curve rather than a triangle. These are caused by normal aberrations present within any monochromator system and do not affect the general principles defined [4]. Detailed investigations of the slit function and its determination were reported in details on [11, 80].

3.6.3 Facility's Monochromator

The monochromator used in the facility, a SpectraPro-300i from Acton Research Company, has a subtractive mode double Czerny-Turner configuration, each part consisting of a grating and two focusing mirrors, the first mirror collimating the light from the entrance slit onto the grating and the second mirror refocusing this light onto the exit slit [77].

The gratings are reflectance gratings. In the spectral range below 690 nm, a 1200 lines/mm (blaze wavelength 500 nm) grating was used, above 690 nm a 600 line/mm (blaze wavelength 1000 nm) grating was used.

The heights of the monochromator slits are kept as large as possible to maximize throughput. The width of the slits determines the bandwidth of the monochromator. The slit widths for entrance, middle and exit are (1.5- 1.75- 1.25) mm, respectively, with the 1200 lines/mm grating, and (2.75 – 3- 2.5) mm with the 600 lines/mm grating, this corresponds to a bandwidth of around 8 nm. The slight difference between slits is to optimize the stability of the signal (see section 3.6.1).

3.7 Order Sorting Filters

Fig. 3.12 Order sorting filter [81]

The main disadvantage of gratings in comparison to prisms is that they reflect light of a particular wavelength into a number of orders [82]. This effect can be decreased by having the gratings blazed in order to increase the reflection into a specific order and a specific wavelength. However, unwanted light of higher

orders still needs to be removed. If white light is used in the monochromator, set to measure 1200 nm light, then, in addition to this light, there will be the second order of 600 nm light, the third order of 400 nm light and so on. To manage with this problem, order sorting filters (long pass filters) are put in front of the monochromator, behind the diffuser on the facility, so that when a certain wavelength is required, light of half that wavelength and below cannot enter the monochromator.

Two order sorting filters from Acton Research Cooperation company are used in the facility, 320 nm in the range (565 nm – 630 nm) and 590 nm in the range (640 nm – 975 nm) [77].

3.8 Monochromator's Detector

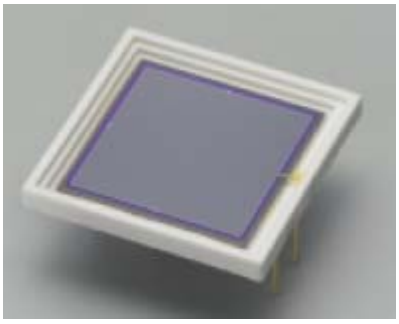

Fig. 3.13 S6337 silicon photodiode [66]

The choice of the detector, at the exit slit of the monochromator, is generally dictated by the light levels to be measured and the stability required. The silicon photodiode used in most medium-to-high light level applications, and the PMT is used at low light levels.

The detector used with the double monochromator is a large area silicon photodiode S6337 (18 mm × 18 mm) from Hamamatsu. The S6337 windowsless photodiode has excellent uniformity even at wavelength longer than 1000 nm, (0.3 % at 1100 nm) [66], that features excellent spatial response uniformity over a wide range from UV to IR. S6337 will prove useful for precision photometry and as a standard detector for spectral response calibration [83].

3.9 Reflection Trap detectors and its Aperture Area

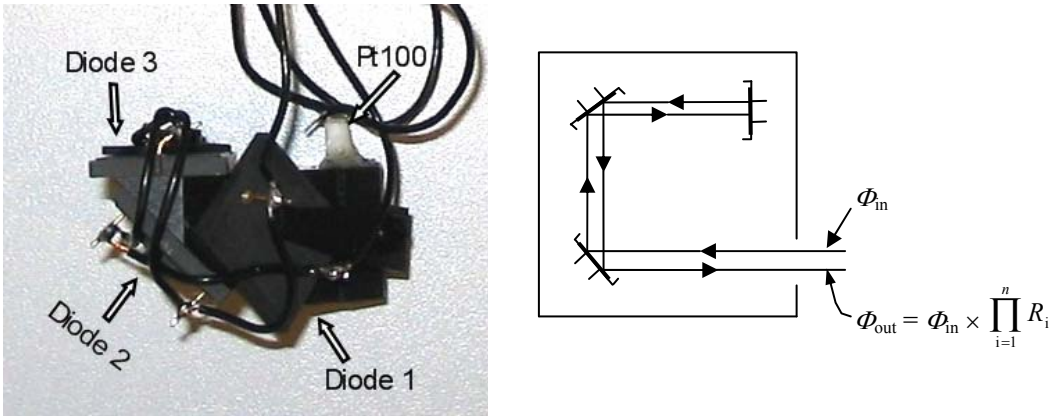

Fig. 3.14 Reflection trap detector [84]

The reflection trap detector used in the facility has three Hamamatsu S1337 PN photodiodes (10 mm × 10 mm). The three diodes are arranged in three dimensions so that light does five reflections (after reflecting onto the final detector it returns along its original path) The incident radiation is reflected successively from the three detectors at 45^o, 45^o, 0^o, 45^o, 45^o until the residual radiation emerges from the trap back along the direction of incidence. The layout of a trap detector is shown in Fig. 3.14. The advantage of this over the four-photodiode arrangement is that the plane of reflection is rotated by 90°, meaning that the polarization dependence is, in principle, removed.

The trap detector was equipped with a well defined aperture area, to determine the irradiance responsivity rather than the power responsivity. The measured area of the aperture is 20.431 mm^2 with a relative standard uncertainty of 0.073 %. The aperture area was measured and calibrated by the "Multisensor Metrology" group in PTB-Braunschweig by Multisensor Coordinate Metrology methods [1, 85].

Fig. 3.15 RTCR cryogenic radiometer

The trap detector was calibrated at the "Detector Radiometry" group in PTB-Berlin against a Cryogenic Radiometer for its power responsivity (see sec. 6.3.1). The cryogenic radiometer RTCR was manufactured by Oxford Instruments Ltd, and its design closely follows the National Physical Laboratory (NPL) cryogenic radiometer (see Fig. 3.15) [1, 27].

3.10 Amplifiers

The signal from a photodiode is a small current, typically picoampere to microampere. This current is converted to voltage in a current-to-voltage amplifier, a so-called transimpedance amplifier. The size of the feedback resistor determines the size of the amplification, e.g. a 1 MΩ resistor will cause an amplification of 10^{6} V/A. All detectors used in the facility, either the trap detector or the detector behind the monochromator as well as the monitor detector, are amplified by transimpedance amplifiers self-made by the working group “Photometry” at PTB. The size of the feedback resistor has 12 levels in the range from 0.1 MΩ to 30275 MΩ with nearly equal multiplying factor between the levels of approximately 3.2, leading to amplifications of 10^{5} V/A to approximately 3×10^{10} V/A. The relative standard uncertainty in the used amplifier levels is in the range from 0.005 % to 0.02 %.

3.11 Transfer Standards

Transfer standards are sources which are used to transfer the spectral radiance and irradiance scales and the photometric scales between different levels of the calibration chain.

3.11.1 FEL-Lamp

Fig. 3.16 FEL lamp

The most common lamp used as a spectral irradiance standard is the FEL tungsten halogen lamp, which has a double coiled filament [86-89]. FEL is the lamp type designation (not an acronym) of the American National Standards Institute (ANSI) [90]. FEL lamps made by different manufacturers can differ in, for example, the number of coils.

The lamp used in the facility is an Osram Sylvania 1000 W modified FEL type quartz halogen lamp potted on a bi-post base [91]. The lamp bulb is clear. This lamp is designed for operation at ~115 V / 8.1 A for a distribution temperature of ~ 3100 K. The lamp is covered by a blackened housing to lower the effect of stray light and to have a well defined constant reflection from the background (see Fig. 3.16). These lamps are mounted on a heat sink to improve thermal uniformity. They also have a plate on the front which is a well-defined surface for distance measurements and which acts as a baffle, screening the lower part of the lamp. The lamp also comes with a removable alignment jig for systematic alignment.

Fig. 3.17 SM 120-25D Power supply [92]

The lamp is operated with SM 120-25D DC power supply from Delta Elektronika Company [92]. Current mode regulation is used rather than voltage regulation because lamp voltage, in general, does not reproduce well due to the variation of sockets used among users. The lamp current is measured as the voltage across a standard resistor of 0.1 Ω, using a high accuracy digital voltmeter (Agilent 3458A). The lamp current was raised slowly to reach the specified value in about 30 sec. Turning the lamp on and off abruptly may cause the filament condition to change due to thermal shocks. After being turned on, the lamp is allowed to stabilize, typically for 20 min, while the lamp current is maintained at the specified value. The lamp current was monitored during the measurement [93, 94]. The stability of this lamp is lower than 0.1 %.

The lamp must be handled carefully to avoid mechanical shocks to the filament. Before measurement, the bulb of the lamp is cleaned with a soft cloth to remove dust accumulated from the packing material. The lamp bulb should not be touched with bare hands.

3.12 Light Tight Boxes

The entrance optics of the spectroradiometer together with the Si-trap as a reference detector are placed on the (x, y, z) translation stage, from ISEL company), of the TULIP setup.

In order to avoid stray light errors, all of the equipment are installed in a light tight box, where all the walls are covered with a very good absorbing material, POLYCON 100 black coating.

4 Model of the Evaluation of Source Irradiance Measurements

In the following section we develop the measurement equations needed for using a detector standard for source irradiance measurement. The basic approach will be classified into three steps:

1. The irradiance of a homogenized laser irradiation, from TULIP, will be determined from a standard trap detector irradiance responsivity.
2. The absolute spectral irradiance responsivity curve of the spectroradiometer will be determined for every wavelength setting from the standard trap detector using the irradiance determined in step (1).
3. The absolute spectral source irradiance of a FEL lamp will be calibrated directly with the calibrated spectroradiometer.

4.1 Irradiance of a Homogenized Laser Irradiation

The general equation for the standard detector output signal I^S in relation with its power responsivity is [62]:

$$I^S = \int s_S^*(\lambda)\Phi_\lambda(\lambda)d\lambda, \tag{4.1}$$

where $s_S^*(\lambda)$ is the known spectral power responsivity of the standard detector in A/W and $\Phi_\lambda(\lambda)$ is the spectral flux of the laser beam at the wavelength λ in W/nm. However, the quantity we want to measure is the spectral irradiance $E_\lambda(\lambda)$, instead of spectral flux, which is defined as:

$$E_\lambda(\lambda) = \frac{d\Phi_\lambda(\lambda)}{dA}, \tag{4.2}$$

where dA is the detector aperture area.

Using in Eq. (4.1) the spectral irradiance responsivity $s_s(\lambda)$ instead of the spectral power responsivity $s_S^*(\lambda)$, with, $s_s(\lambda) = s_S^*(\lambda)\Delta A$ and $\frac{\Phi_\lambda(\lambda)}{\Delta A} = \frac{d\Phi_\lambda(\lambda)}{dA}$, we obtain for the standard detector output signal:

$$I^S = \int s_S(\lambda) E_\lambda(\lambda) d\lambda. \tag{4.3}$$

Note, that I^S is given in Ampere, $s_s(\lambda)$ in A/(W/m^2) and $E_\lambda(\lambda)$ in W/(m^{2}nm).

The laser irradiation used in the experiments is nearly monochromatic, i.e. it consists only of a very narrow spectral line at the laser wavelength λ_L.

This narrow spectral line from the laser can be expressed by delta function $\delta(\lambda)$, when $\delta(\lambda) = \begin{cases} +\infty, \lambda = \lambda_L \\ 0, \quad \lambda \neq \lambda_L \end{cases}$, hence $\int \delta(\lambda) d\lambda = 1$.

Therefore the detector signal can be expressed by:

$$I^S = \int s_S(\lambda) E_{Laser,\lambda_L} \delta(\lambda) d\lambda = s_S(\lambda_L) E_{Laser,\lambda_L}, \tag{4.4}$$

$$\Rightarrow E_{Laser,\lambda_L} = \frac{I^S}{s_S(\lambda_L)}, \tag{4.5}$$

where E_{Laser,λ_L} is the laser irradiance for the spectral line at wavelength λ_L.

Note that $I^S = I_{Detector} - I_{Detector,Background}$.

4.2 Calibration of the Irradiance Responsivity of a Spectroradiometer

In the case of the calibration of a spectroradiometer, the incident irradiance field is transformed to an output signal through the spectral irradiance responsivity function $s(\lambda_M,\lambda_L)$, which amongst others depends on the spectroradiometer wavelength setting λ_M and on the laser wavelength λ_L (see Fig. 4.1).

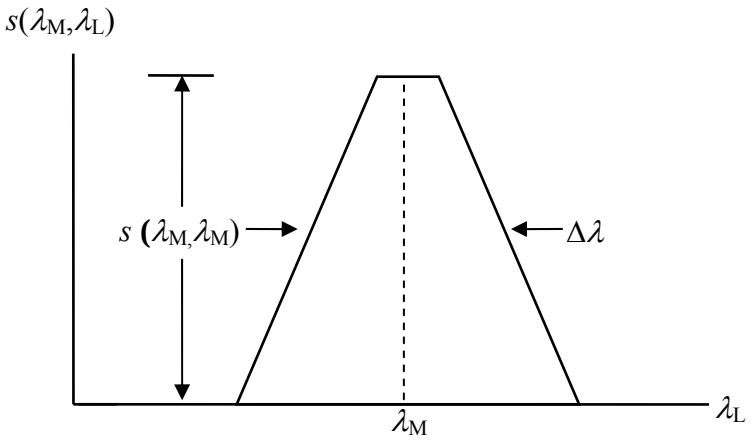

Fig. 4.1 Spectroradiometer responsivity function $s(\lambda_M,\lambda_L)$.

Thus, when the incident irradiance field irradiates the entrance optics of the spectroradiometer, the spectroradiometer output signal I^{M} at the monochromator wavelength setting (λ_{M}) is equal to:

$$I^{M}(\lambda_{M}) = \int s(\lambda_{M}, \lambda) E_{\lambda}(\lambda) d\lambda. \tag{4.6}$$

When the laser irradiation, that is nearly monochromatic at the laser wavelength λ_{L}, is equal to the setting of the spectroradiometer wavelength λ_{M}, thus Eq. (4.6) yields,

$$I^{M}(\lambda_{M}) = \int s(\lambda_{M}, \lambda) E_{Laser,\lambda_{L}} \delta(\lambda) d\lambda = s(\lambda_{M}, \lambda_{M}) E_{Laser,\lambda_{L}}. \tag{4.7}$$

Substituting Eq. (4.5) for $E_{Laser,\lambda_{L}}$, the following equation for the unknown spectral irradiance responsivity of the spectroradiometer $s(\lambda_{M},\lambda_{M})$ holds:

$$\Rightarrow s(\lambda_{M}, \lambda_{M}) = \frac{I^{M}(\lambda_{M}) s_{S}(\lambda_{L})}{I^{S}}. \tag{4.8}$$

4.3 Irradiance Calibration of an Unknown Source

Let us now assume, a uniform irradiance field from a source with an unknown spectral irradiance irradiates the entrance optics of the spectroradiometer. In the case of the calibration of an unknown source, the incident irradiance field is transformed to an output signal through the spectral irradiance responsivity function $s(\lambda_{M},\lambda_{S})$, which amongst others depends on the spectroradiometer wavelength setting λ_{M} and on the source wavelength λ_{S}. Thus, in general, when the incident irradiance field from an unknown source irradiates the entrance optics of the spectroradiometer, the spectroradiometer output signal arising from the unknown source I^{U} at monochromator wavelength setting (λ_{M}) is equal to:

$$I^{U}(\lambda_{M}) = \int s(\lambda_{M}, \lambda) E_{\lambda}^{U}(\lambda) d\lambda, \tag{4.9}$$

where $I^{U}(\lambda_{M})$ is the spectroradiometer output signal arising from the unknown source at the monochromator wavelength setting λ_{M} and $E_{\lambda}{}^{U}(\lambda)$ is the spectral irradiance of the unknown source.

When $E_\lambda^U(\lambda)$ has a linear wavelength dependence over the central region of a symmetric responsivity function, $E_\lambda^U(\lambda)$ can be moved outside the integral. For illustration; let us consider the following (see Fig. 4.2):

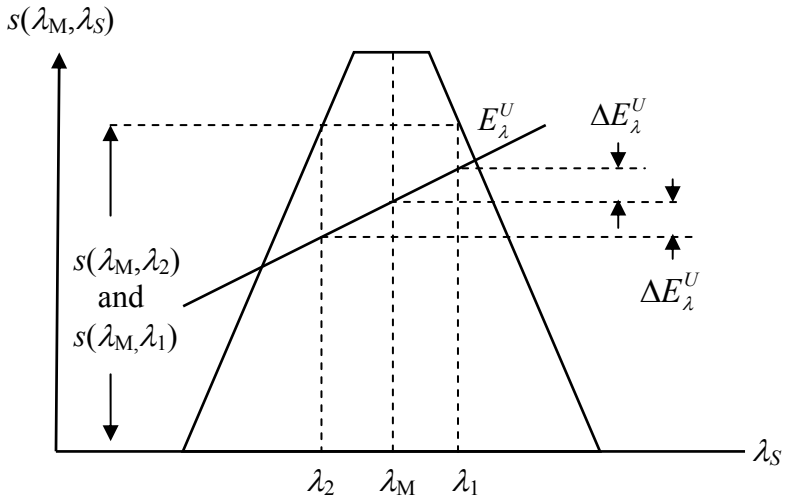

Fig. 4.2 Illustration showing why E_λ^U can be moved outside the integral in Eq. (4.9), when E_λ^U is linear and the central portion of s is symmetric.

For every contribution to the integral at a wavelength shorter than λ_M, say λ_2, the contribution to $I^U(\lambda_M)$ is:

$$s(\lambda_M,\lambda_2)\left[E_\lambda^U(\lambda_M)-\Delta E_\lambda^U\right](\lambda_M-\lambda_2). \tag{4.10}$$

The contribution to $I^U(\lambda_M)$ at a wavelength longer than λ_M, say λ_1 is equal to:

$$s(\lambda_M,\lambda_1)\left[E_\lambda^U(\lambda_M)+\Delta E_\lambda^U\right](\lambda_1-\lambda_M). \tag{4.11}$$

For $\lambda_1 - \lambda_M = \lambda_M - \lambda_2$ and because of the symmetry $s(\lambda_M, \lambda_2) = s(\lambda_M, \lambda_1)$, the combined contribution is:

$$(s(\lambda_M,\lambda_2)+s(\lambda_M,\lambda_1))E_\lambda^U(\lambda_M)\Delta\lambda, \tag{4.12}$$

where $\Delta\lambda = \lambda_1 - \lambda_2$. Thus, the entire integral in Eq. (4.9) is made up of terms such as this and therefore can be written as:

$$I^U(\lambda_M)=E_\lambda^U(\lambda_M)\int s(\lambda_M,\lambda)d\lambda. \tag{4.13}$$

Also, for the symmetric responsivity function it holds:

$$\Delta\lambda = \frac{\int s(\lambda_M, \lambda) d\lambda}{s(\lambda_M, \lambda_M)}, \tag{4.14}$$

where $\Delta\lambda$ is the Full Width at Half Maximum (FWHM), i.e. the monochromator spectral bandpass. Thus Eq. (4.13) yields,

$$I^U(\lambda_M) = E_\lambda^U(\lambda_M) s(\lambda_M, \lambda_M) \Delta\lambda, \tag{4.15}$$

$$\Rightarrow E_\lambda^U(\lambda) = \frac{I^U(\lambda_M)}{s(\lambda_M, \lambda_M)} \frac{1}{\Delta\lambda}, \tag{4.16}$$

or in general form by substituting Eq. (4.8) for $s(\lambda_M, \lambda_M)$ in Eq. (4.16) and using $s_s(\lambda_M) = s_s^*(\lambda_M)\Delta A$, Eq. (4.16) yields,

$$E_\lambda^U(\lambda) = \frac{I^U(\lambda_M) I^S}{I^M(\lambda_M) s_S^*(\lambda_L) \Delta A} \frac{1}{\Delta\lambda}. \tag{4.17}$$

From Eq. (4.17) we can note that when a standard detector is used to calibrate a spectroradiometer for measuring the spectral irradiance, the standard detector aperture area ΔA and the spectral bandpass $\Delta\lambda$ of the spectroradiometer are critical parameters that must be well determined.

5 Results and Discussion

5.1 Experimental Procedure of a Spectroradiometer Irradiance Responsivity Calibration

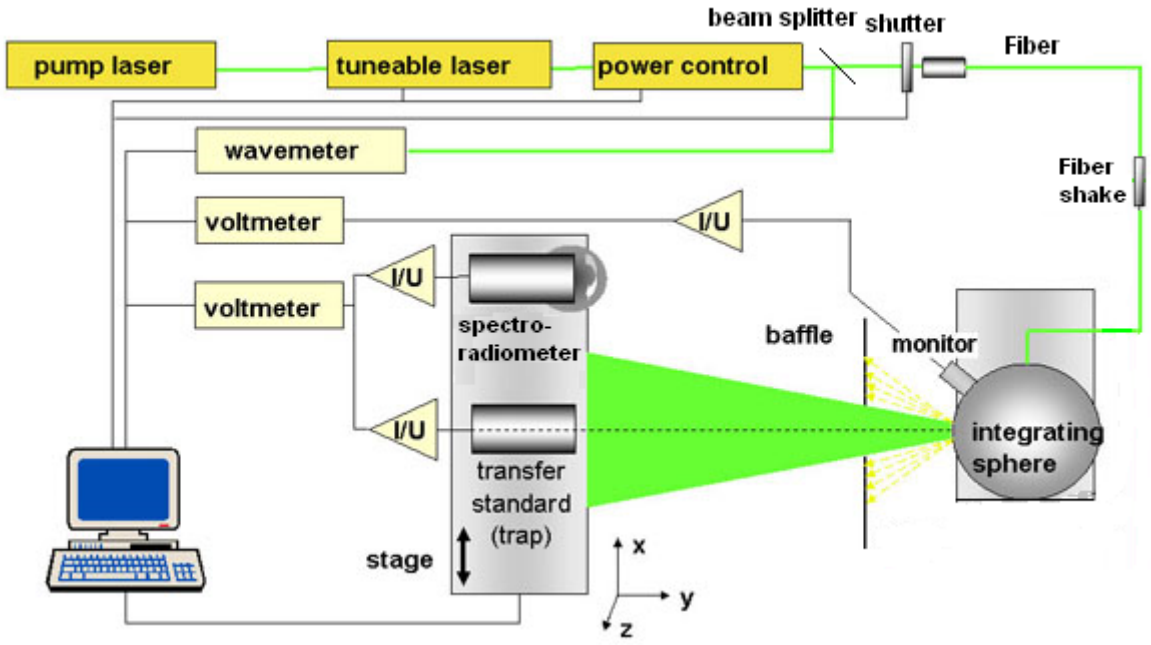

Fig. 5.1 Principal scheme of the TULIP facility for the calibration of detectors

In Fig. 5.1, the principal scheme of the Tunable Laser In Photometry (TULIP) facility for the calibration of detectors is shown. The radiation of a continuous wave (cw) high-power tunable laser is introduced into an integrating sphere to build a uniform, monochromatic, and nearly Lambertian source of high spectral radiant flux [16-19]. A silicon reflection trap (Si-trap) detector with a calibrated aperture is used as standard irradiance detector to determine the irradiance at a reference plane. This Si-trap detector is calibrated against a cryogenic radiometer, the primary standard for optical radiant power.

Within the TULIP setup, the output of the tunable laser is first directed through an intensity stabilizer (model LPC from BEOC company), which controls the relative optical power in the beam to enable long-term stability of 0.03 % at a set wavelength point [95]. The laser beam is sent through a beam splitter, which

reflects a small fraction of the beam into a wavemeter (model WS/7 Super Precision from HighFinesse), which is able to measure the wavelength of the laser radiation with an accuracy of 60 MHz [96]. The main part of the laser radiation is directed via an optical fiber into an integrating sphere. The speckle pattern, originating from the multipath-interference due to the coherent nature of the laser radiation, is effectively removed by shaking the fiber. The speckle pattern is still present, but is altered on a much shorter time scale than the integration time of the multimeter, thus effectively the variations are averaged out. A monitor photodiode at one exit port of integrating sphere is used to correct for radiant flux changes in the sphere output between the measurements with the reference instrument (trap) and with the Device Under Test (DUT) (spectroradiometer). The output radiation from the integrating sphere is used to calibrate the spectroradiometer (a double monochromator with a silicon detector and fiber bundle-based input optics), see Fig. 3.1.a.

The diffuser of the entrance optics is needed in order to uniformly irradiate the entrance slit of the monochromator independent from source geometry. The order-sorting filter would not be necessary for the measurement with the narrow-line laser source, however, in the calibration of broadband radiant sources, the order-sorting filters are necessary in order to avoid higher-order effects. The entrance optics of the spectroradiometer together with the Si-trap as a reference detector are placed on the (x, y, z) translation stage of the TULIP setup (see Fig. 5.1).

In the first step, the calibrated Si-trap detector with known aperture area is moved to a defined position in the radiant field and measures the spectral irradiance at the set wavelength of the tunable laser. In the second step, the entrance optics (opal glass diffuser, order-sorting filter, fiber bundle) of the spectroradiometer is moved to the same position (see Fig. 3.1.a).

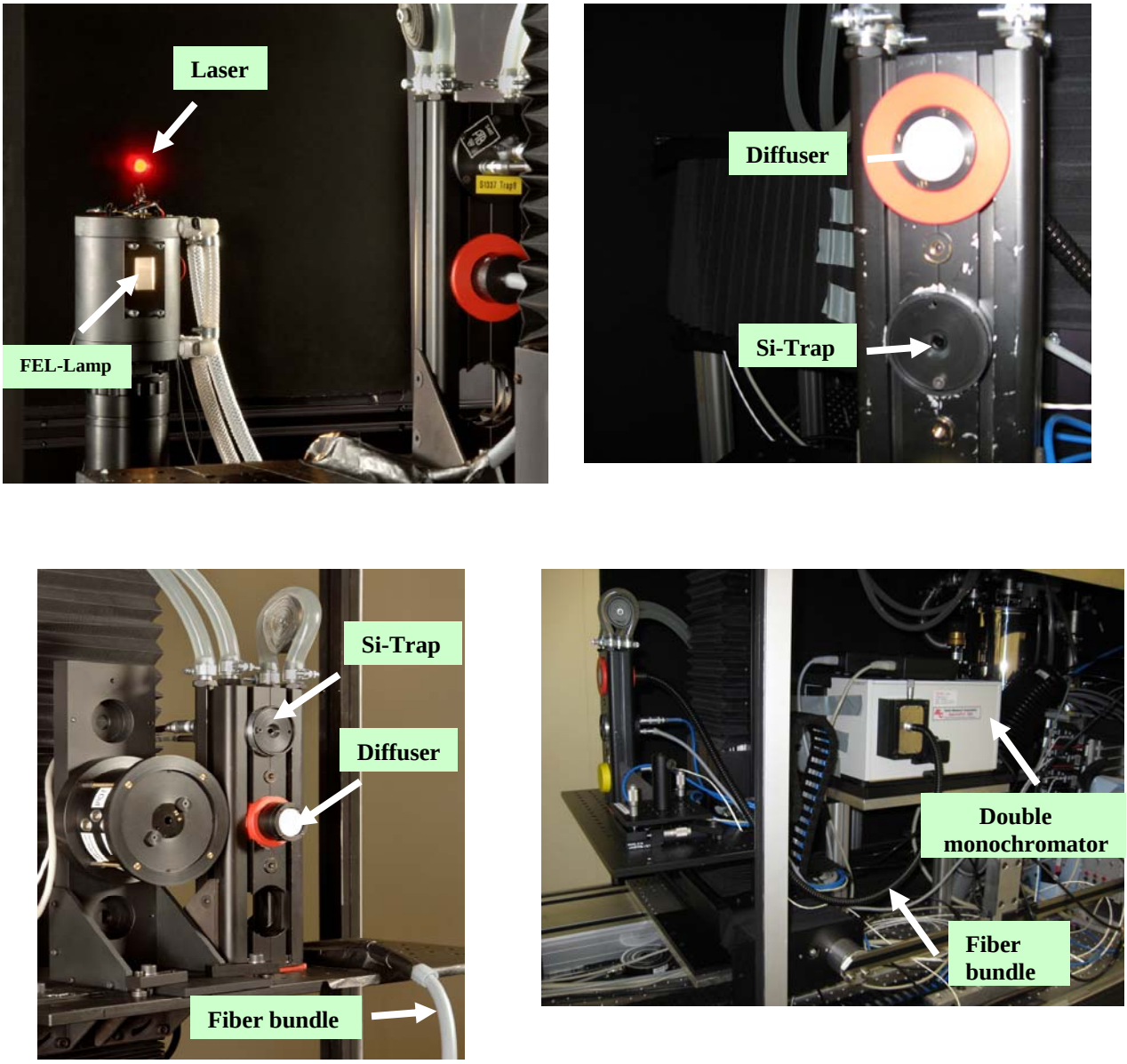

Fig. 5.2 Overview photos inside the facility

The comparison of the spectroradiometer signals and the spectral irradiance values determined by the trap detector measurements allows for determining the spectral irradiance responsivity function of the spectroradiometer. This function is determined for each monochromator setting.

Using the calibrated spectroradiometer, the irradiance at a given distance of any radiant source (e.g. FEL lamps) can be calibrated (see Fig. 3.1.b). For the experiments described here, three different laser sources inside the TULIP setup, covering the spectral range between 565 nm and 975 nm were used (see sec. 3.1). Fig. 5.2 shows some photos of the facility.

5.2 Results of a Spectroradiometer Calibration

5.2.1 Slit Function

At each wavelength, the absolute slit function (or the bandpass) of the monochromator is determined either by tuning the laser wavelength through a fixed monochromator setting in the automated laser range or by scanning the monochromator over a fixed laser wavelength in the non-automated laser range. In practice, the slit function of the monochromator is determined by measuring the output signal of the monochromator as a function of scanning wavelength under monochromatic (laser) irradiation [78, 79].

We choose nearly equal slits (1.5 mm, 1.75 mm, 1.25 mm) as it gives a nearly triangular slit function and provides the maximum signal. The triangular shape is inexact, because of mirror aberrations leading to a non perfect imaging of the entrance slit onto the exit slit. Moreover, there is a small difference between the sizes of the two slits to optimize the stability of the signal (see sec. 3.6.2.).

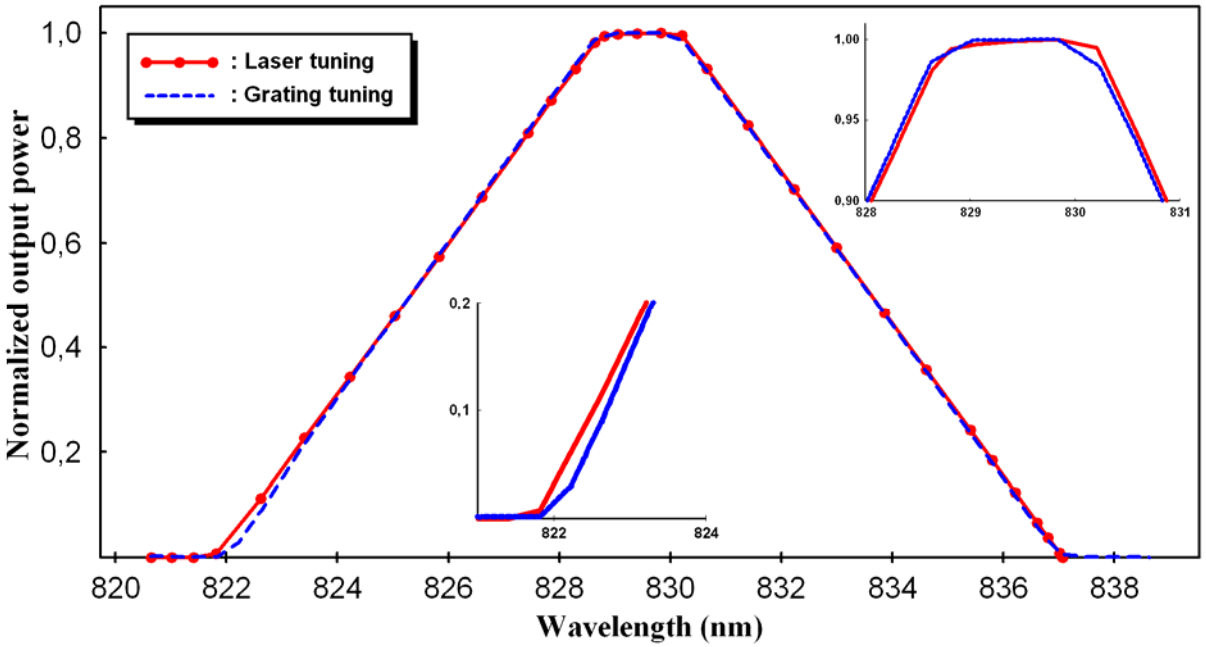

Fig. 5.3 The slit function as determined by scanning the monochromator over a laser line at 830 nm (dashed blue line), and tuning the laser wavelength with the double monochromator fixed at 830 nm (red line).

Only the method using the tunable lasers will lead to the correct integral value of the slit function and hence the bandpass of the monochromator, $\Delta\lambda$. By tuning the laser, the influence caused by mechanical performance during grating movement can be avoided. Presence of this influence affects the integral value of the slit function (bandpass) as well as the effective wavelength of the monochromator. This influence may be different from one monochromator to another where the grating is placed on a large drive wheel with motor control; especially if no angular wavelength decoder is used. Furthermore, the efficiency of the grating is angle dependent which also leads to differences between the two methods.

As an automated tuning of the laser was implemented in the spectral range between 640 nm and 680 nm for this survey, the laser-tuning method was only used in this spectral range and at two selected other wavelengths (830 nm and 850 nm). The difference between the values of the integral of the slit function determined by these two approaches is about 0.68 % at 830 nm (see Fig. 5.3).

5.2.2 Spectroradiometer Irradiance Responsivity

In Fig. 5.4 the spectroradiometer irradiance responsivity $s_S(\lambda)$ for the wavelength ranges from 565 nm to 635 nm, from 640 nm to 680 nm and from 690 nm to 975 nm is shown. The wavelength dependence of the responsivity arises from the wavelength dependence of all optical components of the whole spectroradiometer system, i.e. their transmission and reflection properties, the slit settings and the spectral responsivity of the silicon detector at the output port of the double monochromator. The irradiance responsivity in the spectral range from 640 nm to 680 nm is higher than the values at the neighboring wavelengths, because a new fiber bundle with higher throughput and a diffuser with smaller thickness were used. The increase in the irradiance responsivity for $\lambda > 850$ nm is caused by the wavelength dependence of the grating efficiency, its blaze wavelength is 1000 nm.

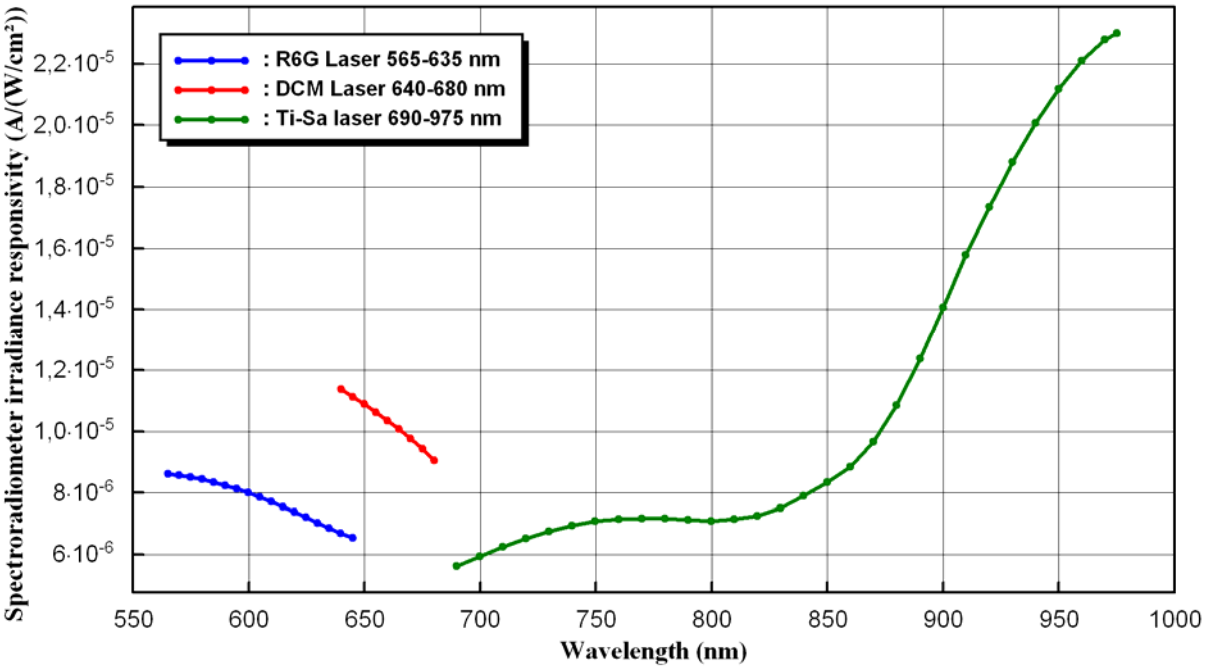

Fig. 5.4 Irradiance responsivity of the spectroradiometer in the wavelength range of the Rhodamine 6G, DCM, and Ti-Sapphire laser sources. The irradiance responsivity in the DCM laser spectral range is higher than the values at the neighboring wavelengths, because a new fiber bundle with higher throughput and a diffuser with smaller thickness were used.

5.3 System Characterization and Correction Factors

In the real case some correction factors, which affect on the value of the irradiance measurement, must be included in the irradiance model of Eq. (4.17), i.e.

$$E_{\lambda}^{U}(\lambda) = \frac{I^{U}(\lambda_M) I^{S}}{I^{M}(\lambda_M) s_S^{*}(\lambda_L) \Delta A} \frac{1}{\Delta\lambda} Corr, \tag{5.1}$$

where $Corr$ is a product of correction factors caused by:

- Response and irradiance uniformity ($f_{\text{Unif}}(\lambda)$).
- Polarization dependence ($f_{\text{Pol}}(\lambda)$).
- Monochromator wavelength shift ($f_{\text{WL}}(\lambda)$).
- Monochromator bandwidth ($f_{\text{BW}}(\lambda)$).
- Distance effect ($f_{\text{Dist-Effect}}$).

5.3.1 Response and Irradiance Uniformity ($f_{\text{Unif}}(\lambda)$)

The non-uniformity of the measured radiant field, the irradiance uniformity, and of the active area of the input optics, the response uniformity, has to be measured when a photodiode is intended to perform high accuracy measurement [97, 98]. A high non-uniformity would produce measurement errors when the detector is used at different positions.

A setup is used to evaluate the response and irradiance uniformity in which the radiant source is a DCM tunable laser beam at 640 nm. The active area of the input optics (diffuser) is placed on a micropositioning stage which permits displacements along two perpendicular axes in a plane perpendicular to the optical axis. Horizontal and vertical scans were made through the active area with 4 mm steps (see Fig. 5.5).

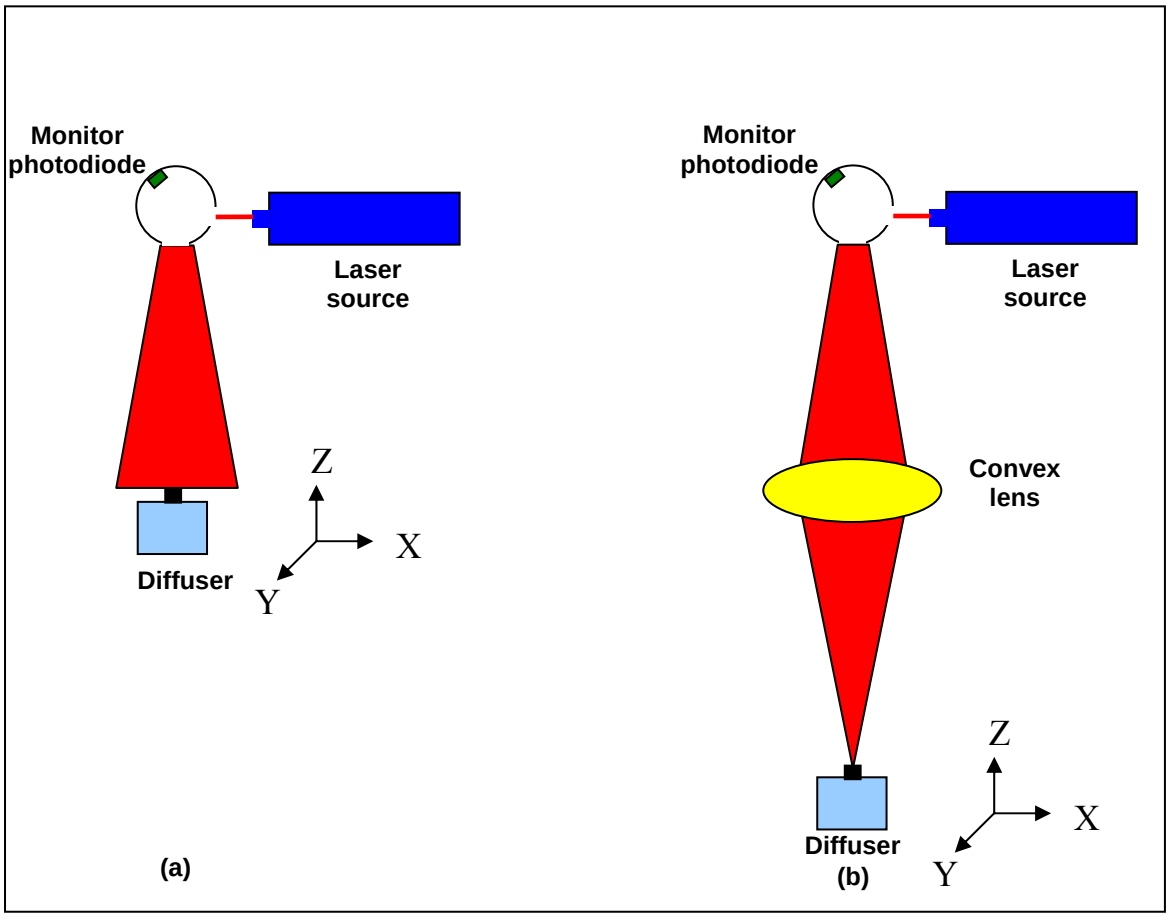

Fig. 5.5 Setup used for non-uniformity caused by: (a) Irradiance of the measured radiant field and (b) Response of the active area of the input optics (diffuser)

The correction factor for the non-uniformities, $f_{\mathrm{Unif}}(\lambda)$, caused by the active area of the input optics (diffuser) $s(x,y,\lambda)$, the reference trap detector $s_{\mathrm{R}}(x,y,\lambda)$ and the real irradiation field E_{real} (x,y,λ), is calculated according to the following formula,

$$f_{Unif}(\lambda) = \frac{\int_A s(x,y,\lambda)dA}{\int_A s(x,y,\lambda)E_{real}(x,y,\lambda)dA} \cdot \frac{\int_A s_R(x,y,\lambda)E_{real}(x,y,\lambda)dA}{\int_A s_R(x,y,\lambda)dA}. \qquad (5.2)$$

Considering in Eq. (5.2) the reference trap detector $s_R(x,y,\lambda)$ has a response uniformity of 100 %.

Results show that the irradiation field coming from the laser-integrating sphere source gives a highly uniform irradiation field (≅ 99.5 %) (see Fig. 5.6). On the other hand, the response uniformity of the input optics gives bad uniformity (≅ 50 %) (see Fig. 5.7). In spite of this bad response uniformity from the input optics, the correction factor is nearly unity as we have a highly uniform irradiation field [99].

The correction factor due to the response and irradiance uniformity, $f_{\mathrm{Unif}}(\lambda)$ is 1.0012 with a relative standard uncertainty of 0.06 %.

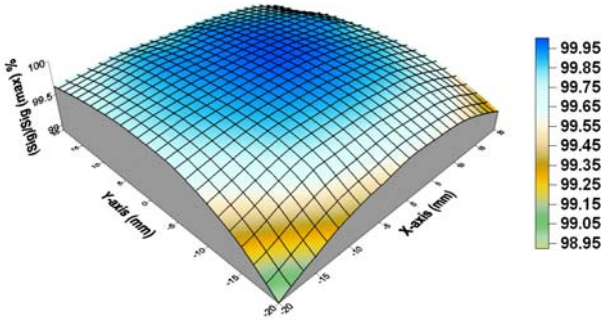

Fig. 5.6 Irradiance uniformity of the radiant field.

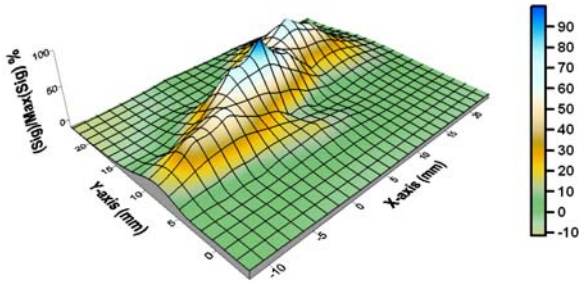

Fig. 5.7 Response uniformity of the active area of the input optics (diffuser).

5.3.2 Polarization Dependence ($f_{\mathrm{Pol}}(\lambda)$)

The polarization dependence of the irradiance field from the laser-integrating sphere was measured with the Si-trap detector.

A diagram of the setup used to determine the degree of polarization of the irradiance field is illustrated in Fig. 5.8a. The laser-integrating sphere, the polarizer and the trap detector are centered on an optical axis. By rotating the polarizer, the polarization dependence of the light emitted from the laser-integrating sphere at 640 nm was analyzed. The influence of the polarization dependence of the trap detector can be neglected [46, 47].

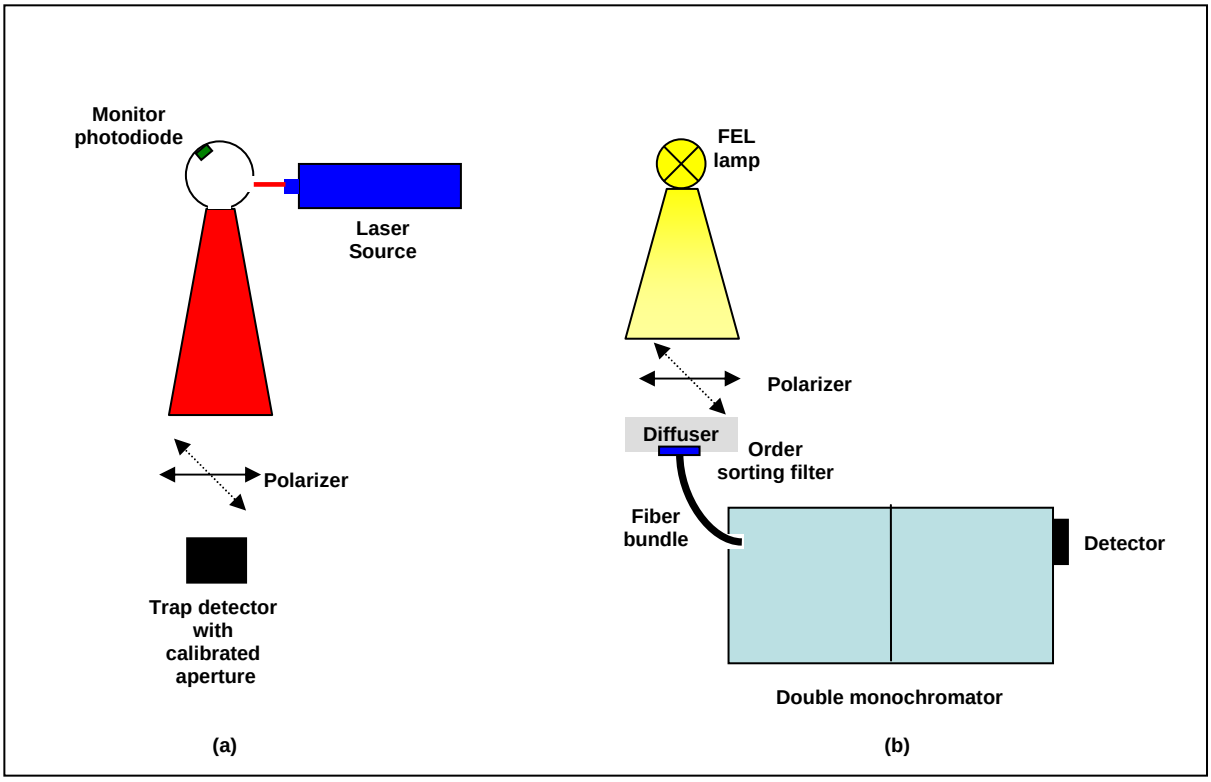

Fig. 5.8 Setup used for polarization dependence from laser and lamp sources

The degree of polarization (P) can be determined by the following equation [100]:

$$P = \frac{E_{MAX}(\lambda) - E_{MIN}(\lambda)}{E_{MAX}(\lambda) + E_{MIN}(\lambda)}, \tag{5.3}$$

where E_{MAX} and E_{MIN} are, respectively, the maximum and minimum irradiance values obtained when the polarizer is rotated.

The laser and integrating-sphere combination in principal provides a source of depolarized light [20, 21]. Indeed the results show that the polarization dependence can be neglected in the irradiance responsivity measurement, because the radiation from the laser-integrating sphere is nearly unpolarized (see Fig. 5.9).

The maximum degree of polarization from the laser-integrating sphere is 0.17 %.

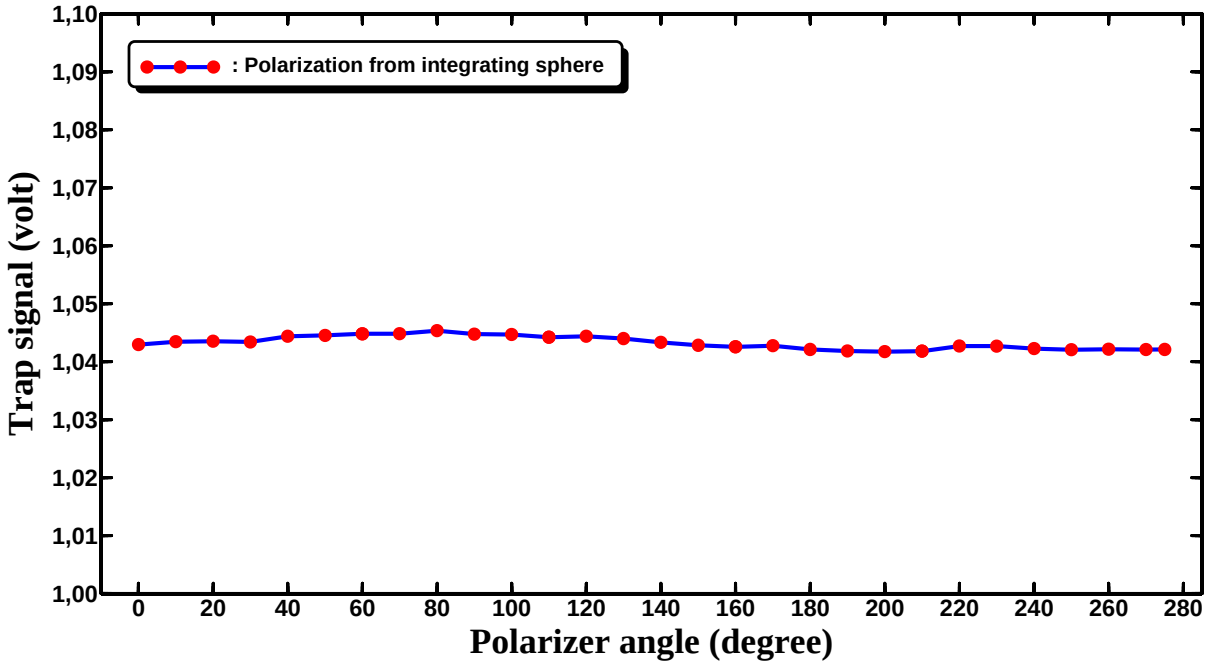

Fig. 5.9 Polarization dependence from the laser-integrating sphere

The polarization dependence of the irradiance field from the FEL-lamp was measured with the spectroradiometer, see Fig. 5.8b. As input optics, a combination of diffuser, order sorting filter and fiber bundle was used for diminishing polarization effects. As reported in [21, 37, 62], such a detection system (input optics + spectroradiometer) has a maximum polarization dependence of 0.7 %.

The degree of polarization obtained from the irradiance measurement of the FEL-lamp is up to 2.1 % (see Fig. 5.10). Radiant light sources (like FEL-lamps) are known to emit partially polarized light [62, 100]. When a source of this type is used as a spectral irradiance transfer standard in conjunction with a polarization sensitive detector, the accuracy of the measurement will be influenced by the degree and orientation of the polarized component of light emitted from the lamp. However, in our case the polarization dependence of the FEL-lamp can be omitted, because the detection system (input optics + spectroradiometer) is nearly polarization insensitive.

Hence, the correction factor due to polarization dependence (f_{Pol} (λ)) in our facility is considered to be 1. However, a possible residual polarization dependence is taken into account by an uncertainty. This uncertainty is determined by worst case considerations:

First, the product of the polarization dependencies of the irradiance field from the integrating sphere of 0.17 % and of the detection system of 0.7 % are taken, giving a total relative standard uncertainty of 0.001 %, i.e. the correction factor due to the irradiance responsivity measurement($f_{Pol(1)}$) is 1.00000 ± 0.001 % at 640 nm.

Second, the product of the polarization dependencies of the FEL lamp of 2.1 % and of the detection system of 0.7 % are taken, giving a total relative standard uncertainty of 0.015 %, i.e. the correction factor due to the FEL lamp irradiance measurement ($f_{Pol\,(2)}$) is 1.00000 ± 0.015 % at 640 nm.

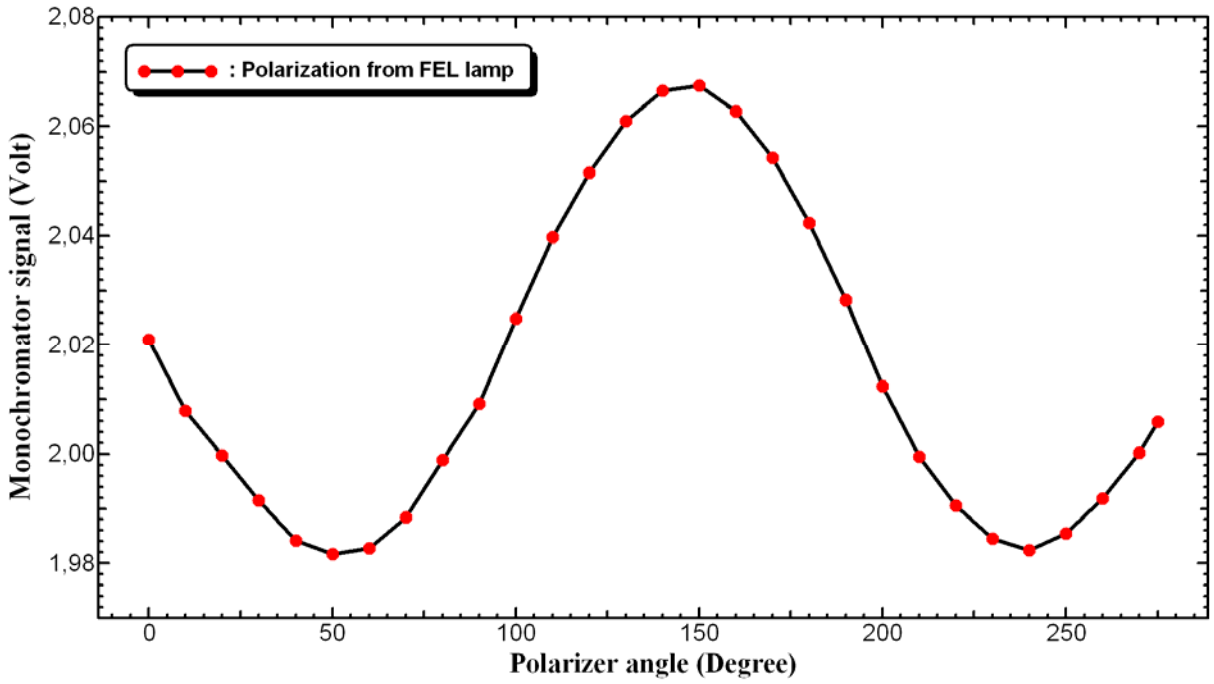

Fig. 5.10 Polarization dependence of the FEL lamp

5.3.3 Monochromator Wavelength Shift ($f_{WL}(\lambda)$)

The correction factor due to the monochromator wavelength shift, $f_{WL}(\lambda)$, is calculated according to the following formula [99]:

$$f_{WL}(\lambda) = \frac{1 - \Delta\lambda_{WLC} \, i'(\lambda)/i(\lambda)}{1 - \Delta\lambda_{WLC} \, i_R'(\lambda)/i_R(\lambda)}, \qquad (5.4)$$

where $i(\lambda)$, $i_R(\lambda)$ is the photocurrent of the irradiated DUT (diffuser-spectroradiometer) and reference (trap) detector respectively. The wavelength correction $\Delta\lambda_{WLC} = \Delta\lambda_1 + \Delta\lambda_2$ has two components, an offset $\Delta\lambda_1 \cong \pm 0.2$ nm, resulting from calibration of the monochromator wavelength by the tunable laser lines, and a correction $\Delta\lambda_2 \cong \pm 0.05$ nm individual for each wavelength due to limited repeatability of the wavelength drive. $i'(\lambda)$ and $i_R'(\lambda)$ are the first derivatives with respect to wavelength, i.e. $i'(\lambda) = di / d\lambda$ and $i_R' = di_R / d\lambda$.

The correction factor due to the monochromator wavelength shift ($f_{WL}(\lambda)$) is in the range from 0.99985 to 1.00166 with a relative standard uncertainty of 0.002 % (see Fig. 5.11).

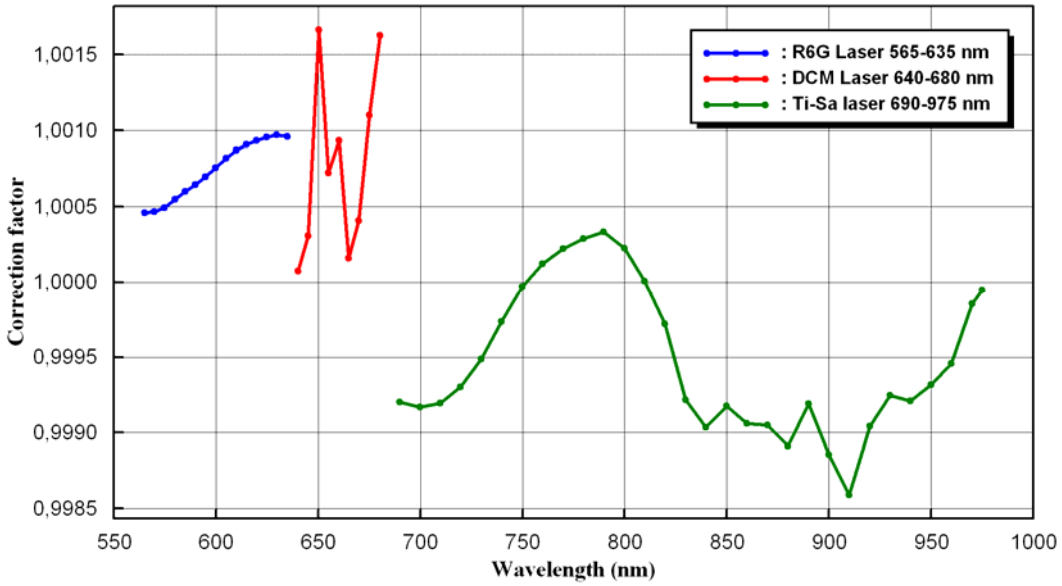

Fig. 5.11 Correction factor due to the monochromator wavelength shift. The sharp structure for the measurements with the DCM laser arises from the adjustment of the distance between the spectroradiometer and the integrating sphere in order to get a higher signal for each wavelength.

5.3.4 Monochromator Bandwidth ($f_{BW}(\lambda)$)

The correction factor for the monochromator bandwidth, $f_{BW}(\lambda)$, considering a triangle slit function, calculated according to the following formula [99]:

$$f_{BW}(\lambda) = \frac{1 - \Delta\lambda^2 . \frac{1}{12} i''(\lambda)/i(\lambda)}{1 - \Delta\lambda^2 . \frac{1}{12} i_R''(\lambda)/i_R(\lambda)}. \qquad (5.5)$$

It depends on differences between the 2nd deviation of the responsivity functions of DUT (spectroradiometer), $i''(\lambda)$, and reference (trap) detector, $i_R''(\lambda)$.

The correction factor due to the monochromator bandwidth ($f_{BW}(\lambda)$) is in the range from 0.999981 to 1.001242 with a relative standard uncertainty of 0.0006 % (see Fig. 5.12).

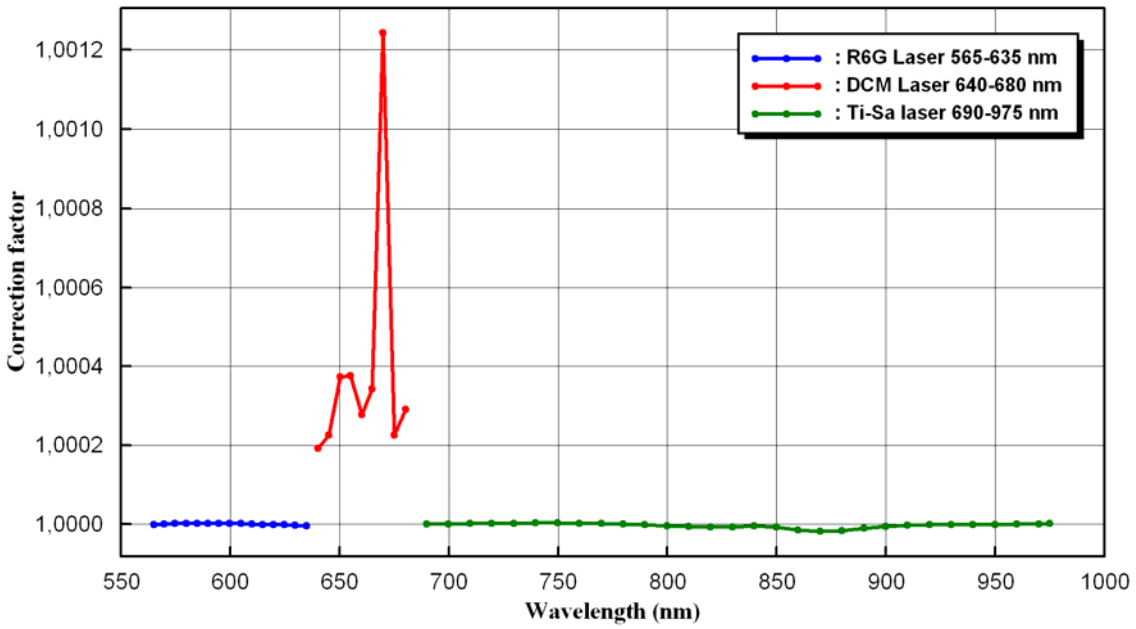

Fig. 5.12 Correction factor due to the monochromator bandwidth. The sharp structure for the measurements with the DCM laser arises from the adjustment of the distance between the spectroradiometer and the integrating sphere in order to get a higher signal for each wavelength.

5.3.5 Distance Effect ($f_{\text{Dist-Effect}}$)

The correction factor due to the source-detector distance effect, $f_{\text{Dist-Effect}}$, is calculated according the following formula:

$$f_{Dist-Effect} = \left(\frac{d_{lamp} + \Delta d}{d_{lamp} + \Delta d + \Delta d_{diffuser}}\right)^2 / \left(\frac{d_{lamp}}{d_{lamp} + \Delta d_{diffuser}}\right)^2, \qquad (5.6)$$

where d_{lamp} is the distance between lamp and diffuser in the irradiance measurement, $\Delta d = d_{\text{laser}} - d_{\text{lamp}}$ is the deviation in the distance between the first step of the spectroradiometer calibration and the second step of the lamp calibration; where d_{laser} is the distance between integrating sphere and diffuser in the irradiance responsivity measurement. $\Delta d_{diffuser}$ is the diffuser offset distance of the effective measurement plane.

The correction factor due to the distance effect is 1.00019 ± 0.001 % as $\Delta d \cong 0$. So it is highly recommended in this system to use $d_{\text{laser}} \cong d_{\text{lamp}}$, i.e. $\Delta d \cong 0$, to minimize the error due to the unknown Δd diffuser. Table 5.1 summarize the list of the correction factors and their values.

Table 5.1 The correction factors that affect in the irradiance measurement and their values.

Correction Factors		Value
Response and irradiance uniformity ($f_{\text{Unif}}(\lambda)$)		1.0012 ± 0.06 % (at 640 nm)
Polarization dependence ($f_{\text{Pol}}(\lambda)$)	Irradiance responsivity ($f_{\text{Pol(1)}}(\lambda)$)	1.00000 ± 0.001 % (at 640 nm)
	FEL-lamp irradiance ($f_{\text{Pol(2)}}(\lambda)$)	1.00000 ± 0.015 % (at 640 nm)
Monochromator wavelength shift ($f_{\text{WL}}(\lambda)$)		(0.99985 - 1.00098) ± 0.002 %
Monochromator bandwidth ($f_{\text{BW}}(\lambda)$)		(0.999981 – 1.001242) ± 0.0006 %
Distance effect ($f_{\text{Dist-Effect}}$)		1.00019 ± 0.001 %

5.4 Method Validation: Spectral Irradiance Calibration of an FEL-Lamp

The validation of the above described method was performed using a 1000 W FEL-type lamp. Instead of the integrating sphere for monochromatic radiation, the FEL lamp was used as an irradiation source (see Fig. 3.1.b). Thus, the spectral irradiance values of this lamp were determined, see Fig. 5.13. The spectral irradiance was also determined by comparison with a blackbody radiator [1, 11, 13] in the working group "Source-based spectroradiometry" at PTB. The comparison showed a very good agreement and the maximum deviation from the spectral irradiance values obtained from the calibration against the blackbody source is 0.7 % and the mean deviation is 0.3 %, see Fig. 5.14, where the deviations between the measured irradiance values and the spectral irradiance obtained from a calibration against the blackbody system are shown. The reproducibility of the measurements is very good, i.e. the results for the calibration of the FEL lamp before and after the calibration with the blackbody system are less than 0.1 %, and this means that spectroradiometer calibrations show essentially only a low drift.

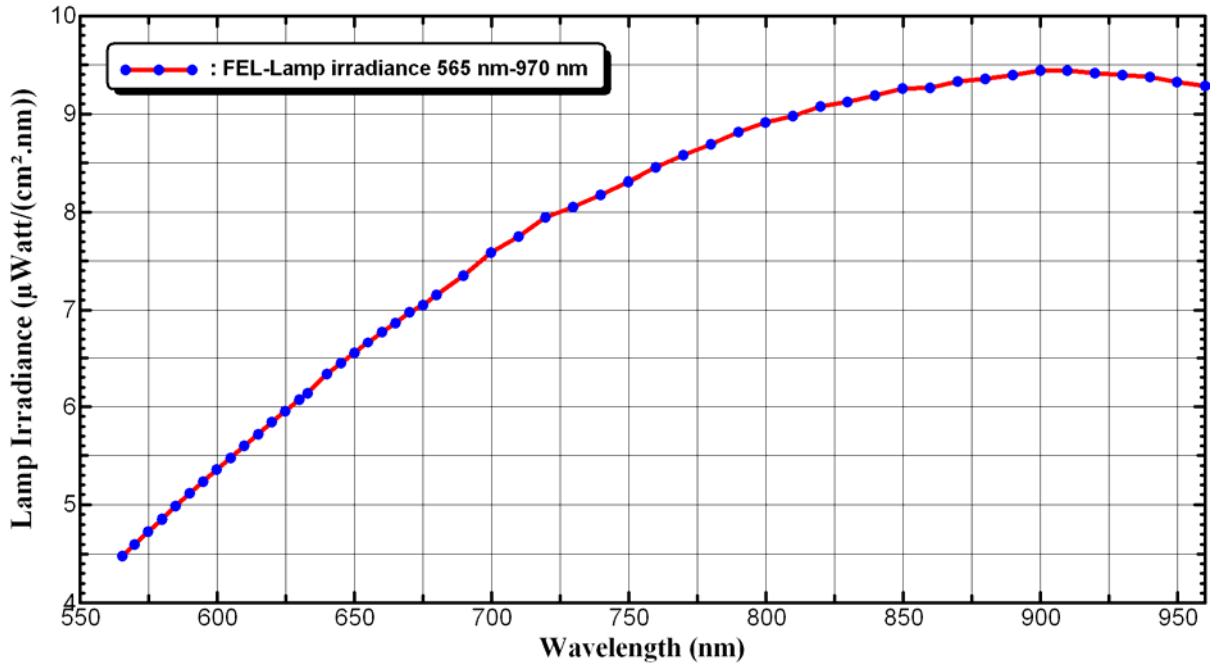

Fig. 5.13 Spectral irradiance of the FEL lamp determined with the calibrated spectroradiometer

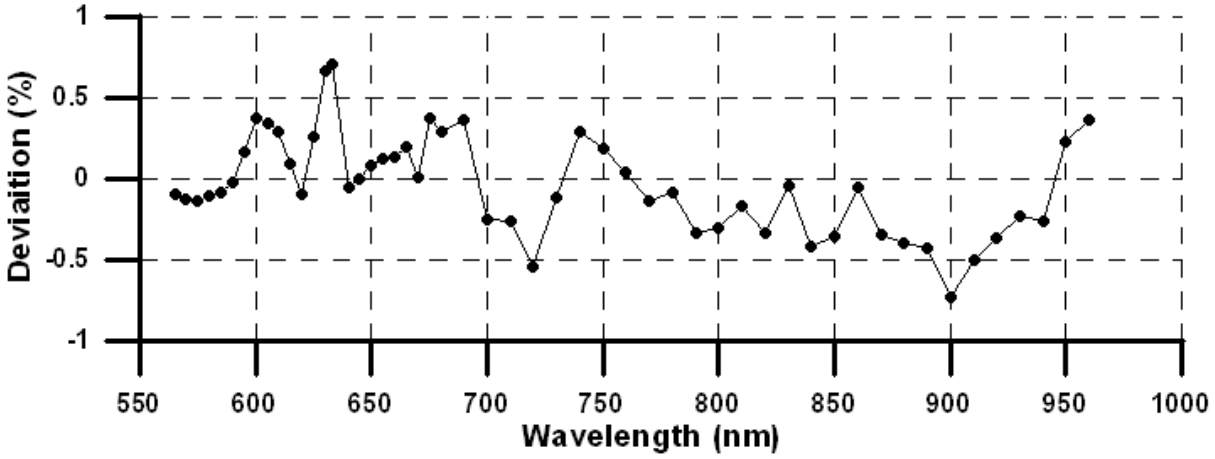

Fig. 5.14 Deviation between the measured irradiance values and the spectral irradiance obtained from a calibration against the blackbody system. Maximum deviation is 0.7 %, the mean deviation is 0.3 %.

6 Estimation of the Measurement Uncertainty

A fundamental part of metrology is the uncertainty analysis. Whenever the result of a measurement is reported, the associated uncertainty must also be stated. This informs the user of the accuracy within which the measurement was made [101-108].

The word “uncertainty” means doubt, and thus “uncertainty of measurement” means doubt about the validity of the result of a measurement. The uncertainty of the result of a measurement reflects the lack of exact knowledge of the value of the measurand. The result of a measurement after correction for recognized systematic effects is still only an estimate of the value of the measurand, because of the uncertainty arising from random effects and from imperfect correction of the result for systematic effects.

The most common methods to evaluate and to express the measurement uncertainty are based on the “Guide to the Expression of Uncertainty in Measurement” (GUM). This guide, published at the first time in 1993, has been adopted worldwide by most of the NMIs, calibration and test laboratories, industry, etc. for evaluating and expressing the measurement uncertainty [101]. On the other hand, a practical alternative to evaluate the uncertainty of a measurement is the Monte Carlo (MC) method, fully described in the GUM-Supplement-1 [105]. In this work, both methods are used depending on the measurand model.

6.1 Evaluation of the Measurement Uncertainty according to GUM (following [84])

Evaluation of the uncertainty by GUM method is adopted and described in details by International Organization for Standardization (ISO) [101], and CIE-2006 [108]. Here we adopt by M. López [84] "According to the GUM, the first step for evaluating the measurement uncertainty consists in defining the measurand. In many cases, a measurand Y is not measured directly, but is determined from N other quantities $X_1, X_2, \ldots, X_N$ through a function f:

$$Y = f(X_1, X_2, \ldots, X_N). \tag{6.1}$$

The second step is the evaluation of the uncertainty of each input quantity. Here the GUM classifies the uncertainty evaluation by two types: the evaluation of the uncertainty by the statistical analysis of series of observations, the so-called Type *A* evaluation, and the evaluation of the uncertainty by means other than the statistical analysis, named Type *B* evaluation. The type *A* evaluation of the standard uncertainty is obtained generally by means of repeated observations of the input quantity X, where the distribution of the random errors is obtained through its standard deviation. That means that the standard uncertainty u_A due to the repeatability of the measurement is estimated by the experimental standard deviation of the mean value $\bar{x}$, that is,

$$u_A(x) = s(\bar{x}) = \frac{1}{\sqrt{n}} \sqrt{\frac{1}{n-1} \sum_{i=1}^{n} (x_i - \bar{x})^2} \tag{6.2}$$

The type *B* evaluation of the standard uncertainty refers to any method different from the statistical analysis. It is based on scientific judgment using all the relevant information available; e.g. manufacturer's specifications, previous measurement data, data provided in the calibration and other reports, etc. The probability distribution may be Gaussian, rectangular, triangular, etc.

The combined standard uncertainty $u_c(y)$ is obtained by combining the individual standard uncertainties u_i, these can be evaluation Type *A* or Type *B*.

That is,

$$u_c^2(y) = \sum_{i=1}^{N} \left[\left(\frac{\partial f}{\partial x_i} \right)^2 u^2(x_i) \right] + 2 \sum_{i=1}^{N-1} \sum_{j=i+1}^{N} \frac{\partial f}{\partial x_i} \frac{\partial f}{\partial x_j} u(x_i) u(x_j) r(x_i, x_j). \qquad (6.3)$$

Eq. (6.3) is also known as the law of propagation of uncertainty, which is based on the first-order Taylor series approximation. The partial derivatives $\partial f / \partial x_i$ are known as the sensitivity coefficients and $u(x_i)$ and $u(x_j)$ are the standard uncertainties associated to the inputs quantities x_i and x_j, respectively, and $r(x_i, x_j)$ is the correlation coefficient. The correlation coefficient characterizes the degree of correlation between x_i and x_j, its value can be found between -1 and +1. If the estimates x_i and x_j are independent, then $r(x_i, x_j) = 0$, and Eq. (5.3) is reduced to

$$u_c^2(y) = \sum_{i=1}^{N} \left(\frac{\partial f}{\partial x_i} \right)^2 u^2(x_i). \qquad (6.4)$$

Eq. (6.4) is most commonly used for calculating the measurement uncertainty assuming that the input quantities are not correlated.

The combined standard uncertainty $u_c(y)$ can be used to express the uncertainty of a measurement result y in many practical measurement situations. However, because its probability distribution is approximately normal in most of the cases, it is believed that the measurand Y is found between the interval $y\text{-}u_c(y) \le Y \le y+u_c(y)$ with a level of confidence p. A confidence level p of 95.45 % is recommended in most of the fields. In this case, the uncertainty of the measurement result is frequently expressed as an expanded uncertainty $U(y)$, and is obtained by multiplying $u_c(y)$ by a coverage factor k. That is,

$$U(y) = k \cdot u_c(y). \qquad (6.5)$$

The coverage factor $k(v, p)$ depends on the "degree of freedom" v of the output quantity and the confidence levels p wished or required in the application."

6.2 Evaluation of the Measurement Uncertainty by using the Monte Carlo Method (following [84]).

Monte Carlo (MC) simulations are based on the principal of random sampling by the MC method including a pseudo-random number generator. It requires a definition of the Probability Density Function (PDF) for each input quantity associated with the measurand**.**

The Monte Carlo method is a practical alternative to the GUM for evaluating the measurement uncertainty, especially for the case when the mathematical model of the measurand is non-linear. The standard GUM-method is valid only for "linear" models. That means in practice, that the signs of the partial derivatives $(\partial y / \partial x_i)$ of the output quantity y determined with respect to all input quantities x_i must not change within the intervals limited by (at minimum) twice the associated standard uncertainties $(x_i \pm 2u(x_i))$ [108].

The Monte Carlo method is adopted and described by International Organization for Standardization (ISO) [105] and CIE-2006 [108]. Here we adopt from M. López [84] "The Monte Carlo method is a numerical procedure valid practically for any model. Here, the value and the associated uncertainty of the output quantity Y, represented by y, are assigned by a large number of simulated observations (see Fig. 6.1). The values of the output quantity y are evaluated from the values of the input quantities x_i with the associated standard uncertainty $u(x_\mathrm{i})$.

The shape of the probability distribution of such quantities may be Gaussian $N(x_\mathrm{i}, u(x_\mathrm{i}))$, rectangular $R(x_\mathrm{i}, u(x_\mathrm{i}))$, or any other type. The related probability distributions are generated by means of random values.

As an example, for a single input quantity $N_{i,j} = N_j(x_i, u(x_i))$ the output quantity $y_{i,j} = f(x_1, x_2, ..N_{i,j}, .., x_N)$ can be evaluated for $1 < j < m$. Thus, the variance u_i^2 of the simulated values can be seen as the combined uncertainty of the mean values y_i.

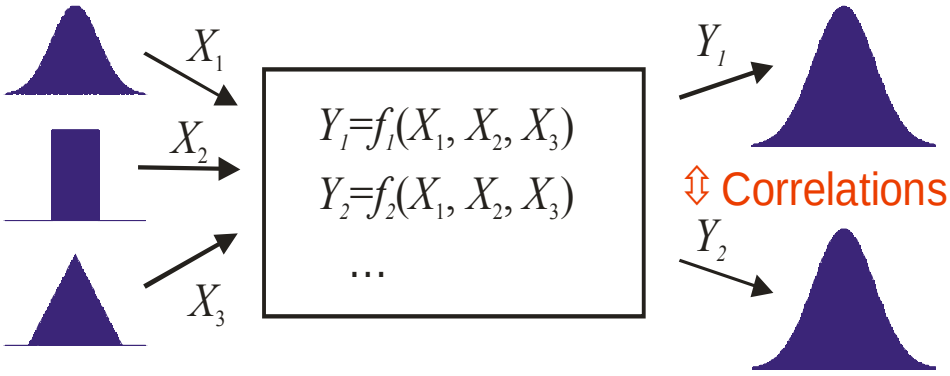

Fig. 6.1 Principle of the Monte Carlo method. The numerical simulation is as follow: First, a complete set of random input variables X_i with appropriate distributions are generated. Second, the generated input variables X_i are used to calculate all results Y_j. Third, all important variable and results are stored. The cycle is repeated several times until an appropriated distribution function is reached. The stored results may used to calculate the standard deviation, the distribution functions and correlations between the input or output quantities [99].

The values of all input quantities are simulated independently and in order to form an appropriate distribution, m is chosen often higher than 10000. Thus, from the simulated values of the output quantity, the mean value y and its associated variance $u(y)$ are calculated by:

$$y = \frac{1}{m}\sum_{j=1}^{m} f\left(N_{1,j}, N_{2,j}, \ldots, N_{i,j}, \ldots, N_{N,j}\right), \tag{6.6}$$

$$u(y) = \sqrt{\frac{1}{m(m-1)}\sum_{j=1}^{m\cdot N}\left[f\left(N_{1,j}, N_{2,j} \ldots, N_{i,j} \ldots, N_{N,j}\right) - y\right]^2}. \tag{6.7}$$”

6.3 Uncertainty Results

According to the model of the Eq. 5.1 of the irradiance measurement:

$$E_{\lambda}^{U}(\lambda) = \frac{I^{U}(\lambda_M) I^{S}}{I^{M}(\lambda_M) s_S^{*}(\lambda_L) \Delta A} \frac{1}{\Delta\lambda} Corr,$$

the following section will show how the uncertainty of each component is determined.

6.3.1 Uncertainty in the Trap Detector Absolute Responsivity (S_S^*):

The uncertainty in the absolute spectral responsivity of the trap detector is determined by the calibration against the cryogenic radiometer primary standard. This information is given with the trap detector responsivity calibration report from the "Detector Radiometry" group in PTB-Berlin [1, 27]. The relative standard uncertainty caused by S_S^* is shown in Fig. 6.2.

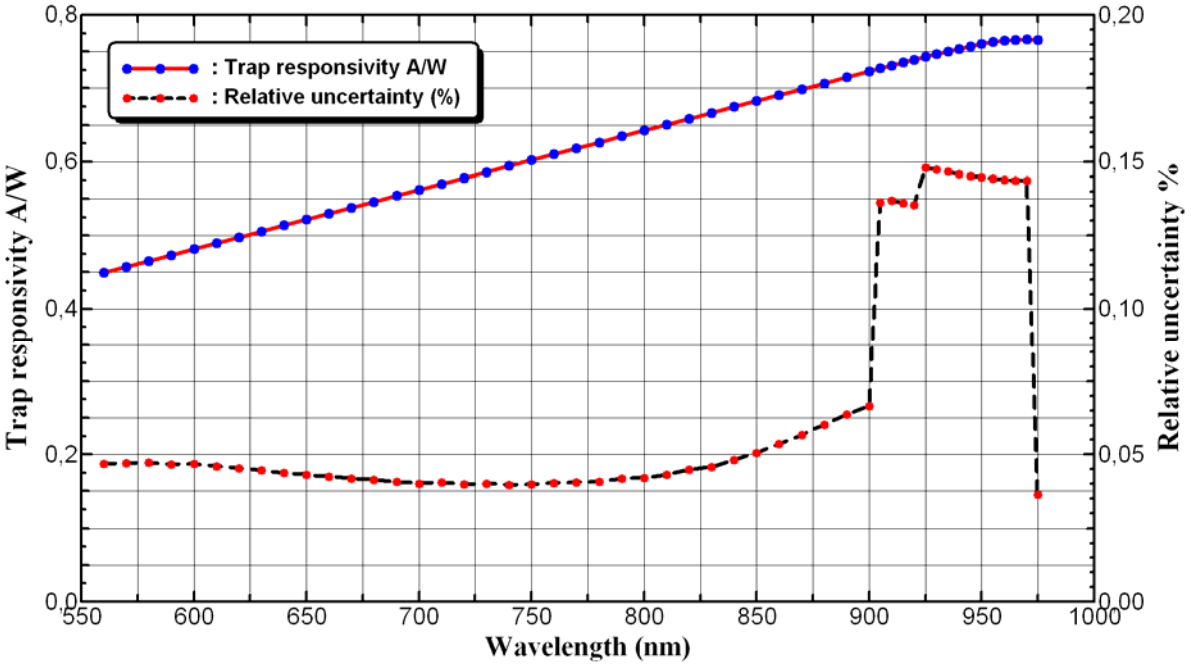

Fig. 6.2 Relative uncertainty in percentage caused by trap detector absolute responsivity S_S^*.

6.3.2 Uncertainty in the Signal Levels (I^S, I^M, I^U):

The current signals from a photodiode; either I^S, I^M or I^U, are small currents. This is converted to a larger voltage in a current-to-voltage amplifier. The signal level used in Eq. (4.18) is the current signal level minus the dark signal; both corrected by the signal of a monitor photodiode minus the dark signal of the monitor photodiode. The standard uncertainty in the detector output current signal is calculated according to the following formula:

$$u^2_{I(\lambda)} = u^2_{VL(\lambda)} + u^2_{VD(\lambda)} + u^2_{VLM(\lambda)} + u^2_{VDM(\lambda)} + u^2_{GM} + u^2_{GD},$$

where $u^2_{I(\lambda)}$ is the standard uncertainty in the detector output current signal at a wavelength λ. $u^2_{VL(\lambda)}, u^2_{VD(\lambda)}$ are the uncertainties of the detector output volt signal in the light and dark respectively. $u^2_{VLM(\lambda)}, u^2_{VDM(\lambda)}$ are the uncertainties of the monitor output volt signal in the light and dark respectively. The signals of the photodiodes are divided by the related monitor signal to eliminate the correlations and the statistics of the ratios are used in the evaluation process 99].

u^2_{GD} is the uncertainty in the detector amplifier gain, and u^2_{GM} is the uncertainty in the monitor amplifier gain. The relative standard uncertainty caused by I^S, I^U and I^M are shown in Fig. 6.3.

6.3.3 Uncertainty in the Aperture Area (ΔA):

The uncertainty in the aperture area comes from how it was calibrated. This information is given with the aperture area calibration facility from "Multisensor Metrology" group in PTB [1, 85]. The relative standard uncertainty of the calibration is 0.073 %.

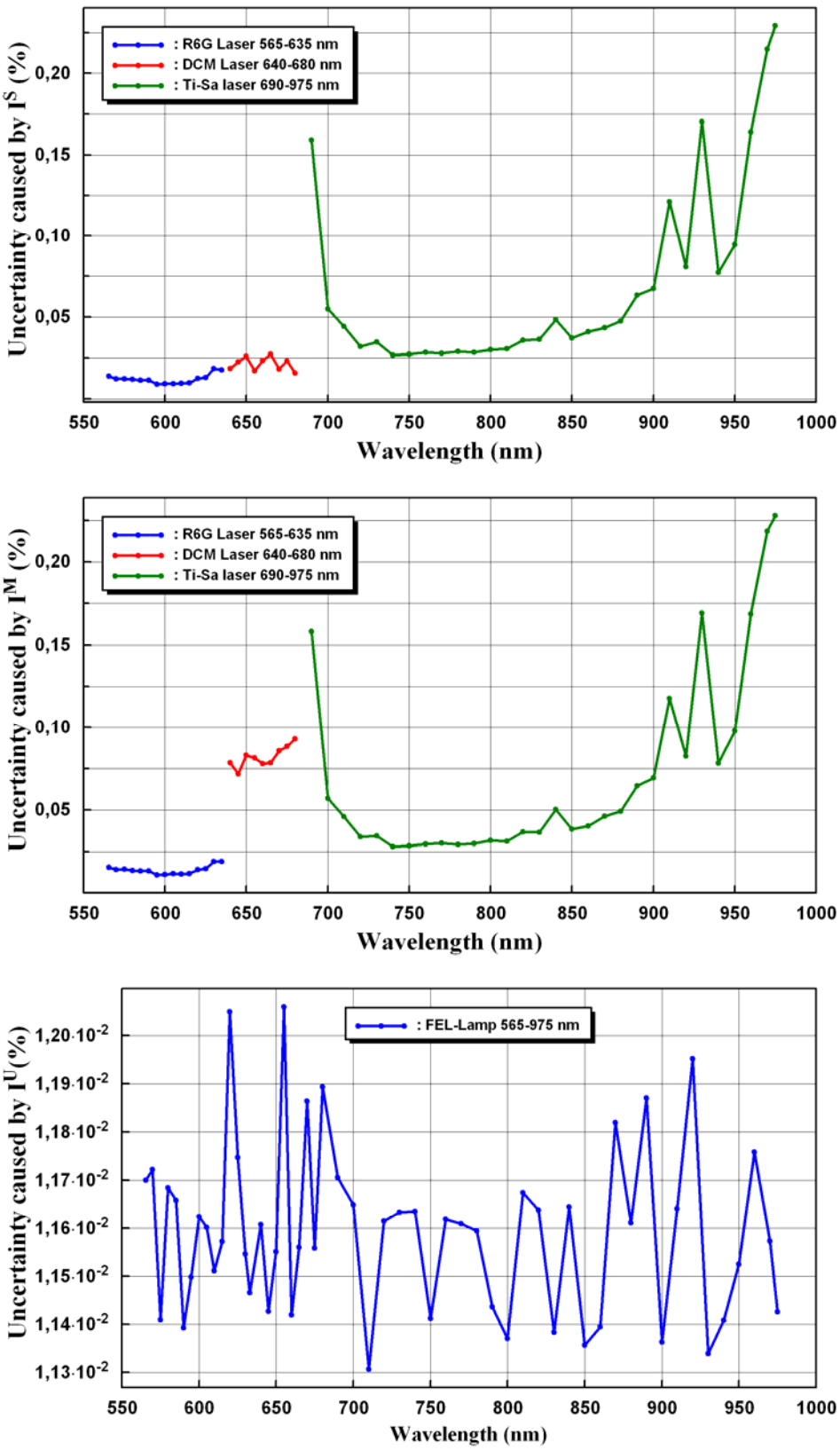

Fig. 6.3 Relative standard uncertainty caused by signal levels I^S, I^M and I^U.

6.3.4 Uncertainty in the Monochromator Slit Function ($\Delta\lambda$):

The uncertainty in the slit function has two components:

i- Uncertainty results from determining the slit function experimentally either by using laser or grating tuning methods.

ii- Uncertainty results from taking the slit function by tuning the grating instead of laser tuning in the non-automated laser range.

Certainly, the uncertainty in the slit function obtained by tuning a spectral line through a fixed monochromator setting is lower than the uncertainty in the slit function obtained by the monochromator scanning over a fixed spectral line (see Fig. 6.4). The relative standard uncertainty in the second case, tuning monochromator, is calculated considering rectangle distribution with half width 0.34 %, as we do not know exactly the error at all wavelengths. The estimation of the half width comes from the experiment that done at wavelength 830 nm by the two methods (see Fig. 5.3).

It is highly recommended in this system to be fully automated to remove this part of the uncertainty.

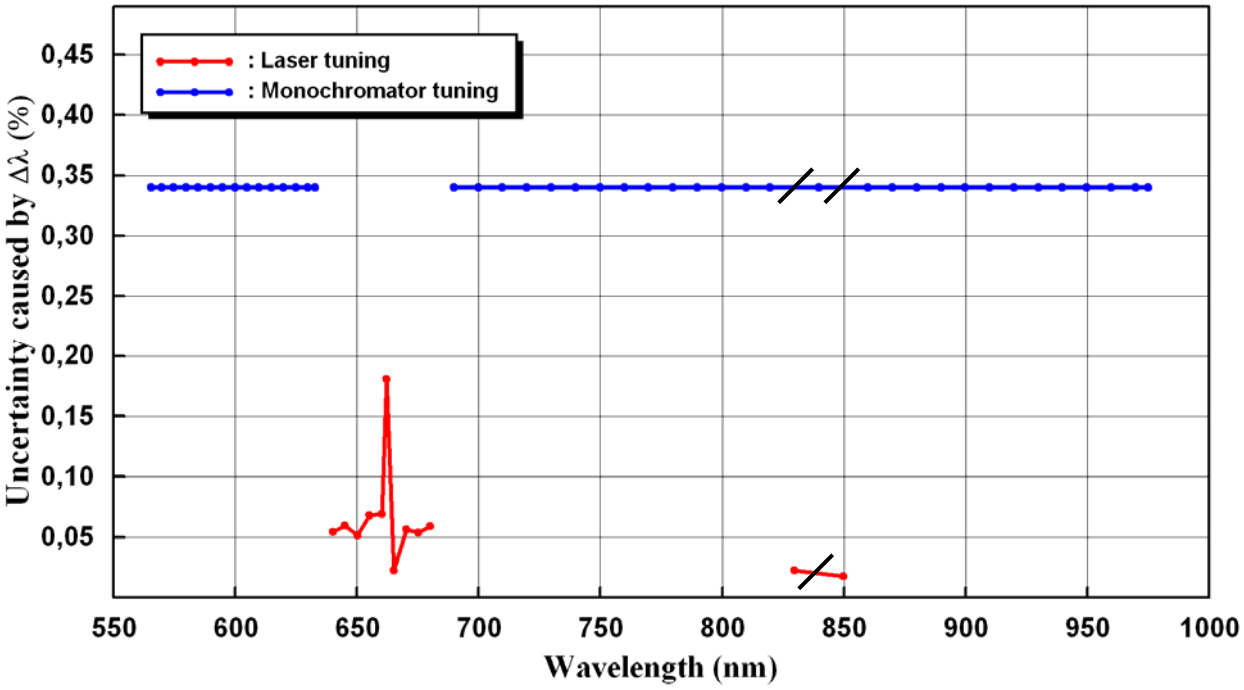

Fig. 6.4 Relative uncertainty in percentage due to monochromator slit function.

6.3.5 Uncertainty in the Correction Factors (*Corr*):

Correction factors are determined and calculated in section 5.3. Each factor has its own uncertainty value according to its model equation. It is difficult to determine the correction factors caused by, e.g. the uniformity and the polarization dependence, at all measured wavelengths, so the uncertainty caused by the correction factors are estimated like the calculation done at 640 nm for all factors.

Relative standard uncertainty due to correction factors is 0.08 % at 640 nm and this value is considered for all measured wavelengths.

6.4 Uncertainty Propagation Software

Uncertainty calculations with the Monte Carlo method are carried out by using the Hypradata software program [109]. For the GUM method, calculations are performed by using the workbench software program to reveal the standard uncertainty for each component inside the irradiance model, for example at 700 nm (see Table 5.2) [110]. The expanded uncertainties in the irradiance measurements are found to be lower than 1 % for $k = 2$, as shown in Fig. 6.5. At some wavelengths in this figure, like at 830 nm and 860 nm, the deviation between blackbody and detector-based is lower than the uncertainty at these points (see Fig. 5.14), and this may be caused from the uncertainty of the blackbody system itself. Comparison in associated uncertainty with blackbody and detector-based facility is shown in Fig. 6.6.

As can be seen from Fig. 5.14 and Fig. 6.6, the deviation is smaller than the combined standard uncertainties for nearly the whole wavelength range investigated.

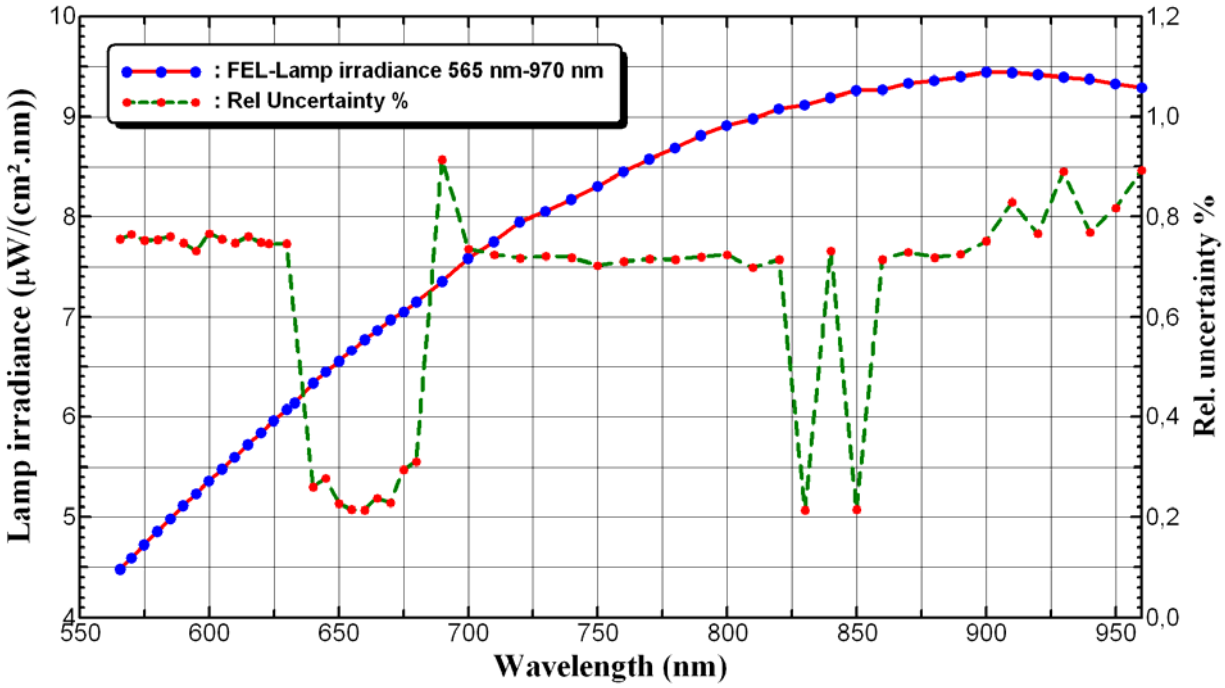

Fig. 6.5 Associated relative expanded uncertainty with the spectral irradiance measurement ($k = 2$), calculated by the Monte Carlo method using the Hypradata software [109].

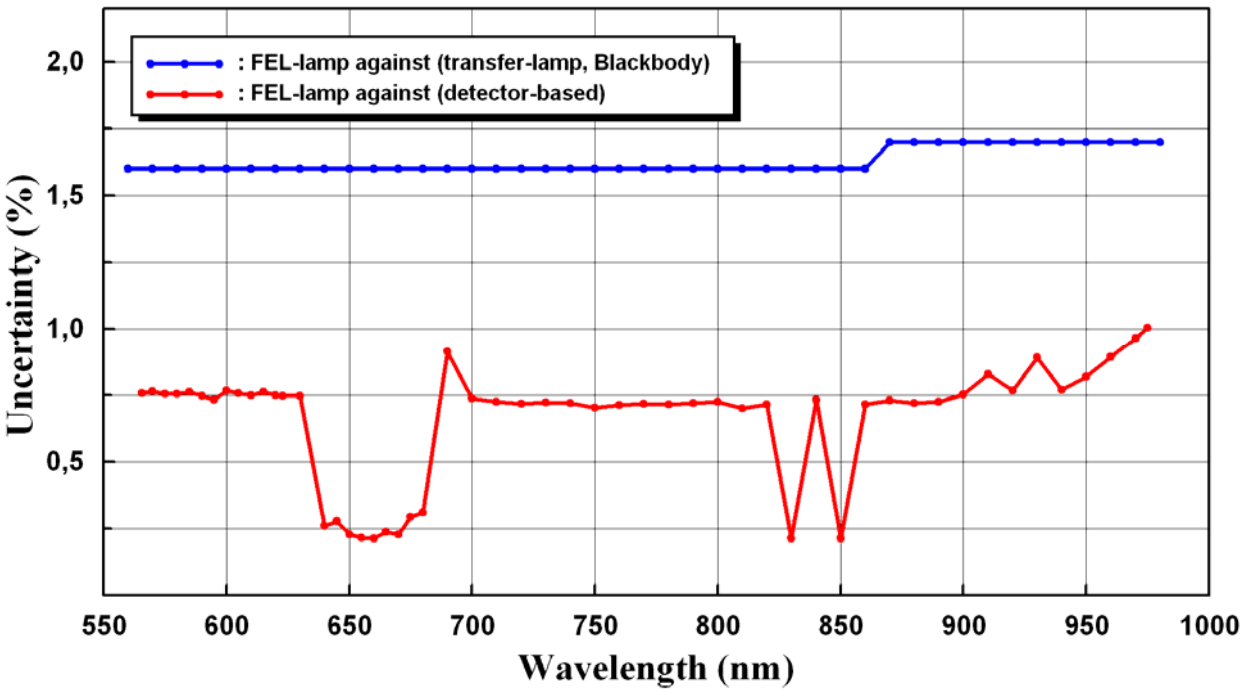

Fig. 6.6 Detector-based versus PTB-Blackbody facility relative expanded uncertainty ($k = 2$), measured against transfer FEL-lamp, not directly to Blackbody.

Table 6.2 Uncertainty contribution in the irradiance measurement at 700 nm calculated by the GUM method using the workbench software [110].

Uncertainty component	**Relative Standard Uncertainty %**
Trap detector responsivity (s_s^*)	0.04
Aperture area (ΔA)	0.073
Standard detector output signal (I^S)	0.057
Spectroradiometer output signal (I^M)	0.062
Unknown source signal (I^U)	0.014
bandpass ($\Delta\lambda$)	0.34
correction factors (*Corr*)	0.08
Expanded uncertainty (k = 2)	**0.74**

7 Summary and Outlook

A new setup for a completely detector-based traceability chain for spectral irradiance calibrations has been built at PTB. The characterization of the setup with the help of the tunable laser facility TULIP is described in this thesis. The detector-based traceability chain is realized using a spectroradiometer, which is calibrated for the absolute spectral irradiance responsivity using a Si-trap as a transfer-standard detector. Thus the spectral irradiance measurements are in principal traceable to the PTB cryogenic radiometer, thus the use of radiant sources like the blackbody radiator with its related problems as primary standards is principally not necessary.

The new setup also reveals the importance of obtaining the slit function and hence the bandpass of the monochromator, $\Delta\lambda$, by tuning the laser wavelength through a fixed monochromator setting rather than a monochromator scanning over a fixed laser wavelength. The bandpass is a critical parameter that must be well determined in the irradiance model equation. It can affect in the irradiance calculation within 0.68 % as seen in the thesis at 830 nm.

The spectral irradiance values of the FEL lamp, as measured by the new setup, were compared with those determined by a blackbody radiator. The comparison showed a very good agreement and the maximum deviation from the spectral irradiance values obtained from the calibration against the blackbody source is 0.7 %, the mean deviation is 0.3 %.

At present, the irradiance calibrations of the FEL lamps in the spectral range between 565 nm and 975 nm were measured with expanded uncertainties lower than 1 %. Thus, this completely detector-based traceability chain for the spectral irradiance calibrations has the potential to reduce the measurement uncertainty compared to the traditional source-based methods, e.g. using blackbody

radiators. But tunable lasers over the whole spectrum range from 250 nm to 2500 nm are needed in radiometry, between 380 nm and 830 nm in photometry.

The new method might have many applications like a more precise spectral irradiance or illuminance calibration of a variety of light sources, realization of the Candela, solar irradiance for outdoor solar cell calibration and spectral calibration of most light sources.

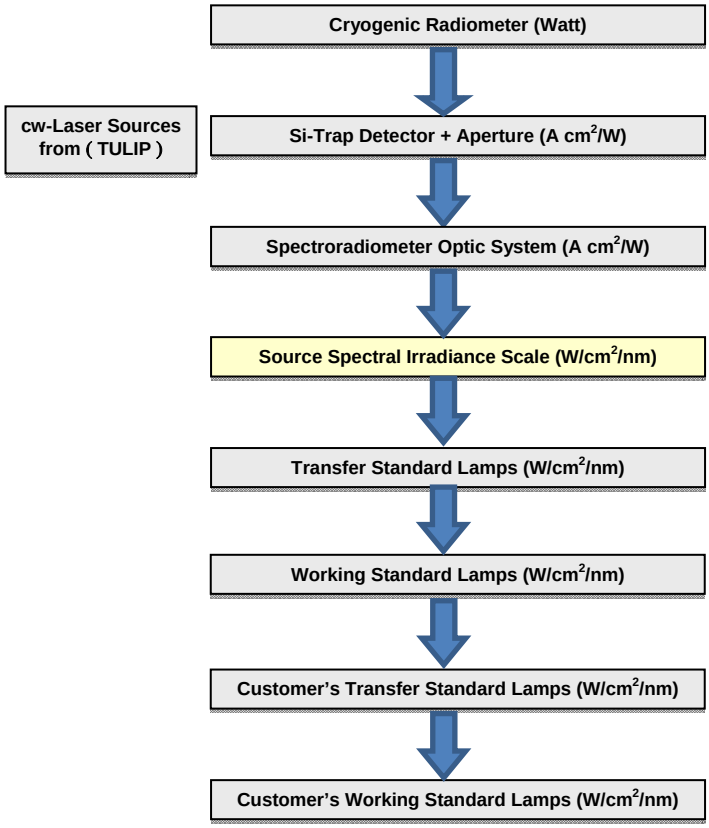

Fig. 7.1 Possible new chain leading to spectral irradiance scale

With this new chain (see Fig. 7.1) the two commonly used calibration steps to measure the blackbody temperature using calibrated filter-radiometers are replaced by the single calibration of the responsivity of the spectroradiometer against a trap detector (see Fig. 1.2).

A further reduction of the uncertainty and an extension of the method to the IR and the UV spectral ranges will be pursued as soon as the TULIP facility at PTB will be complemented by a new automated quasi-cw laser system.

8 References

1. Physikalisch-Technische Bundesanstalt (PTB), Germany, http://www.ptb.de.
2. Le Bureau International des Poids et Mesures (BIPM), France, http://www.bipm.org.
3. National Institute of Standards and Technology (NIST), "Optical radiation measurements based on detector standards." NIST Technical Note 1621, March (2009).
4. E. Woolliams, "Development and evaluation of a high temperature blackbody source for the realisation of NPL's primary spectral irradiance scale." Ph.D thesis, University of Manchester, United Kingdom, (2003).
5. F. Grum, R. Becherer; *Optical radiation measurements*; Academic Press, Volume 1 - Radiometry, (1979).
6. A. Abd-Elmageed, "Establishing the NIS spectral responsivity scale." M.Sc thesis, Helwan University, Egypt, (1999).
7. Santa Cruz Institute for Particle Physics (SCIPP), http://scipp.ucsc.edu.
8. C. DeCusatis, *Handbook of Applied Photometry*, Optical Society of America (1998).
9. A. C. Parr, R. U. Datla, *Optical Radiometry*, Elsevier Academic Press, First edition (2005).
10. N. P. Fox, "Primary radiometric quantities and units." Metrologia 37, 507–513 (2000).
11. P. Sperfeld, "Entwicklung einer empfängergestützten spektralen Bestrahlungsstärkeskala." Ph.D thesis, Braunschweig University, Germany (1999). http://www.biblio.tu-bs.de/ediss/data/19990628a/19990628a.html
12. P. Sperfeld, S. Pape, B. Khlevnoy, A. Burdakin, "Performance limitations of carbon-cavity blackbodies due to absorption bands at the highest temperatures," Metrologia. 46, 170-173, (2009).

13. P. Sperfeld, J. Metzdorf, S. Yousef, K. Stock, W. Möller, “Improvement and extension of the black-body-based spectral irradiance scale,” Metrologia. 35, 267-271, (1998).
14. K. D. Mielenz, R. D. Saunders, J. B. Shumaker, “Spectroradiometric determination of the freezing temperature of Gold.” J. Res. Nat. Inst. Stand. Technol. 95, (1990).
15. E. W. M van der Ham, H. C. D. Bos, C. A. Schrama, “Primary realization of a spectral irradiance scale employing monochromator-based cryogenic radiometry between 200 nm and 20 μm.” Metrologia 40, 177–180 (2003).
16. S. Nevas, A. Sperling, S. Winter, A. Abd-Elmageed, P. Blattner, “Measurements of the spectral responsivity and f_1' values of photometers.” Proceedings of the CIE Expert Symposium on Advances in Photometry and Colorimetry, (CIE X: 033), Turin, 07-08 July, (2008).
17. T. Keawprasert, K. Anhalt, R. D. Taubert, A. Abd-Elmageed, A. Sperling, J. Hartmann, “Absolute calibration of spectral responsivity for a radiation thermometer.” Proceedings of NEWRAD 2008, 10^{th} International Conference on New Developments and Applications in Optical Radiometry Daejeon, 12-15 October (2008).
18. A. Abd-Elmageed, S. Winter, S. Nevas, P. Sperfeld, S. Kück, A. Sperling, “Detector based traceability chain for spectral irradiance using tunable lasers, independent from blackbody radiators.” Proceeding of BulLight 2010, ISSN 1314-0787, Varna-Bulgaria, 10-12 June (2010).
19. T. Keawprasert, K. Anhalt, R. D. Taubert, A. Abd-Elmageed, A. Sperling, J. Hartmann, “Monochromator based absolute calibration of radiation thermometers.” Proceeding of TEMPMEKO&ISHM 2010, Portorož - Slovenia, 31 May-04 June (2010).
20. V. E. Anderson, N. P. Fox, D. H. Nettleton, “Highly stable, monochromatic and tunable optical radiation source and its application to high accuracy spectrophotometry.” Applied Optics 31, No. 4, (1992).

21. S. Brown, G. Eppeldauer, K. R. Lykke, “Facility for spectral irradiance and radiance responsivity calibrations using uniform sources.” Applied Optics 45, No.32, (2006).
22. G. P. Eppeldauer, S. W. Brown, T. C. Larason, M. Rácz, K. R. Lykke, “Realization of a spectral radiance responsivity scale with a laser-based source and Si radiance meters.” Metrologia 37, 531–534 (2000).
23. R. Monshouwer, H.C.D. Bos, E. W. M. van der Ham, “New method for the primary realization of the spectral irradiance scale from 400 to 900 nm.” Proceedings of the CIE Expert Symposium on Advances in Photometry and Colorimetry , (CIE X: 033), Turin, 07-08 July, (2008).
24. E. F. Zalewski and C. R. Duda, “Silicon photodiode device with 100 % external quantum efficiency.” Applied Optics 22, No.18, (1983).
25. L. Werner, J. Fischer, U. Johannsen, J. Hartmann, “Accurate determination of the spectral responsivity of silicon trap detectors between 238 nm and 1015 nm using a laser-based cryogenic radiometer.” Metrologia 37, 279-284 (2000).
26. Ö. Bazkır, F. Samadov, “Comparison characterization of silicon photodiode-based trap detectors and establishment of spectral responsivity scale.” Optics and Lasers in Engineering 43, 131–141 (2005).
27. F. Lei, J. Fischer, “Characterization of photodiodes in the UV and visible spectral region based on cryogenic radiometry.” Metrologia 30, 297–303 (1993).
28. L. Werner, R. Friedrich, U. Johannsen, A. Steiger, “Precise scale of spectral responsivity for InGaAs detectors based on a cryogenic radiometer and several laser sources.” Metrologia 37, 523–526 (2000).
29. K. D. Stock, H. Hofer, “PTB primary standard for optical radiant power: transfer-optimized facility in the clean-room centre.” Metrologia 32, 545–549 (1995/96).

30. K. D. Stock, H. Hofer, “Present state of the PTB primary standard for radiant power based on cryogenic radiometry.” Metrologia 30, 291–296 (1993).
31. K. D. Stock, H. Hofer, M. Pawlak and J. Metzdorf, “Improvements to the German national primary standard of radiant power above 200 nm.” Metrologia 35, 279–282 (1998).
32. C. C. Hoyt, P. V. Foukal, “Cryogenic radiometers and their application to metrology.” Metrologia 28, 163–167 (1991).
33. N. P. Fox, “Radiometry with cryogenic radiometers and semiconductor photodiodes.” Metrologia 32, 535–543 (1995/96).
34. J. E. Martin, N. P. Fox, P. J. Key, “A cryogenic radiometer for absolute radiometric measurements.” Metrologia 21, 147–155 (1985).
35. C. L. Cromer, G. Eppeldauer, J. E. Hardis, T. C. Larason, A.C. Parr, “National Institute of Standards and Technology detector-based photometric scale.” Applied Optics 32, No.16, (1993).
36. Albert C. Parr, “A national measurement system for radiometry, photometry, and pyrometry based upon absolute detectors.” National Institute of Standards and Technology (NIST), Technical Note 1421, September (1996).
37. W. Budde, *Optical radiation measurements*, Academic Press, Volume (4)-Physical Detectors of Optical radiation, (1983).
38. Y. Ohno, Photometrie-Seminar, Braunschweig, Germany (2004).
39. A. Haapalinna, “Characterization Methods for Silicon Photodiode and Silicon Sub-Surface Properties.” Ph.D thesis, Helsinki University of Technology, Finland, (2004).
40. A. C. Parr, “The candela and photometric and radiometric measurements.” J. Res. Natl. Inst. Stand. Technol. 106, 151-186 (2000).

41. C. A. Schrama, R. Bosma, K. Gibb, H. Reijn, P. Bloembergen, “Comparison of monochromator-based and laser-based cryogenic radiometry.” Metrologia 35, 431–435 (1998).
42. V. Ahtee, S. W. Brown, T. C. Larason, K. R. Lykke, E. Ikonen, M. Noorma, “Comparison of absolute spectral irradiance responsivity measurement techniques using wavelength-tunable lasers.” Applied Optics 46, No. 20, (2007).
43. E. F. Zalewski, J. Geist, “Silicon photodiode absolute spectral response self-calibration.” Applied Optics 19, No. 8, (1980).
44. H. W. Yoon, C. E. Gibson, P. Y. Barnes, “Realization of the National Institute of Standards and Technology detector-based spectral irradiance scale.” Applied Optics 41, No. 28, (2002).
45. J. Walker, R. D. Saunders, J. Jackson, D. McSparron, “ Spectral irradiance calibrations.” National Bureau of Standards (NBS), Special publication 250-20, September (1987).
46. T. Kübarsepp, P. Kärhä, E. Ikonen, “Characterization of a polarization-independent transmission trap detector.” Applied Optics 36, No.13, (1997).
47. R. Goebel, S. Yilmaz, R. Pello, “Polarization dependence of trap detectors.” Metrologia 33, 207–213 (1996).
48. F. Hengstberger, *Absolute Radiometry* (Academic Press, Inc., Boston, 1989), ISBN0-12-340810-5.
49. W. W. Coblentz, "Studies of instruments for measuring radiant energy in absolute value: an absolute thermopile," Bulletin of the Bureau of Standards **12,** 503 (1915); also issued as Scientific Papers of the Bureau of Standards #261, March 1916.
50. National Institute of Standards and Technology (NIST), “Spectroradiometric detector measurements: ultraviolet, visible, and near-infrared detectors for spectral power.” NIST special publication 250-41, (2008).

51. G. Eppeldauer, M. Rácz, “Spectral power and irradiance responsivity calibration of InSb working-standard radiometers.” Applied Optics 39, No.31, (2000).
52. T. C. Larason, S. S. Bruce, C. L. Cromer, “The NIST high accuracy scale for absolute spectral response from 406 nm to 920 nm.” J. Res. Natl. Inst. Stand. Technol. 101, 133-140 (1996).
53. P. Shaw, T. C. Larason, R. Gupta, S. W. Brown, K. R. Lykke, “Improved Near-Infrared Spectral Responsivity Scale.” J. Res. Natl. Inst. Stand. Technol. 105, 689-700 (2000).
54. M. Johnson, *Photodetection and Measurement: Maximizing Performance in Optical Systems*, McGraw-Hill companies, ISBN 0-07-140944-0 (2003).
55. National Physical Laboratory (NPL), United Kingdom, http://www.npl.co.uk/.
56. J. L. Gardner, “On the use of the term “scale(s)” in radiometric and photometric metrology.” Metrologia 37, 547 (2000).
57. Deutsche Akkreditierungsstelle GmbH (DAkkS), http://www.dakks.de.
58. F. Sametoglu, O. Bazkir, O. Celikel, “Detector Based Traceability Chain Established at the UME.” Proceedings of NEWRAD 2005, 9th International Conference on New Developments and Applications in Optical Radiometry Davos, Switzerland, 17-19 October (2005).
59. K. Hauer, A. Höpe, “High-grade uniform light source for radiometric and photometric applications.” MAPAN 24, 175-182 (2009).
60. P. C. Knee, “Investigation of the uniformity and ageing of integrating spheres.” Analytica Chimica Acta 380, 391-399 (1999).
61. Labsphere company, *A guide to integrating sphere radiometry and photometry*, http://www.labsphere.com.
62. H. J. Kostkowski, *Reliable Spectroradiometry*, Spectroradiometry Consulting, (1997).

63. S. W. Brown, G. P. Eppeldauer, K. R. Lykke, “NIST facility for Spectral Irradiance and Radiance Responsivity Calibrations with Uniform Sources.” Metrologia 37, 579-582 (2000).
64. P. Shaw, Z. Li, “On the fluorescence from integrating spheres.” Applied Optics 47, No.21, (2008).
65. Oriel integrating sphere, http://www.newport.com.
66. Hamamatsu Photonics company, http://www.hamamatsu.com.
67. Physikalisch-Technische Bundesanstalt (PTB), “Reflectometry” group, Braunschweig, Germany.
68. G. P. Eppeldauer, M. Racz, T. C. Larason, “Optical characterization of diffuser-input standard irradiance meters.” SPIE Proceeding, Volume 3573, (1998).
69. P. Manninen, “Characterization of diffusers and light emitting diodes using radiometric measurements and mathematical modeling.” Ph.D thesis, Helsinki University of Technology, Finland, (2008).
70. J. Gröbner, “Improved entrance optic for global irradiance measurements with a Brewer spectrophotometer.” Applied Optics 42, No.18, (2003).
71. J. Hovila, M. Mustonen, P. Kärhä, E. Ikonen, “Determination of the diffuser reference plane for accurate illuminance responsivity calibrations.” Applied Optics 44, No. 28, (2005).
72. L. P. Boivin, “Diffusers in silicon-photodiode radiometers.” Applied Optics 21, No.5, (1982).
73. Heraeus, Quartz glass plates datasheet, http://www.heraeus.com.
74. The Society of Photo-Optical Instrumentation Engineers (SPIE), http://spie.org/.
75. Lot-Oriel company, “Light sources for research, development and industry”, http://www.lot-oriel.com/
76. Roper Scientific company, http://www.roperscientific.de/
77. Acton Research Corporation, http://www.princetoninstruments.com/

78. L. Boivin, “Study of bandwidth effects in monochromator-based spectral responsivity measurements.” Applied Optics 41, No. 10, (2002).
79. R. D. Saunders, J. B. Shumaker, “Apparatus function of a prism-grating double monochromator.” Applied Optics 25, No.20, (1986).
80. H. J. Kostkowski, “Self study manual on optical radiation measurements.” Part I - chapter 7, (June 1997).
81. Spectral Products company, USA, http://www.spectralproducts.com.
82. C. Palmer, *Diffraction Grating Handbook*, Newport Corporation, 6th edition (2005).
83. L. Boivin, “Spectral responsivity of various types of silicon photodiode at oblique incidence: comparison of measured and calculated values.” Applied Optics 40, No.4, (2001).
84. M. López, “Optical characterization of Ge- and InGaAs-semiconductor detectors for high accuracy optical radiant power measurements in the near infrared.” Ph.D thesis, Braunschweig University, Germany (2008). http://bib1lp1.rz.tu-bs.de/docportal/servlets/MCRZipServlet?id=DocPortal_derivate_00004809.
85. R. Christoph, H. Neumann “*Multisensor Coordinate Metrology*.” sv cooporate media, Munich, 2007 ISBM 978-3-937889-66-5.
86. J. Metzdorf, K. D Stock, P. Sperfeld, A. Sperling, S. Winter and T. Wittchen, “A new FEL-type quartz-halogen lamp as an improved standard of spectral irradiance.” Metrologia 35, 423–426 (1998).
87. A. Sperling and V. Bentlage, “A stabilized transfer-standard system for spectral irradiance.” Metrologia 35, 437–440 (1998).
88. T. F. Gerald, E. G. Charles, W. Y. Howard, C. P. Albert, “ “Once is Enough” in Radiometric Calibrations.” J. Res. Natl. Inst. Stand. Technol. 112, 39-51 (2007).

89. Y. Ohno and J. K. Jackson, “Characterization of modified FEL quartz-halogen lamps for photometric standards.” Metrologia 32, 693–696 (1995/96).
90. American National Standards Institute (ANSI), http://www.ansi.org.
91. Osram Sylvania Inc., http://www.sylvania.com.
92. Delta Elektronika BV, SM120-25D power supply Datasheet, http://www.delta-elektronika.nl.
93. J. Metzdorf, K. D Stock, P. Sperfeld, A. Sperling, S. Winter and T. Wittchen, “Aspects of quality assurance in monitoring solar UV irradiance.” Metrologia 40, 66–69 (2003).
94. P. Kärhä, J. Hovila, P. Manninen, “Instruction manual for operating standard lamps.” Metrology Research Institute, Helsinki University of Technology, Version 1.6, February (2010).
95. Brockton Electro-Optics Corp (BEOC), Laser Power Controller (LPC), http://www.brocktoneo.com.
96. HighFinesse GmbH, WS/7 Super Precision, http://www.highfinesse.de.
97. J. Campos, A. Corróns, A. Pons, “Response uniformity of silicon photodiodes.” Applied Optics 27, No.24, (1988).
98. L. C. Alves, F. Reis, M. C. Torres, G. B. Almeida, I. B. Couceiro, “Spatial uniformity of the silicon photodiodes for establishment of spectral responsivity scale.” XIX IMEKO World Congress Fundamental and Applied Metrology; Lisbon, Portugal, ISBN 978-963-88410-0-1, September 6−11 (2009).
99. S. Winter, A. Sperling, “Uncertainty analysis of a photometer calibration at the DSR setup of the PTB.” 2nd Expert Symposium on Measurement Uncertainty, CIE x029:2006, ISBN 3-9810021-4-8, Braunschweig, Germany, 139-142, (2006).
100. R. K. Kostuk, “Polarization characteristics of a 1000-W FEL type filament lamp.” Applied Optics 20, No.13, (1981).

101. International Organization for Standardization (ISO) ”Guide to the expression of uncertainty in measurement”, (1993).
102. United Kingdom Accreditation Service (UKAS), “The expression of uncertainty and confidence in measurement.” Edition 2, January (2007).
103. M. G. Cox, B. R. L. Siebert, “The use of a Monte Carlo method for evaluating uncertainty and expanded uncertainty,” Metrologia 43, 178–188 (2006).
104. European co-operation for accreditation (EA), “Expression of the Uncertainty of Measurement in Calibration.” EA-4/02. December (1999).
105. BIPM Joint Committee for Guides in Metrology, “Evaluation of measurement data — Supplement 1 to the “Guide to expression of the uncertainty in measurement” — Propagation of distribution using a Monte Carlo method.” Final draft September (2006).
106. M. Cox, P. Harris, B. R. L. Siebert, “Evaluation of measurement uncertainty based on the propagation of distributions using Monte Carlo simulation.” Measurement Techniques 46, (2003).
107. National Institute of Standards and Technology (NIST), “Guidelines for evaluating and expressing the uncertainty of NIST measurement results.” NIST Technical Note 1297, Edition (1994).
108. Proceedings of the 2nd CIE Expert Symposium on measurement uncertainty, (ISBN 3-9810021-4-8), Braunschweig, Germany, 12-13 June, (2006).
109. S. Winter, Hypradata software, Scientific Software Development Company, http://www.ssd.de/
110. Metrodata GMBH, Workbench software, http://www.metrodata.de/.